UNIVERSITY OF CALIFORNIA

Los Angeles

Prediction and Ecological Consequences of Variation in Leaf Drought Response Traits

A dissertation submitted in partial satisfaction of the

requirements for the degree Doctor of Philosophy

in Biology

by

Marvin Browne

2023

ABSTRACT OF THE DISSERTATION

Prediction and Ecological Consequences of Variation in Leaf Drought Response Traits

by

Marvin Browne

Doctor of Philosophy in Biology

University of California, Los Angeles, 2023

Professor Lawren Sack, Chair

Among the many constituents of a plant's environment, water is critical to the functionality of most of a plant's physiological processes. Therefore, it is imperative to clarify how plants acquire, retain, utilize, and lose water to understand how these organisms will perform in a changing environment. Improving the capacity to determine tissue water status at organ, whole plant, canopy, and regional scales is necessary to resolve the drought responses and water requirements of crop and wild species, for agricultural and urban sustainability of water use. The most salient metrics of plant responses to dehydration at leaf scale are pressure volume (PV) curve traits, estimated from the relationship between water potential of a leaf (Ψ_{leaf}) and relative water content (RWC). These indices are correlated for a given dehydrating leaf; and notably, Ψ_{leaf} can provide mechanistic insight of the driving force for water movement within tissues. Pressure-volume curves have long been used for detailed analysis of tissue water status and its determinants (e.g.,

modulus of elasticity (ε), leaf water potential at turgor loss point (π_{tlp}), and cell capacitance before wilting (C_{ft})), exhibiting many physical relationships among parameters. However, while pressure-volume traits are central in the analysis and prediction of drought tolerance there has been much less characterization of the variation of PV parameters across leaves within species. Further, estimation of Ψ_{leaf} and RWC require destruction of leaf tissues, whereas remote sensing tools provide opportunities to improve throughput and enable water stress measurements at coarser scales.

Therefore, in this dissertation, I constructed a model to discern and explain the patterns of changes in water status as Ψ_{leaf} scaled from water content measured by terahertz radiation in-situ remote sensing. Then, I estimated the impact of intraspecific variation and inter-relationships of pressure volume curve parameters on prediction and interpretation, establishing a novel concept of baseline variation among sun leaves on similarly grown plants of 50 species. Last, I quantified intraspecific plasticity in the osmotic potential at full turgor (π_o) ($\Delta\pi$, or osmotic adjustment), an important drought tolerance trait, among ecotypes of a model species, *Arabidopsis thaliana*, and test for associations among osmotic adjustment, drought survival, growth under well-watered conditions, and native climate. This work provides new resolution of the determinants of tissue water status, with applications at both the leaf scale, such as clarifying the mechanistic traits underlying drought tolerance within species, and at ecosystem scales, such as for spectroscopic estimation of plant water status.

This dissertation of Marvin Browne is approved.

Mona Jarrahi

Elsa Marianne Ordway

Van Maurice Savage

Lawren Sack, Committee Chair

University of California, Los Angeles

2023

To my cherished family and friends, thank you for all the love and support.

Table of Contents

List of Tables

typically, the sources and scales cannot be fully disentangled. The cell in **bold-face** represents the types of variation involved in the baseline, "reference" intraspecific trait variation (ITV_{ref}) considered in this study, that is, variation across individuals in "typical" sun leaves.

Table 3.3. Simulations testing the influence of error in variables on the prediction of leaf water potential scaling up from the log transformed peak field ratio, ln (PFR), which relates to water mass per area (WMA; Figure 3.1). For each bootstrapping simulation I used either the mean value of each parameter or values sampled from a constructed distribution with the same mean and standard deviation from published data (Browne et al., 2020), or using my own database of traits.

Chapter 4.

Table 4.1. Leaf water status, osmotic adjustment, climate and growth variables, symbols, units, and definitions. Full list of climate variables is available in Supplemental Table 4.2.

Table 4.2. In response to drought stress, three types of strategies may arise: resistance, i.e., the maintenance of function under stress; avoidance, i.e., the ability to grow rapidly under ideal conditions; and ambivalence, i.e., strong stress sensitivity for ecotypes adapted to moist conditions. Tabled are osmotic, growth and allocation traits, the expected response under resistant, avoidant and ambivalent strategies and the associated reasoning for the response.

Table 4.3. Ecotypes of *Arabidopsis thaliana* grown experimental presented with their origin group, pre and post drought osmotic potential at full turgor ($\pi_{o,w}$ and $\pi_{o,d}$), leaf mass per area (LMA), time until death (TTD), flowering time, and climate variables (mean annual temperature (MAT) and mean annual precipitation (MAP)).

List of Figures

Chapter 2.

Figure 2.7. Association of water mass per area with the terahertz transmission peak field ratio, generalizing across leaves within and across three species. Each species' measurement points, regression line and ordinary least squares R^2 values are presented: *Arabidopsis thaliana*, purple; *Hedera canariensis*, blue; *Platanus racemosa,* yellow; all species together, black. Statistical significance: *, p<0.05; **, p<0.01; ***, p<0.001.

Figure 2.8. Species specific predictions of leaf water status using terahertz spectroscopy. Plots of observed values against predicted values for leaf water mass per area (WMA), relative water content (RWC), and leaf water potential (Ψ_{leaf}). Species level and all species level WMA were predicted for each measurement of PFR using species-specific and all species regression parameters respectively (Table S2.2). Statistical significance: not significant, ns; *, p<0.05; **, p<0.01; ***, p<0.001.

Chapter 3.

Figure 3.1. Diagram of inputs used to predict of leaf water status variables from spectroscopy-based measurements and leaf traits from spectroscopy approaches (S) (extended from Browne et al. (2020)). Energy transmitted from leaf tissue is indicative of the tissue "equivalent water thickness" or water mass per area (WMA). A function relating WMA to the spectroscopic measurement (Sm) across leaves varying in hydration state enables prediction of WMA. Relative water content (RWC) is then estimated by including the saturated water mass per area (i.e., the product of leaf mass per area and saturated water content). Last, leaf water potential is determined using species-mean pressure-volume (PV) curve parameters.

Figure 3.2. Mean intraspecific variation among sun leaves of plants growing in similar conditions (ITV_{ref}) for pressure volume curve parameters of 50 species and other morphological and compositional leaf traits for 39 species, separated by the dotted line and in each category ordered by increasing median coefficient of variation (n=12-50 species). Error bars indicate the standard error of the mean and asterisks denote the significant difference between mean of pressure volume curve and morphological and compositional leaf traits (***p<0.001; Nested ANOVA).

Figure 3.3. Tests of observed versus predicted values of leaf water potential at turgor loss point (π_{tlp} and $\widehat{\pi_{tlp}}$, respectively), relative water content at turgor loss point (RWC_{tlp} and $\widehat{RWC_{tlp}}$, respectively) and capacitance at full turgor (C_{ft} and $\widehat{C_{ft}}$, respectively) for 5-6 leaves of 40-44 species. Each point represents a leaf, and lines are plotted for all significant within-species regressions (grey dashed lines), with 1:1 line (solid black line). Values were predicted using equations 8, 9 and 11 for $\widehat{\pi_{tlp}}$, $\widehat{RWC_{tlp}}$, and $\widehat{C_{ft}}$, respectively.

Figure 3.4. Correlations across species of the coefficient of variation (CV) across individual sun leaves of plants grown in similar, well-watered conditions (a measure of ITV_{ref}) for total (C_{ft}) and symplastic ($C_{ft,s}$) capacitance, total and symplastic relative water content at turgor loss point (RWC_{tlp} and $RWC_{tlp,s}$, respectively), and leaf water potential at turgor loss point (π_{tlp}) with their mechanistic drivers according to biophysical theory, the leaf osmotic potential at full turgor (π_o) and modulus of elasticity (ε) for 53 species records2. Statistical significance; *p<0.05; **p<0.01; ***p<0.001). There is a strong relationship among variation in "higher level" parameters and their constituents. Black solid lines were drawn with standard major axis.

Figure 3.5. Test of model sensitivity to increasing parameters values for *Hedera canariensis* (A) and *Platanus racemosa* (B). I estimated the error in predicted leaf water potential (Ψ_{leaf}) using the root mean square error (RMSE; MPa) by increasing the sampled parameters, i.e., for pressure volume curve (PV) parameters (π_{tlp} and ε); for saturated water mass per area (SWMA); and for PV parameters and SWMA together, in my model (Figure 1). I increased sampled parameters by 5-100%, represented here as multiplying parameters by 1.05 to 2.0.

Figure 3.6. Root mean squared error of predictions (RMSE $\widehat{\Psi_{leaf}}$) for five values across the typical measured range of the log transformed peak field ratio, ln (PFR), which relates to water mass per area (WMA) and can thus be scaled up to give $\widehat{\Psi_{leaf}}$ for *Hedera canariensis* (A) and *Platanus racemosa* (B) (analysis using PFR data from (Browne et al., 2020)). For each ln (PFR), I predicted 1000 $\widehat{\Psi_{leaf}}$ values based on the approach presented in Figure 1, and for each term either using the mean value, or adding error by sampling from a normal distribution based on the measured mean and standard deviation (Table 3) to: (Simulation A) the pressure volume (PV) curve parameters; (Simulation B) the saturated water mass per area (SWMA); and (Simulation C) both the PV parameters and SWMA.

Chapter 4.

Figure 4.1. Map of provenance for 26 ecotypes of *Arabidopsis thaliana* catalogued in the 1001 Genome Project (A). Individuals from each provenance were grown in a climate-controlled glasshouse at the University of California, Los Angeles. Each point represents the provenance of an ecotype and each scaled color represents the aridity index (AI) of the associated climate. Individuals were allowed to dehydrate and by the end of the drought cycle, they showed a range of change in their osmotic potential at full turgor ($\Delta\pi$) from -0.91 to 0.17 MPa (B). Negative values indicate osmotic adjustment that would provide drought resistance. Light green points and lines represent ecotypes which had not osmotically adjusted, and darker green points represent those which had adjusted. Statistical significance; *p<0.05; **p<0.01; ***p<0.001.

Figure 4.2. After five of 12 individuals of *Arabidopsis thaliana* from each ecotype exhibit strong negative signs to the drought experiment, I harvested the control and droughted individuals of 29 and 26 genotypes respectively. Before rehydration, I equilibrated and estimated leaf water potential (Ψ_{leaf}; A). Then, entire plants were rehydrated overnight, and I estimated the post drought osmotic potential at full turgor ($\pi_{o,d}$; B) and the change in osmotic potential at full turgor from well-watered to post drought conditions ($\Delta\pi$; C). Light green points and lines represent ecotypes which had not osmotically adjusted, and darker green points represent those which had adjusted. Statistical significance; *p<0.05; **p<0.01; ***p<0.001.

Figure 4.3. I estimated correlations among well-watered osmotic potential at full turgor ($\pi_{o,w}$) droughted osmotic potential at full turgor ($\pi_{o,d}$) and the change in osmotic potential at full turgor ($\Delta\pi$) across all my genotypes and among those that had or had not adjusted osmotically. Across ecotypes, $\pi_{O,w}$ did not predict osmotic adjustment (A) but $\pi_{O,d}$ was strong associated (B). When I considered osmotic adjustment strategies, the adjusters' $\pi_{O,d}$ strongly predicted osmotic adjustment. Further, only the non-adjusters' $\pi_{O,w}$ was significantly related to $\pi_{O,d}$ (C). Light green points and lines represent ecotypes which had not osmotically adjusted, and darker green points represent those which had adjusted. Statistical significance; *p<0.05; **p<0.01; ***p<0.001.

Figure 4.4. I tested for kinship-informed correlations among drought resilient traits, $\pi_{o,w}$, $\pi_{o,d}$, $\Delta\pi$, leaf mass per area (LMA) and root mass fraction (RMF), and drought survival time as the time until death from the beginning of the drought experiment until 5/12 individuals had died (TTD). I found significant correlations among $\pi_{O,w}$, $\pi_{O,d}$, $\Delta\pi$, LMA and RMF with survival where "less-resilient" ecotypes survived for shorter periods of the drought. Light green points and lines represent ecotypes which had not osmotically adjusted, and darker green points represent those which had adjusted. Statistical significance; *p<0.05; **p<0.01; ***p<0.001.

Figure 4.5. I tested for kinship-informed correlations among drought avoidant traits, flowering time at 16°C, relative growth rate, leaf area ratio, unit leaf rate, leaf mass fraction and reproductive mass fraction (ReMF) and drought survival time as the time until death from the beginning of the drought experiment until 5/12 individuals had died (TTD). I found significant correlations among flower time, relative growth rate, leaf area ratio, leaf mass fraction, and reproductive mass fraction with survival where longer-lived ecotypes grew less, allocate more of their biomass to leaves over flowers and flower later. Light green points and lines represent ecotypes which had not osmotically adjusted, and darker green points represent those which had adjusted. Statistical significance; *p<0.05; **p<0.01; ***p<0.001.

Figure 4.6. Kinship-informed correlations among osmotic variables relative growth (RGR) and its component traits (unit leaf rate (ULR), leaf area ratio (LAR), and leaf mass per area (LMA)). Many strong relationships among osmotic and growth traits were significant for the ecotypes which had osmotically adjusted. The non-adjusting ecotypes only presented strong relationships between $\pi_{o,w}$ and LMA. Light green points and lines represent ecotypes which had not osmotically adjusted, and darker green points represent those which had adjusted. Statistical significance; *p<0.05; **p<0.01; ***p<0.001.

Acknowledgements

"Revocate animos, maestumque timorem mittite:

forsan haec et olim meminisse iuvabit.

Per varios casus, per tot discrimina rerum tendimus"

Book 1, The Aeneid, Virgil

I wanted to start my acknowledgements with this quote because it is something that has stuck with me since I translated it in my Latin class in high school. In it, Aeneas, the protagonist of the story, and his crew have recently landed on shore after losing family and friends at sea and in the Trojan war. He asks the remaining people to "recall your spirits and cast away sorrow and fear: perhaps it will be pleasing to have remembered this. Through various misfortunes, through so many crises of things, I strive." I appreciate this quote but often when look it up again to make sure I'm spelling it correctly, I see people asking if remembering a difficult moment in life will be worth it. For me, at least, I will be glad to not only remember the knowledge I've gained but also the people that have supported, taught, and loved me throughout this journey.

To my parents, thank you all the moments thanked and unthanked that have led me to this moment. You have sacrificed a tremendous amount coming to this country and dedicating yourselves to Safiya and I. I hope you have look at this document and my degree as our accomplishment and success. Safiya thank you for all the many laughs that helped bring joy to my days away from you all. Chelsea for being my home away from home. You have always been tremendously supportive of all my work from the beginning.

To Lawren, thank you for being mentor and guiding me along towards this point. I was welcomed by your lab and over these many years, I appreciate all the opportunities that you have provided through collaborations with engineers, chemists and science policy of these six years. I

am fortunate to have been trained by you. To Gretchen, thank you for introducing me to the world of plant physiology and, advocating and mentoring me through the years.

To the Sack lab folks, my Ph.D. was supported all your contributions to my life and work—it's been a fun ride! Alec, we started this journey together and I'm glad to have had the chance to do so. I admire your love for the natural world and the immense knowledge you have masterfully wield. Marissa, you are not only talented scientist and amazing organizer for scientists of color on this campus and I'm glad you always remembered me when there was some event or some chisme or Costco deals. Leila, that osmotic adjustment project was a doozy, but it was so fun having you around to share our love for SpongeBob references and thanks for always remembering birthdays! It brought us all together and united us through the long days and weeks in lab. Camila, thank you for always being a support system and someone to bounce ideas off even when I tried to do it with poor Portuguese abilities. Christian, the one the only, the guy, the legend. Thanks for helping create a home away from home from our pizza creations to bike rides to the beach, and miscellaneous missions to undisclosed locations to source plant cuttings. Santiago, thank you showing me what life as a scientist should be rigor during the day and dancing the night away. Joseph, I admire the tenacity you've shown on your untraditional path and I'm glad I got to meet you along the way. Also, thank you for teaching me the ways of hydraulics and feeding me that one day. Anna, your fiery spirit and love for food and the fire R&B classics made field work and all the manifold bubbles a joy, thank you. Nidhi, your ability to connect with and bring others together with your curiosity is something I aspire to live by. Grace, thanks for always letting me come to talk and ask for help in your office. Jessica, the hidden gem of the Sack lab. Thanks for all the chats and horror movie suggestions.

To Mary and Chris—Thanks for all the adventures from day 1. Chris I've enjoyed all our food adventures and hope to have many more. Mary thanks for all the warm and adventures to the Sierras and Joshua Tree. You're both amazing friends.

I am grateful to my collaborators and to my committee members, Mona Jarrahi, Elsa Ordway and Van Savage for their guidance, encouragement and feedback on my work across the years.

Coauthored work: Chapter 2 is from Browne, M.G., Yardimci, NT, Scoffoni, C, Jarrahi, M, Sack, L. Prediction of leaf water potential and relative water content using terahertz radiation spectroscopy published in *Plant Direct* in 2020. Chapter 3 is from Browne, M.G., Bartlett, MK, Henry,C., Jarrahi, M., John, G., Scoffoni, C., Yardimci, T., Sack, L. (2023) Low baseline intraspecific variation in leaf pressure-volume traits: biophysical constraints and implications for spectroscopic sensing published in *Physiologia Plantarum* in 2023. Chapter 4 is from Browne, M.G., Fletcher L., Farell C., Sack L. The contribution of osmotic adjustment to drought adaptation in *Arabidopsis thaliana* which is *in prep.*

Professional Preparation

2016 BA in Biology (emphasis: Environmental Science) (Occidental College)

Publications

Browne, M.G., Bartlett, MK, Henry,C., Jarrahi, M., John, G., Scoffoni, C., Yardimci, T., Sack, L. (2023) Low baseline intraspecific variation in leaf pressure-volume traits: biophysical constraints and implications for spectroscopic sensing. *Physiologia Plantarum.* https://doi.org/10.1111/ppl.13974.

Panescu P., **Browne M.**, Chen K., Sack L., Maynard H. (2022) Effects of Trehalose and Polyacrylate-Based Hydrogels on Tomato Growth Under Drought. *AoBP Plants*, https://doi.org/10.1093/aobpla/plac030

Browne, M.G., Yardimci, NT, Scoffoni, C, Jarrahi, M, Sack, L. (2020) Prediction of leaf water potential and relative water content using terahertz radiation spectroscopy. *Plant Direct* 4: 1–16. https://doi.org/10.1002/pld3.197 . ***Plant Direct Article of the Year 2020 (#3)***

North, G. B., Brinton, E. K., **Browne, M.G.**, Gillman, M. G., Roddy, A. B., Kho, T. L., Wang, E., Fung, V. A., and Brodersen, C.R (2019) Hydraulic conductance, resistance, and resilience: how leaves of a tropical epiphyte respond to drought. *American Journal of Botany* 7: 943– 957. https://doi.org/10.1002/ajb2.1323.

North, G. B., **Browne, M.G.**, Fukui, K., Maharaj, F. D. R., Phillips, C. A., and Woodside, W. T. (2016) A tale of two plasticities: leaf hydraulic conductances and related traits diverge for two tropical epiphytes from contrasting light environments. *Plant, Cell & Environment* 39: 1408– 1419. doi: 10.1111/pce.12697.

Selected Awards and Grants

2022 Dissertation Year Fellowship, The Graduate Division, UCLA (3 quarters of funding)
2020 Ecology and Evolutionary Biology Department Summer Fellowship, UCLA($7,500).
2020 UCLA/NRT Integrated Urban Solutions for Food, Energy, and Water Management (INFEWS) Graduate Traineeship (1 year funding)
2020 Graduate Student Researcher funded through California AB1668-SB606 Project.
2019 Ecology and Evolutionary Biology Department Fellowship, UCLA ($8,300).
2018 Graduate Student Researcher (6 quarters) funded through UCLA Sustainable Grand Challenge and the Anthony and Jeanne Pritzker Family Foundation.

***Presentations*:**

Browne, M.G., Yardimci, NT, Scoffoni, C, Jarrahi, M, Sack, L. (2020) Prediction of leaf water potential and relative water content using terahertz radiation spectroscopy. Uri Hochberg Lab Meeting.

Browne, M.G., Bartlett, MK, Henry,C., Jarrahi, M., John, G., Scoffoni, C., Yardimci, T., Sack, L. Intraspecific variation in leaf pressure-volume traits:biophysical constraints and implications for in-situ and remote sensing, Ecological Society of America, Montreal

Browne, M.G., Yardimci, NT, Scoffoni, C, Jarrahi, M, Sack, L. (2020) Prediction of leaf water potential and relative water content using terahertz radiation spectroscopy. Ecological Society of America Annual Meeting, Virtual.

Browne, M.G. Sorrel. Botany of the Holidays 2019. Mildred Mathias Botanical Garden, Los Angeles, CA.

Synergistic activities*:*
2023 Entering Mentoring Training, UCLA Center for the Improvement of Mentored Experience in Research
2020 Leaders in Sustainability Certificate, UCLA Institute of the Environment and Sustainability IoES
2019-Present Member of Mildred Mathias Botanical Garden Campus Advisory Committee
Mentor to UCLA honors research in Ecology and Evolutionary Biology students: 2019-2020: Julia Lok, Suzanne Reyes-Ingwersen**; 2020-2021:** Joshua Matsuda

Chapter 1: Premise of the Dissertation

Climate change is predicted to increase the frequency of extended dry periods especially in places like California (Swain et al., 2018). Thus, plants will be challenged to be resilient and adapt or acclimate in response to water stress or else dehydrate and experience mortality. In response to short term dehydration species, can stave off further dehydration by closing stomata or buffer transient environmental changes using tissue water storage (Sack et al. 2003; Henry et al., 2019). Over longer periods, species may accumulate solutes to maintain turgor pressure with further water stress (Bartlett et al., 2014) or invest more in structural components of tissues in response to greater solar irradiance (Sack et al., 2006). Plant ecophysiologists use many morphological and physiological traits to explain patterns and processes of plant water use from organ and species-level physiology to ecosystem function. Indeed, plant functional traits, which explain plant responses to water availability are widely used to estimate resource capture and physiological vulnerability and draw associations between patterns of drought tolerance and climate (Bartlett et al., 2012; Fletcher et al. 2019; Medeiros et al., 2019). Given the increasing availability of species mean trait values (Kattge et al., 2020) and their use for parameterizing models for remotely sensed ecosystem hydraulic function (Moment et. al., 2017; Lu et al. 2022), it is imperative to quantify and determine the influence of intraspecific variation in hydraulic traits on prediction of plant water status. My work aims to address two questions: what are the limitations in estimating physiological traits, and what can we learn about trait-trait relationships through variation among and within species.

Common practice for estimating species vulnerability to drought is to analyze the relationship between declines in physiological functioning with dehydration and then to establish thresholds of irreparable damage. For example, pressure volume (PV) curves quantify the loss in water content with dehydration state. Leaf water potential, a measure of how strongly water is

held within plant cells, is regularly used to estimate leaf water status. PV curves and leaf water potential have a long history of use (Tyree and Hammel, 1972) but require destruction of leaves, which diminishes reproducibility and throughput. To address these concerns, I collaborated with engineers using terahertz radiation (THz, i.e., electromagnetic radiation in 10–1,000 μm wavelength range), which is highly sensitive to water within tissues at small scales.

Intra-specific trait variation (ITV) is a complex and multi-contextual topic in plant ecology. Plants exhibit ITV due to genetic variation among individuals within and between populations, phenotypic plasticity due to variation in growing conditions, trait variation linked with ontogeny and plant size, and developmental plasticity due to variation in gene expression that might occur even if genes and environment were identical (i.e., as found between two adjacent leaves on a shoot) (Albert et al., 2011; Bolnick et al., 2011; Violle et al., 2012; Siefert et al., 2015). For example, ITV in traits related to sun versus shade acclimation can be significant with leaf mass per area varying up to 2-fold between interior and full exposed leaves (Sack et al. 2006) and leaf hydraulic conductance ranging up to 67% higher in sun leaves than shade leaves (Sack et al. 2003). Considering the diversity of drivers of ITV, I examined ITV among fully developed sun leaves of well-watered plants, a 'reference' ITV that would add to the understanding of variation associated with different "scales" or "underlying processes."

Lastly, plasticity in hydraulic traits under patchy resource supply can confer greater resilience and variation in species' abundances (Grime and Mackey, 2002; de Bello et al., 2011; Bartlett et al. 2014). Thus, traits plasticity in traits such as the osmotic potential at full turgor (π_o) can provide resilience for species when water is limiting. Osmotic adjustment, or the accumulation of osmotica, allows the maintenance of cell turgor, delaying stomatal closure and further physiological decline (Bartlett et al. 2012; Zivcak et al., 2016). Therefore, the capacity to maintain turgor under drought via osmotic adjustment is essential for many species during water

deficit. To examine plasticity in osmotic adjustment, I quantified variation π_o among ecotypes of model species *Arabidopsis thaliana* and tested for associations with native climate, other osmotic variables (well-watered π_o, droughted π_o), and growth.

In Chapter 1, I developed a physically based model for the prediction of leaf water potential from electromagnetic radiation (i.e., terahertz time domain spectroscopy). In Chapter 2, I highlight the importance of the intraspecific variation in pressure volume curve parameters, critical traits that influence drought tolerance, and use these to better constrain predictions of leaf water potential using the method described in Chapter 1. In Chapter 3, I examine intraspecific variation in drought tolerance by focusing on osmotic adjustment among 29 genotypes of *Arabidopsis thaliana*. Overall, this work examines and tests broad trends of drought tolerance relationships across scales, contributing insights into the role of intraspecific variation in shaping drought tolerance, species distributions and ultimately ecosystem function.

References

Albert, C. H., F. Grassein, F. M. Schurr, G. Vieilledent, and C. Violle. 2011. When and how should intraspecific variability be considered in trait-based plant ecology? *Perspectives in Plant Ecology, Evolution and Systematics* 13: 217–225.

Bartlett, M. K., C. Scoffoni, and L. Sack. 2012. The determinants of leaf turgor loss point and prediction of drought tolerance of species and biomes: a global meta-analysis: Drivers of plant drought tolerance. *Ecology Letters* 15: 393–405.

Bartlett, M.K., Zhang, Y., Kreidler, N., Sun, S., Ardy, R., Cao, K., Sack, L., 2014. Global analysis of plasticity in turgor loss point, a key drought tolerance trait. Ecol Lett 17, 1580–1590. https://doi.org/10.1111/ele.12374

Bolnick, D. I., P. Amarasekare, M. S. Araújo, R. Bürger, J. M. Levine, M. Novak, V. H. W. Rudolf, et al. 2011. Why intraspecific trait variation matters in community ecology. *Trends in Ecology & Evolution* 26: 183–192.

de Bello, F., Lavorel, S., Albert, C.H., Thuiller, W., Grigulis, K., Dolezal, J., Janeček, Š., Lepš, J., 2011. Quantifying the relevance of intraspecific trait variability for functional diversity. Methods in Ecology and Evolution. https://doi.org/10.1111/j.2041-210X.2010.00071.x

Dong, N., I. C. Prentice, I. J. Wright, B. J. Evans, H. F. Togashi, S. Caddy-Retalic, F. A. McInerney, et al. 2020. Components of leaf-trait variation along environmental gradients. *New Phytologist* 228: 82–94.

Fletcher, L.R., Cui, H., Callahan, H., Scoffoni, C., John, G.P., Bartlett, M.K., Burge, D.O., Sack, L. 2018. Evolution of leaf structure and drought tolerance in species of Californian Ceanothus. American Journal of Botany 105, 1672–1687. https://doi.org/10.1002/ajb2.1164

Grime, J.P., Mackey, J., 2002. The role of plasticity in resource capture by plants. Evolutionary Ecology.

Givnish, T. 1988. Adaptation to sun and shade: a whole-plant perspective. *Functional Plant Biology* 15: 63–92.

Henry, C., John, G.P., Pan, R., Bartlett, M.K., Fletcher, L.R., Scoffoni, C., Sack, L., 2019. A stomatal safety-efficiency trade-off constrains responses to leaf dehydration. *Nature Communications*. https://doi.org/10.1038/s41467-019-11006-1

Kattge, J., G. Bönisch, S. Díaz, S. Lavorel, I. C. Prentice, P. Leadley, S. Tautenhahn, et al. 2020. TRY plant trait database – enhanced coverage and open access. *Global Change Biology* 26: 119–188.

Lu, Y., Sloan, B., Thompson, S.E., Konings, A.G., Bohrer, G., Matheny, A., Feng, X. 2022. Intra-specific variability in plant hydraulic parameters inferred from model inversion of sap flux data. *Journal of Geophysical Research: Biogeosciences* 127, e2021JG006777. https://doi.org/10.1029/2021JG006777

Medeiros, C. D., C. Scoffoni, G. P. John, M. K. Bartlett, F. Inman-Narahari, R. Ostertag, S. Cordell, et al. 2019. An extensive suite of functional traits distinguishes Hawaiian wet and dry forests and enables prediction of species vital rates. *Functional Ecology* 33: 712–734.

Messier, J., B. J. McGill, and M. J. Lechowicz. 2010. How do traits vary across ecological scales? A case for trait-based ecology. *Ecology Letters* 13: 838–848.

Momen, M., Wood, J.D., Novick, K.A., Pangle, R., Pockman, W.T., McDowell, N.G., Konings, A.G. 2017. Interacting effects of leaf water potential and biomass on vegetation optical depth: effects of LWP and biomass on VOD. *Journal of Geophysical Research: Biogeosciences* 122, 3031–3046. https://doi.org/10.1002/2017JG004145.

Niinemets, Ü., O. Kull, and J. D. Tenhunen. 1998. An analysis of light effects on foliar morphology, physiology, and light interception in temperate deciduous woody species of contrasting shade tolerance. *Tree Physiology* 18: 681–696.

Sack, L., Cowan, P.D., Jaikumar, N., Holbrook, N.M. 2003. The 'hydrology' of leaves: co-ordination of structure and function in temperate woody species. Plant, Cell & Environment. https://doi.org/10.1046/j.0016-8025.2003.01058.x

Sack, L., Melcher, P.J., Liu, W.H., Middleton, E., Pardee, T. 2006. How strong is intracanopy leaf plasticity in temperate deciduous trees? American Journal of Botany. https://doi.org/10.3732/ajb.93.6.829

Sanders, G. J., and S. K. Arndt. 2012. Osmotic adjustment under drought conditions R. Aroca [ed.]. *Plant responses to drought stress: From morphological to molecular features*: 199–229.

Siefert, A., C. Violle, L. Chalmandrier, C. H. Albert, A. Taudiere, A. Fajardo, L. W. Aarssen, et al. 2015. A global meta-analysis of the relative extent of intraspecific trait variation in plant communities. *Ecology Letters* 18: 1406–1419.

Swain, D. L., B. Langenbrunner, J. D. Neelin, and A. Hall. 2018. Increasing precipitation volatility in twenty-first-century California. *Nature Climate Change* 8: 427–433.

Tyree, M. T., and H. T. Hammel. 1972. The measurement of the turgor pressure and the water relations of plants by the pressure-bomb technique. *Journal of Experimental Botany* 23: 267–282.

Valladares, F., S. J. Wright, E. Lasso, K. Kitajima, and R. W. Pearcy. 2000. Plastic phenotypic response to light of 16 congeneric shrubs from a panamanian rainforest. *Ecology* 81: 1925–1936.

Violle, C., B. J. Enquist, B. J. McGill, L. Jiang, C. H. Albert, C. Hulshof, V. Jung, and J. Messier. 2012. The return of the variance: intraspecific variability in community ecology. *Trends in Ecology & Evolution* 27: 244–252.

Zivcak, M., M. Brestic, and O. Sytar. 2016. Osmotic adjustment and plant adaptation to drought stress M. A. Hossain, S. H. Wani, S. Bhattacharjee, D. J. Burritt, and L.-S. P. Tran [eds.],. *Drought stress tolerance in plants, vol 1: Physiology and biochemistry*: 105–143.

Chapter 2: Prediction of leaf water potential and relative water content using terahertz radiation

Received: 26 November 2019 | Accepted: 3 December 2019

DOI: 10.1002/pld3.197

ORIGINAL RESEARCH

American Society of Plant Biologists | SEB | WILEY

Prediction of leaf water potential and relative water content using terahertz radiation spectroscopy

Marvin Browne[1] | Nezih Tolga Yardimci[2] | Christine Scoffoni[3] | Mona Jarrahi[2] | Lawren Sack[1]

[1]Department of Ecology and Evolutionary Biology, University of California Los Angeles, Los Angeles, CA, USA

[2]Department of Electrical and Computer Engineering, University of California Los Angeles, Los Angeles, CA Los Angeles, CA, USA

[3]Department of Biological Sciences, California State University, Los Angeles, Los Angeles, CA, USA

Correspondence
Lawren Sack, Department of Ecology and Evolutionary Biology, University of California, Los Angeles, 621 Charles E. Young Dr. South, Los Angeles, CA 90095, USA.
Email: lawrensack@ucla.edu

Funding information
U.S. National Science Foundation, Grant/Award Number: IOS-145727; NRT-INFEWS, Grant/Award Number: DGE-1735325; the UCLA Sustainable LA Grand Challenge; Anthony and Jeanne Pritzker Family Foundation

Abstract

Increases in the frequency and severity of droughts across many regions worldwide necessitate an improved capacity to determine the water status of plants at organ, whole plant, canopy, and regional scales. Noninvasive methods have most potential for simultaneously improving basic water relations research and ground-, flight-, and space-based sensing of water status, with applications in sustainability, food security, and conservation. The most frequently used methods to measure the most salient proxies of plant water status, that is, water mass per leaf area (WMA), relative water content (RWC), and leaf water potential (Ψ_{leaf}), require the excision of tissues and laboratory analysis, and have thus been limited to relatively low throughput and small study scales. Applications using electromagnetic radiation in the visible, infrared, and terahertz ranges can resolve the water status of canopies, yet heretofore have typically focused on statistical approaches to estimating RWC for leaves before and after severe dehydration, and few have predicted Ψ_{leaf}. Terahertz radiation has great promise to estimate leaf water status across the range of leaf dehydration important for the control of gas exchange and leaf survival. We demonstrate a refined method and physical model to predict WMA, RWC, and Ψ_{leaf} from terahertz transmission across a wide range of levels of dehydration for given leaves of three species, as well as across leaves of given species and across multiple species. These findings highlight the powerful potential and the outstanding challenges in applying in vivo terahertz spectrometry as a remote sensor of water status for a range of applications.

KEYWORDS

Arabidopsis, drought tolerance, hydraulics, pressure–volume curves, remote sensing, turgor loss point

1 | INTRODUCTION

Understanding plant responses to water is increasingly urgent given drought-induced losses in crop productivity and tree mortality in many ecosystems worldwide (Allen et al., 2010; IPCC, 2014). Improving the capacity to determine tissue water status at organ, whole plant, canopy, and regional scales is necessary to resolve the drought responses and water requirements of crop and wild species,

for food security and sustainability of agricultural and urban water use.

The most salient metrics of leaf water status at leaf scale are water mass per leaf area (WMA; numerically equal to the "leaf equivalent water thickness"; Tucker, 1980; Hunt & Rock, 1989; all terms and abbreviations summarized in Table 1), relative water content (RWC), and leaf water potential (Ψ_{leaf}; Jones, 2014). These indices are correlated for a given dehydrating leaf and provide different information. Whereas the WMA represents the absolute tissue water content normalized by leaf area, the RWC, normalized by the saturated water content, also provides information of cell volume shrinkage (Sack, John, & Buckley, 2018) and thereby captures more specifically the plant-experienced water stress. Even more mechanistic insight is provided by $\Psi_{leaf,}$ which enables quantification of the balance of osmotic and turgor pressures, and represents the driving force for water movement, enabling estimation of hydraulic conductances (Bartlett, Scoffoni, & Sack, 2012; Scoffoni et al., 2018; Scoffoni, McKown, Rawls, & Sack, 2012). However, typical methods for measuring these variables require the excision of tissues and laboratory analysis, either gravimetric in the case of WMA and RWC, or using the Scholander pressure chamber or psychrometry for $\Psi_{leaf,}$ and thus, measurement of plant water status has often been limited to relatively low throughput and small study scales (Jones, 2014). By contrast, noninvasive methods have great potential for improving ground-based and remote sensing in water relations research and their applications in agriculture and conservation, especially as WMA, RWC, and Ψ_{leaf} can in principle be estimated not only for leaves, but also at coarser scales, for whole canopies (Table S1). We present a refined method and physically based model to estimate WMA, RWC, and Ψ_{leaf} from terahertz radiation during mild, moderate, and severe leaf dehydration, for given leaves, across leaves of a given species, or across multiple species, validated for three species (*Arabidopsis thaliana*, *Hedera canariensis*, and *Platanus racemosa*; Table 2).

Water within a plant absorbs electromagnetic radiation across the visible, infrared, and terahertz wavelengths distinctly from other structural plant components (Jones, 2014; Knipling, 1970). Accordingly, many studies have shown correlations of radiation variables with leaf water status variables at the scale of individual leaves, whole plants, and forest stands (Table S1; Claudio et al., 2006; Cotrozzi et al., 2017; Danson, Steven, Malthus, & Clark, 1992; Hunt & Rock, 1989; Hunt, Rock, & Nobel, 1987; Peñuelas, Filella, Biel, Serrano, & Savé, 1993; Peñuelas & Inoue, 1999; Rapaport, Hochberg, Cochavi, Karnieli, & Rachmilevitch, 2017; Rapaport, Hochberg, Shoshany, Karnieli, & Rachmilevitch, 2015; Sancho-Knapik et al., 2011). The power of these approaches at large scales is shown by the use of airborne hyperspectral or microwave data to detect canopy water content across large forest ranges (Asner et al., 2016; Rao, Anderegg, Sala, Martínez-Vilalta, & Konings, 2019). Yet, heretofore, the bulk of studies has focused on statistical correlations of water status variables across well-hydrated and strongly dehydrated leaves, without clear resolution for mildly to moderately dehydrated leaves (Table S1). Thus, further development is needed to sense WMA, RWC, and Ψ_{leaf} in mild and moderately dehydrated leaves, that is, in the important range of leaf dehydration for the control of gas exchange, between full turgor and turgor loss point (Bartlett, Klein, Jansen, Choat, & Sack, 2016; Trueba et al., 2019), as well as at stronger levels of dehydration below turgor loss point.

Electromagnetic radiation in the terahertz regime (loosely 100 GHz-10 THz frequency range or 10–1,000 μm wavelength range) (Mittleman, Jacobsen, & Nuss, 1996) has exceptional promise for measuring plant water status and dynamics. Transitions between vibrational and rotational states of many polar molecules, such as water, fall in the terahertz region of the electromagnetic spectrum (Mittleman, Jacobsen, Neelamani, Baraniuk, & Nuss, 1998), and thus, terahertz wave propagation is very sensitive to the sample water content (Hecht, 2002; Rønne, Åstrand, & Keiding, 1999; Thrane, Jacobsen, Uhd Jepsen, & Keiding, 1995). In addition, terahertz radiation can offer higher resolution imaging compared with microwave frequencies. Imaging and spectroscopy at terahertz frequencies are harmless since the energy of the photon is very small, compared to lower-wavelength radiation such as ultraviolet and X-rays (Sun et al., 2011). Terahertz time-domain spectroscopy (THz-TDS) employs short pulses of electromagnetic radiation, which have a broad terahertz frequency range (Skoog, Holler, & Crouch, 2017). The transmitted and reflected pulses through and from the sample are detected to extract the time- and frequency-domain responses (Yardimci, Cakmakyapan, Hemmati, & Jarrahi, 2017; Yardimci & Jarrahi, 2017). Because of these specifications, there has been great interest in predicting plant water status using THz-TDS systems (Table S1; Hu & Nuss, 1995; Hadjiloucas, Karatzas, & Bowen, 1999; Jördens, Scheller, Breitenstein, Selmar, & Koch, 2009; Castro-Camus, Palomar, & Covarrubias, 2013; Gente et al., 2013; Born et al., 2014; Gente, Rehn, & Koch, 2015; Santesteban et al., 2015; Baldacci et al., 2017; Gente et al., 2018). However, as for other wavelengths, previous terahertz studies have generally compared only well-hydrated versus strongly dehydrated leaves in absolute water content (Born et al., 2014; Castro-Camus et al., 2013; Gente et al., 2013; Jördens et al., 2009; Li et al., 2018), WMA (Baldacci et al., 2017; Gente et al., 2018), or Ψ_{leaf} (Hadjiloucas et al., 1999), with limited resolution for moderately dehydrated leaves. Physical models have been proposed to relate absolute water content or WMA to terahertz absorption (Gente et al., 2013; Jördens et al., 2009; Baldacci et al., 2017), but not yet extended to enable scaling to RWC and Ψ_{leaf}. Further, while it is important to follow individual leaves in their WMA, RWC, and Ψ_{leaf} during dehydration, tests are needed of whether the water status of multiple leaves of a species or different species can be estimated from generalized relationships of water status to terahertz radiation, as even for given species leaves can vary more than twofold in hydrated thickness and WMA independently of RWC and Ψ_{leaf} (Scoffoni, Vuong, Diep, Cochard, & Sack, 2014).

Our aim was to clarify the relationship between leaf terahertz spectroscopy responses and key water status variables, that is,

TABLE 1 Terms, abbreviations, and definitions for terahertz spectroscopy and the measurement of leaf water status and underlying leaf structural and compositional variables

Term	Symbol	Units	Definitions and Significance
Terahertz spectroscopy			
Terahertz time-domain spectroscopy	THz-TDS	–	System used to generate terahertz wavelength pulses and detect them after interaction with a sample to extract the time-domain and frequency-domain response of the sample
Peak field ratio	PFR	dBs	Ratio of transmitted terahertz radiation through sample to radiation transmitted through an empty system
Reference signal amplitude	E_{Ref}	dBs	Peak electric field detected by the THz-TDS system when no sample is placed in the system
Sample signal amplitude	E_T	dBs	Peak electric field detected by the THz-TDS system when a leaf sample is placed in the system
Absorption coefficient	α	m^{-1}	Indication of the attenuation of radiation by a medium
Absorption coefficient of water	α_w	m^{-1}	Indication of the attenuation of radiation by water
Absorption coefficient of solid or dissolved leaf materials	α_S	m^{-1}	Indication of the attenuation of radiation by nonwater leaf materials
Reflectivity	R	unitless	Characteristic of a surface distinguishing its capacity to reflect incident radiation
Leaf water status and structural composition			
Leaf water potential; predicted values	Ψ_{leaf}; $\widehat{\Psi_{leaf}}$	MPa	Water status variable indicating the bulk leaf average chemical potential of water within leaf cells
Osmotic potential	Ψ_S	MPa	Solute potential, determined by the concentration of cell solutes
Pressure potential	Ψ_P	MPa	Turgor pressure against the cell walls
Relative water content; predicted values	RWC; $\widehat{RWC}$	$g \cdot g^{-1}$	Ratio of mass of leaf water to leaf water in saturated leaf
Water thickness	WT	m	Thickness of water within leaf
Water mass per area; predicted values	WMA; $\widehat{WMA}$	$g \cdot m^{-2}$	Mass of water within leaf per leaf area
Saturated water mass per area	SWMA	$g \cdot m^{-2}$	Mass of water within fully hydrated (saturated) leaf per leaf area
Saturated water content	SWC	g	Mass of water in fully hydrated (saturated) leaf
Leaf mass per area	LMA	$g \cdot m^{-2}$	Ratio of mass of dry leaf lamina to leaf area
Pressure–volume curve parameters			
Water potential at turgor loss point	Ψ_{tlp}	MPa	The chemical potential of water within leaf cells at "wilting point"
Modulus of elasticity	ε	MPa	Stiffness of cell walls
Osmotic potential at full turgor	π_o	MPa	Osmotic potential in cells at full turgor
Relative water content at turgor loss point	RWC_{tlp}	$g \cdot g^{-1}$	RWC at dehydration stage at which cells lose turgor

WMA, RWC, and Ψ_{leaf}. We used a THz-TDS system to characterize for given dehydrating leaves the terahertz transmission peak field ratio (PFR). We tested the hypothesis that a novel, physically based model, by which WMA would decline linearly with ln (PFR) (see *Methods*), can be applied to terahertz radiation for prediction of WMA, RWC, and Ψ_{leaf} during mild, moderate, and severe leaf

TABLE 2 Species are listed with family, geographic origin, growth habit, and calculated pressure–volume curve parameters, including water potential at turgor loss point (Ψ_{tlp}), modulus of elasticity (ε), osmotic potential at full turgor (π_o), and the relative water content at turgor loss point (RWC_{tlp})

Species	Family	Origin	Plant Habit	Ψ_{tlp} MPa	ε MPa	π_o MPa	RWC_{tlp} %
Arabidopsis thaliana	Brassicaceae	Eurasia and Africa	Herbaceous	−0.41	0.26	−0.28	67.2
Hedera canariensis	Araliaceae	Canary Islands	Climber	−2.32	7.85	−1.71	78.3
Platanus racemosa	Platanaceae	Southern California	Tree	−1.39	9.69	−1.16	86.4

dehydration. We also tested the ability to predict leaf water status from generalized equations across leaves of a given species, and across multiple species using physical relationships.

2 | MATERIALS AND METHODS

2.1 | Plant material and sample preparation

Measurements were conducted on three species diverse in phylogeny, habitat type, and responses to drought: *Arabidopsis thaliana* (Col-0), *Hedera canariensis*, and *Platanus racemosa* (Table 2). Large individuals of climber *H. canariensis*, and tree *P. racemosa* were sampled on and around the campus of the University of California, Los Angeles. *A. thaliana* Col-0, an annual herb, was grown in a climate-controlled greenhouse at the University of California, Los Angeles (minimum, mean, and maximum values for temperature, 18.3, 22.4, 35.7°C; for relative humidity 8.3%, 44.4%, 83.8%; and for irradiance 1.2, 67.6, 1,300 μmol photons/m^2 s^{-1}). Seeds were cold-acclimated at 4°C for three days and sown in pots (7.95 cm width × 12.4 cm length × 5.87 cm deep) in soil (1:1:2:1:1 mixture of washed plaster sand, loam, peat moss, perlite, vermiculite). After approximately a week, plants were thinned to one individual per pot, and plants were studied after 5–6 weeks of growth.

For *H. canariensis* and *P. racemosa*, shoots with at least six fully developed leaves were harvested in the afternoon of the day prior to measurements and transported to the laboratory in plastic bags with wet paper towels. From each shoot, two nodes were recut under deionized water, and shoots were rehydrated overnight under plastic. For *A. thaliana*, trays of potted individuals were watered to saturation with deionized water and sealed with a dark plastic cover and wet paper towels for overnight rehydration. Two leaves from each of 3 individuals of *H. canariensis* and *P. racemosa*, and one leaf from each of five individuals of *A. thaliana* (a sixth leaf was not successful) was used for measuring terahertz transmission and leaf water status during dehydration.

2.2 | Terahertz time-domain spectroscopy

A Ti:Sapphire laser (Coherent MIRA-HP, Coherent Inc.) was used to generate femtosecond optical pulses at a 780 nm wavelength (Figure 1a). The beam of light was split into two, with the first beam used to pump a terahertz source to generate terahertz pulses, which were guided and focused on a terahertz detector, and the second beam passed through a linear delay stage to the terahertz detector. Plasmonic photoconductive nano-antenna arrays were used as the terahertz source and detector to provide high-power terahertz radiation and high terahertz detection sensitivity over a broad terahertz frequency range (Yardimci & Jarrahi, 2017; Yardimci, Yang, Berry, & Jarrahi, 2015). By moving the linear delay stage and changing the time delay between the optical pump and probe pulses incident on the terahertz source and detector, respectively, the time-domain electric field profile of the terahertz pulses incident on the terahertz detector was resolved with a sub-picosecond resolution over a 400 ps time-window. Lock-in detection was used to increase the signal-to-noise ratio of the resolved signal. To further increase the signal-to-noise ratio of the resolved signal, 10 time-domain traces were captured and averaged. By taking the Fourier transform of the averaged time-domain signal, the frequency-domain data were obtained with a 2.5 GHz frequency resolution (Figure 1b). The THz-TDS system used for the measurements reported in this work offered a 100-dB dynamic range and a frequency range of 0.1–5.5 THz.

2.3 | Measurements of dehydrating leaves for terahertz transmission and leaf water status

Before starting measurements with the THz-TDS system, a reference signal was acquired without placing any leaf samples on the terahertz beam path.

To determine the potential influence of variation in the angle of terahertz radiation incident on the leaf samples, leaves of *H. canariensis* were measured at 90°, perpendicular to the beam, as well as at ±5.0° off the perpendicular direction. We found negligible changes in the terahertz measurement results within this angle range.

Hydrated leaves were sealed in bags (Whirl-Pak, Nasco, Fort Atkinson, WI, USA) that had been exhaled into to generate a moist, high CO_2 environment to minimize transpiration, and placed in a larger plastic bag with wet paper towels to equilibrate at least 30 min before weighing with an analytical balance (0.01 mg; MS205DU Mettler Toledo, Toledo, OH). Then, each leaf sample was placed on a motorized XY translation stage and the position of the leaf was adjusted such

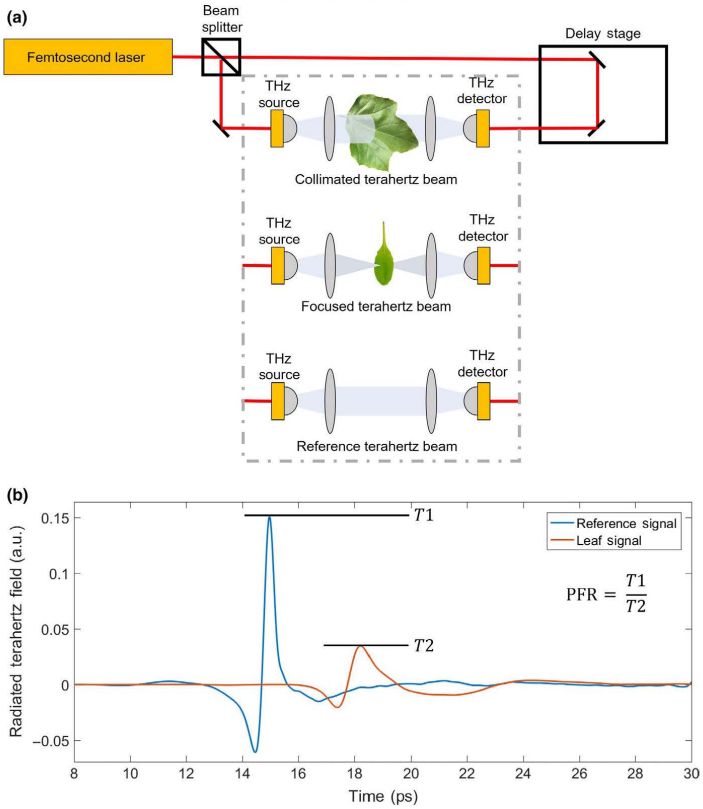

FIGURE 1 Schematic of the terahertz time-domain spectroscopy and its output (THz-TDS). The THz-TDS system is based on a terahertz source that emits femtosecond pulses of light. These pulses of light were distributed between the terahertz source, where they were used for sample analyses, and the terahertz detector, where they were used for detecting the terahertz pulses that transmitted through the leaf samples. At the beginning of measurements, a reference signal was recorded. A delay stage was used to change the time delay between the light pulses that were incident on the terahertz source and detector to scan across the terahertz bandwidth. *Hedera canariensis* and *Platanus racemosa* samples were measured using a collimated terahertz beam, and *Arabidopsis thaliana* were measured using a focused terahertz beam (a). For each measurement, a time-domain reference signal was recorded (E_{Ref}; blue curve) along with a signal transmitted through the leaf sample (E_{Ref}; red curve) (b)

that a section of lamina between two secondary veins was exposed to the terahertz radiation which was incident on the adaxial leaf face. A collimated terahertz beam with ~1.5-cm-diameter beam spot size was used for the *H. canariensis* and *P. racemosa* leaves. The smaller and more fragile leaves of *A. thaliana* were placed on a glass slide to ensure proper alignment during dehydration, and the terahertz beam was focused to produce a ~3-mm-diameter beam spot size for the measurements (Figure 1a). Because *A. thaliana* samples were smaller than the beam from the terahertz source, reduction the beam size incident on the sample was necessary to avoid including radiation propagating through air around the leaf, which would have led to large errors in the extracted water status parameters, as the data analysis assumes that the entire terahertz radiation interacts with the leaf sample.

The measurements with the THz-TDS system were repeated for each leaf during dehydration, with the position of the terahertz beam on the leaves marked to return to approximately the same spot for each measurement. However, given that leaves were removed from the system and replaced for repeated measurements, there were shifts in the exact position of the terahertz beam on the leaf sample in successive measurements; thus, for each dehydration stage, 25 measurements (at 1 mm steps) were made within the marked 5 × 5 mm^2 area for each *H. canariensis* and *P. racemosa* sample and averaged to improve the precision of the mean (Figure 2). Since a beam with much smaller spot size was incident on *A. thaliana*, 169 measurements (at 0.5 mm steps) were taken within a 6 × 6 mm^2 area. The THz-TDS system can image the leaf surface with even greater resolution (Figure 3) but that requires significant measurement times, which may result in dehydration of excised tissues. After each THz-TDS measurement, the leaf and bag were weighed with the analytical balance, and Ψ_{leaf} was determined with a pressure chamber (0.001 MPa resolution, Plant Moisture Stress Model 1000; PMS Instruments Co). Then, the leaves were bench dried on a fan to reduce Ψ_{leaf} by 0.1–0.2 MPa, and the terahertz measurements were repeated. Once at least two measurements were completed below the species' previously published turgor loss point (Scoffoni et al., 2018, 2014), an image of the leaf was taken using a flatbed scanner (Epson Perfection 4490 Photo, Seiko Epson Corporation) and the leaf lamina area (LA) was determined using Fiji (Schindelin et al., 2012). After the experiment, the mass of the bag was determined and subtracted for calculation of fresh leaf mass (FM) values for each leaf dehydration stage.

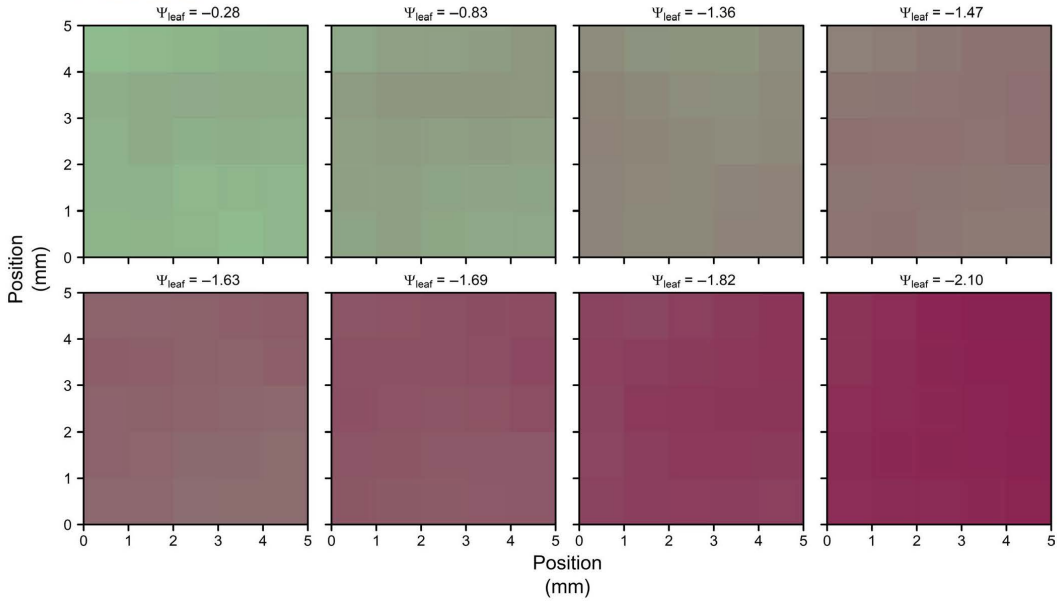

FIGURE 2 Terahertz transmission as a function of dehydration. Leaves were dehydrated to a range of leaf water potentials from full turgor to turgor loss point and beyond. At each measurement point for *Hedera canariensis* and *Platanus racemosa*, transmission of terahertz radiation through the leaf between major veins was characterized at 1-mm steps. Depicted above are sequential images produced for a *H. canariensis* leaf at leaf water potential values of −0.28 to −2.10 MPa, illustrating an increase in the transmitted radiation with dehydration

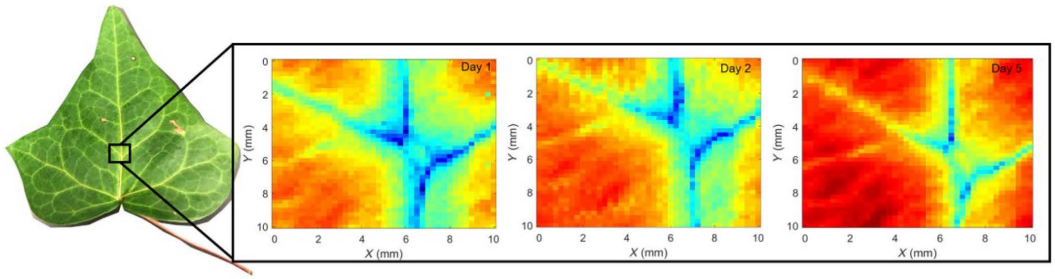

FIGURE 3 High-resolution images of leaf water thickness during dehydration may be taken with the terahertz time-domain spectroscopy system. Depicted are images of a *Hedera canariensis* leaf imaged after 1, 2, and 5 days of dehydration near major veins

Leaf dry mass (DM) was determined after oven drying for 48 hr at 70°C to enable determination of leaf mass per area (LMA):

$$\mathrm{LMA} = \frac{\mathrm{DM}}{\mathrm{LA}} \quad (1)$$

For each leaf, the saturated mass (SM) was estimated as the intercept of standard major axis regression lines (Table S2) fitted for the relationship between the leaf water mass and Ψ_{leaf} (Sack & Pasquet-kok, 2011). Then, RWC was determined for each stage of leaf dehydration as

$$\mathrm{RWC} = \frac{\mathrm{FM} - \mathrm{DM}}{\mathrm{SM} - \mathrm{DM}} \quad (2)$$

And saturated water content (SWC) as:

$$\mathrm{SWC} = \frac{\mathrm{SM}}{\mathrm{DM}} \quad (3)$$

Species-specific pressure–volume curves were constructed using RWC and Ψ_{leaf} data for the leaves that had more than three data points more negative than turgor loss point, that is, for three leaves of *H. canariensis* and five leaves of *P. racemosa*. For *A. thaliana*, given the fewer data available for dehydration sequences of individual leaves, data for all six leaves were pooled together into an overall pressure–volume curve (Scoffoni et al., 2018). From the pressure–volume

curves, parameters were extracted including turgor loss point (Ψ_{tlp}), osmotic potential at full turgor (π_o), and relative water content values at turgor loss point (RWC_{tlp}) (Sack & Pasquet-kok, 2011). When "plateau effects" were detected during early dehydration, that is, minute changes in Ψ_{leaf} despite substantial declines of leaf water mass, representing the dehydration of water-filled leaf airspaces, these points were removed before the estimation of pressure–volume parameters (Kubiske & Abrams, 1990).

A control was established to ensure that the change in the measured terahertz pulse during leaf dehydration was due to declining leaf water status, rather than simply associated with time duration. Thus, for *H. canariensis*, leaves that were maintained fully hydrated were measured over time (Figure 4). Shoots of *H. canariensis* were rehydrated, and then leaves were excised near the base of the petiole in a petri dish under filtered ultra-pure degassed water (0.22 μm Thornton 200 CR; Millipore). The petioles were wrapped in parafilm and connected under filtered water to clear poly-vinyl chloride tubing containing filtered water. Terahertz transmission measurements were recorded for these leaves at 1-hr intervals for 4 hr. For each measurement, the leaves were removed, weighed for the determination of RWC, and reconnected to the tubing under water. Leaf dry mass was determined after oven drying for 48 hr at 70°C. No variation was found in terahertz absorption with time for the hydrated leaves (Figure 4).

2.4 | A physically based model for leaf water status from terahertz signal analysis

During the terahertz measurements, the electromagnetic radiation was partially reflected from the leaf surface and partially absorbed within the leaf. The absorbed terahertz radiation can be estimated by comparing the time-domain reference signal with that obtained after transmission through the leaf. The peak field ratio (PFR) used to estimate leaf water status (Figure 1b) was calculated as:

$$\mathrm{PFR} = \frac{\max(E_T)}{\max(E_{Ref})} \tag{4}$$

where E_{Ref} and E_T are the peak electric field amplitudes of the reference and transmitted terahertz signals through the leaf in the time domain (Hecht, 2002). The amplitude of the transmitted terahertz field has a strong dependence on the total absorbed power within the leaf over a broad terahertz frequency range. We note that the use of the PFR rather than other metrics, such as, for example, the power integrated over the time domain would not change our analysis as the values are dominated by the low-frequency components of the terahertz pulse and, therefore, are strongly correlated, arising from the same absorption parameters. The relationship between the peak amplitudes of the reference and transmitted terahertz fields can be estimated as:

$$|E_T| = |E_{Ref}| \cdot |1-R| \cdot e^{-\alpha d} \tag{5}$$

where R and α are, respectively, assumed to be the reflectivity and the absorption coefficient effective across the measured terahertz frequency band, and d to be the leaf thickness (Hecht, 2002). The absorption coefficient, α, has a strong dependence on the thickness of water within the leaf:

$$\alpha = \frac{WT \cdot \alpha_W + VT \cdot \alpha_V + ST \cdot \alpha_S}{WT + VT + ST} \tag{6}$$

where WT is the thickness of water in the leaf; VT is the thickness of the vapor-saturated leaf airspaces; ST is the thickness of other nonair leaf materials; α_W, α_V, and α_s are the absorption coefficients of liquid water, vapor, and other nonwater (solid or dissolved) leaf materials. The absorption coefficients used in these equations were assumed to be an average value over terahertz frequency bandwidth of the THz-TDS system used for these measurements. Combining Equations 5 and 6, with d = WT+VT + ST:

$$|E_T| = |E_{Ref}| \cdot |1-R| \cdot e^{-(WT \cdot \alpha_W + VT \cdot \alpha_V + ST \cdot \alpha_S)} \tag{7}$$

To relate our measured PFR values to measured leaf water status, we divided both sides of Equation 7 by $|E_{Ref}|$, substituted PFR for $\frac{E_T}{E_{Ref}}$ using Equation 4, and ln-transformed both sides:

$$\ln(\mathrm{PFR}) = \ln(|1-R|) - WT \cdot \alpha_W - VT \cdot \alpha_V - ST \cdot \alpha_S \tag{8}$$

We assumed that WT and VT were of similar magnitude, and $\alpha_V \ll \alpha_W$ (Kindt & Schmuttenmaer, 1996; Rønne et al., 1999; Yang, Shutler, & Grischkowsky, 2011), and thus that $VT \cdot \alpha_V$ was negligible. Solving for WT:

$$WT = \frac{-\ln(PFR)}{\alpha_W} + \frac{\ln(|1-R|) - ST \cdot \alpha_S}{\alpha_W} \tag{9}$$

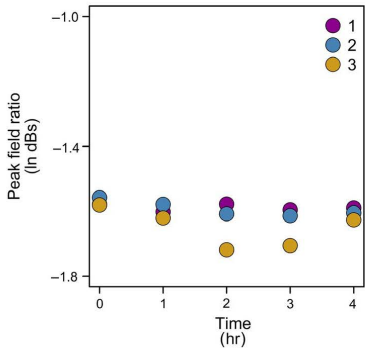

FIGURE 4 Testing for an influence of time on terahertz transmission for leaves maintained at full hydration. As a control, excised leaves were connected to a water source, while measurements were taken every hour for 4 hr, for *H. canariensis* (each symbol color represents a different leaf)

We assume that as a given leaf dehydrates, R remains constant, following (Sun et al., 2011), and further, that α_W, α_V, α_s, and α_S remain constant. Thus, WT can be predicted as a linear function of ln PFS in drying leaves.

$$WT = \frac{-\ln(PFR)}{\alpha_W} + c \quad (10)$$

where $c = \frac{\ln(|1-R|)-ST\cdot\alpha_S}{\alpha_W}$.

Notably, as the density of water = 1.0 g/cm^3, and water thickness (WT) is equivalent to water volume per unit leaf area, WT is numerically equivalent to the total leaf water mass per area (WMA). Thus, for each leaf of a given species, we fitted lines for WMA as a linear function of ln PFR (Table 3).

$$WMA = a\cdot\ln(PFR) + b \quad (11)$$

From these fitted lines, for each dehydration stage of each leaf, we predicted WMA values from PFR, that is, $\widehat{WMA}$. To predict the relative water content ($\widehat{RWC}$), we divided by the saturated water mass per area for each leaf (SWMA), where

$$\widehat{RWC} = \frac{\widehat{WMA}}{SWMA} \quad (12)$$

Notably,

$$SWMA = LMA\cdot SWC \quad (13)$$

where SWC is the saturated water content, that is, the water mass in saturated leaf divided by leaf dry mass, and LMA is the leaf dry mass per area.

We then predicted from $\widehat{RWC}$, using pressure–volume curve parameters derived from curves fitted according to pressure–volume theory (Sack et al., 2018). Ψ_{leaf} is the sum of the pressure potential (Ψ_P) and the solute potential (Ψ_S):

$$\Psi_{leaf} = \Psi_S + \Psi_P \quad (14)$$

and

$$\Psi_S = \frac{\pi_{o}\cdot\Psi_{tlp}(1-RWC_{tlp})}{\pi_{o}(1-RWC)+\Psi_{tlp}(RWC-RWC_{tlp})} \quad (15)$$

TABLE 3 Ordinary least squares (OLS) regression model parameters with lower and upper confidence limits (CL) and tests of common slope (ANCOVA) among leaves. Relationships for each leaf, species, and across multiple species of water mass per area (WMA) with terahertz transmission (ln PFR) were tested and used to predict relative water content and leaf water potential. *P*-values for individual leaves represent the fit of the linear model, and for common slopes, represent a test for the significance of variation in slope among individual leaves or among species

Species	Leaf	Slope (Lower CL, Upper CL)	Intercept (Lower CL, Upper CL)	R^2	*p* value
Arabidopsis thaliana	1	−343 (−656, −30.2)	−3.24 (−210, 203)	.88	.0421
	2	−332 (−566, −97.0)	−72.8 (−320, 174)	.83	.0205
	3	−223 (−263, −182)	19.7 (−8.57, 48.0)	.99	.0004
	4	−1002 (−1727, −277)	−521 (−1095, 49.9)	.95	.0277
	5	−312 (−582, −42.7)	−63.0 (−333, 207)	.93	.038
A. thaliana common slope					.0370
Hedera canariensis	1	−322 (−377, −268)	−211 (−286, −135)	.99	<.0001
	2	−300 (−496, −103)	−165 (−417, 87.8)	.82	.0130
	3	−179 (−193, −164)	−33.3 (−51.9, −14.6)	.99	<.0001
	4	−281 (−357, −205)	−114 (−203, −24.4)	.96	.001
	5	−340 (−664, −16.4)	−357 (−895, 181)	.59	.043
	6	−353 (−575, −132)	−3.45 (−721, 30.2)	.77	.009
H. canariensis common slope					.001
Platanus racemosa	1	−347 (−523, −172)	−139 (−311, 33.3)	.85	.005
	2	−128 (−164, −91.1)	13.0 (−33.9, 59.8)	.95	<.001
	3	−151 (−272, −30.6)	−9.70 (−149, 130)	.69	.025
	4	−97.1 (−110, −84.5)	16.9 (4.90, 29.0)	.98	<.0001
	5	−147 (−173, −122)	−27.3 (−49.5, 50.0)	.97	<.0001
	6	−89.5 (−107, −72.3)	39.4 (28.6, 50.2)	.96	<.0001
P. racemosa common slope					.003
Arabidopsis thaliana		−133 (−172, −96.5)	82.0 (−28.5, 44.9)	.55	1.28×10^{-5}
Hedera canariensis		−91.7 (−135, −48.6)	90.3 (28.0, 153)	.34	.0001
Platanus racemosa		−245 (−339, −151)	90.0 (−71.7, 89.7)	.57	9.17×10^{-9}
All species		−125	48.0	.37	2.25×10^{-12}
All-species common slope					.022

American Society of Plant Biologists SEB WILEY

TABLE 4 Inputs for using measured terahertz spectroscopy peak field ratio (PFR) to predict leaf water status variables, water mass per area ($\widehat{WMA}$), relative water content ($\widehat{RWC}$), and leaf water potential ($\widehat{\Psi_{leaf}}$). Predictions were made for each individual leaf during dehydration ($\widehat{WMA}_{leaf}$, $\widehat{RWC}_{leaf}$ and $\widehat{\Psi}_{leaf,leaf}$, left column), based on the relationship of water mass per area (WMA) to ln(PFR) for each dehydrating leaf, and from individual leaf values for saturated water mass per leaf area (SWMA) and species-level mean pressure–volume curve (PV) parameters. Predictions were also tested using species-level relationships of WMA to ln(PFR) ($\widehat{WMA}_{species}$, $\widehat{RWC}_{species}$, and $\widehat{\Psi}_{leaf,species}$, middle column) and all-species-level relationships of WMA to ln(PFR) ($\widehat{WMA}_{all}$, $\widehat{RWC}_{all}$, and $\widehat{\Psi}_{leaf,all}$, right column), using species-level mean values for SWMA and PV parameters

	Individual leaf level prediction	Species-level prediction	All-species-level prediction
$\widehat{WMA}$	$\widehat{WMA}_{leaf}$, from WMA ~ ln (PFR) relationship for each leaf	$\widehat{WMA}_{species}$, from WMA ~ ln (PFR) relationship for all leaves of given species	$\widehat{WMA}_{all}$, from WMA ~ ln (PFR) relationship for all leaves of all species
$\widehat{RWC}$	$\widehat{RWC}_{leaf}$, from $\widehat{WMA}_{leaf}$ and SWMA of each leaf	$\widehat{RWC}_{species}$, from $\widehat{WMA}_{species}$ and species-level mean SWMA	$\widehat{RWC}_{all}$, from $\widehat{WMA}_{all}$ and species-level mean SWMA
$\widehat{\Psi_{leaf}}$	$\widehat{\Psi}_{leaf,leaf}$, from RWC_{leaf} and species-level mean P-V parameters	$\widehat{\Psi}_{leaf,species}$, from $RWC_{species}$ and species-level mean P-V parameters	$\widehat{\Psi}_{leaf,all}$, from RWC_{all} and species-level mean P-V parameters

where π_o, RWC_{tlp}, and Ψ_{tlp} were determined from pressure–volume curves as described previously, and

$$\Psi_P = \begin{cases} \pi_o \cdot \left(\frac{RWC - RWC_{tlp}}{1 - RWC_{tlp}}\right), & \text{if } RWC > RWC_{tlp} \\ 0, & \text{if } RWC < RWC_{tlp} \end{cases} \quad (16)$$

Thus, using this physical model, $\widehat{WMA}$, $\widehat{RWC}$, and $\widehat{\Psi_{leaf}}$ were estimated from terahertz measurements during dehydration (Figure 5). Based on the relationship of water mass per area (WMA) to ln (PFR) (Equation 11), predictions are made of water mass per area ($\widehat{WMA}$). Then, relative water content ($\widehat{RWC}$) is estimated, accounting for saturated water mass per leaf area (SWMA), which is the product of leaf dry mass per area (LMA) and saturated water content (SWC) (Equations 12-13). Finally, leaf water potential ($\widehat{\Psi_{leaf}}$) is estimated using pressure–volume curve (PV) parameters (Equations 14-16).

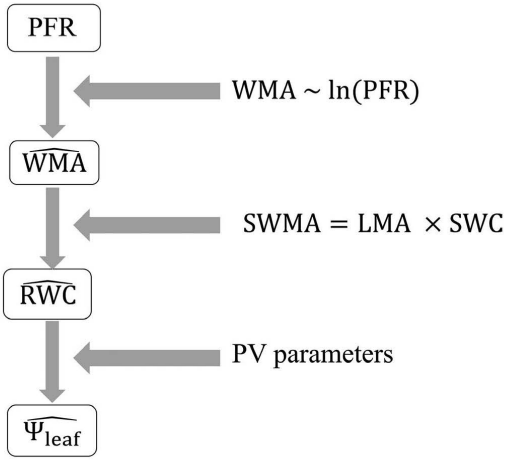

FIGURE 5 Flowchart illustrating the inputs to for the hierarchical prediction of water status variables from terahertz spectroscopy peak field ratio (PFR) and leaf traits (see Equations and Table 1 for further information about variables and symbols). Based on the relationship of water mass per area (WMA) to ln (PFR) for each dehydrating leaf, predictions are made of water mass per area ($\widehat{WMA}$). Then, relative water content ($\widehat{RWC}$) is estimated, accounting for saturated water mass per leaf area (SWMA), which is the product of leaf dry mass per area (LMA) and saturated water content (SWC). Finally, leaf water potential ($\widehat{\Psi_{leaf}}$) is estimated using pressure–volume curve (PV) parameters. These predictions were tested using the relationship of water mass per area (WMA) to ln (PFR) for individual leaves, or all leaves of given species, or across all leaves for the three species tested (Table 4)

2.5 | Statistics

We used Pearson correlation coefficients (r) to test the strength of the association of variables, and the coefficient of determination (R^2) to express the goodness of fit of models to data (Sokal & Rohlf, 1995).

Applying the physically based model statistically, we used measured terahertz spectroscopy peak field ratio (PFR) to predict leaf water status variables, leaf water mass per area ($\widehat{WMA}$), relative water content ($\widehat{RWC}$), and leaf water potential ($\widehat{\Psi_{leaf}}$). Predictions were made for each individual leaf during dehydration (Table 4, left column), based on the relationship of water mass per area (WMA) to ln (PFR) for each dehydrating leaf, and from individual leaf values for saturated water mass per leaf area (SWMA) and species-level mean pressure–volume curve (PV) parameters. Predictions were also tested using species-level relationships of WMA to ln (PFR) (Table 4, middle column) and all-species-level relationships of WMA to ln (PFR) (Table 4, right column), using species-level mean values for SWMA and PV parameters. We then tested how well these estimates corresponded to observed values of WMA, RWC, and Ψ_{leaf}.

To estimate the relationships of ln (PFR) to WMA at individual leaf, or species, or all-species scale, we fitted lines using ordinary least squares (OLS) regression with the *lm* function in the stats R package (R Core Team, 2019). We tested for the similarity of

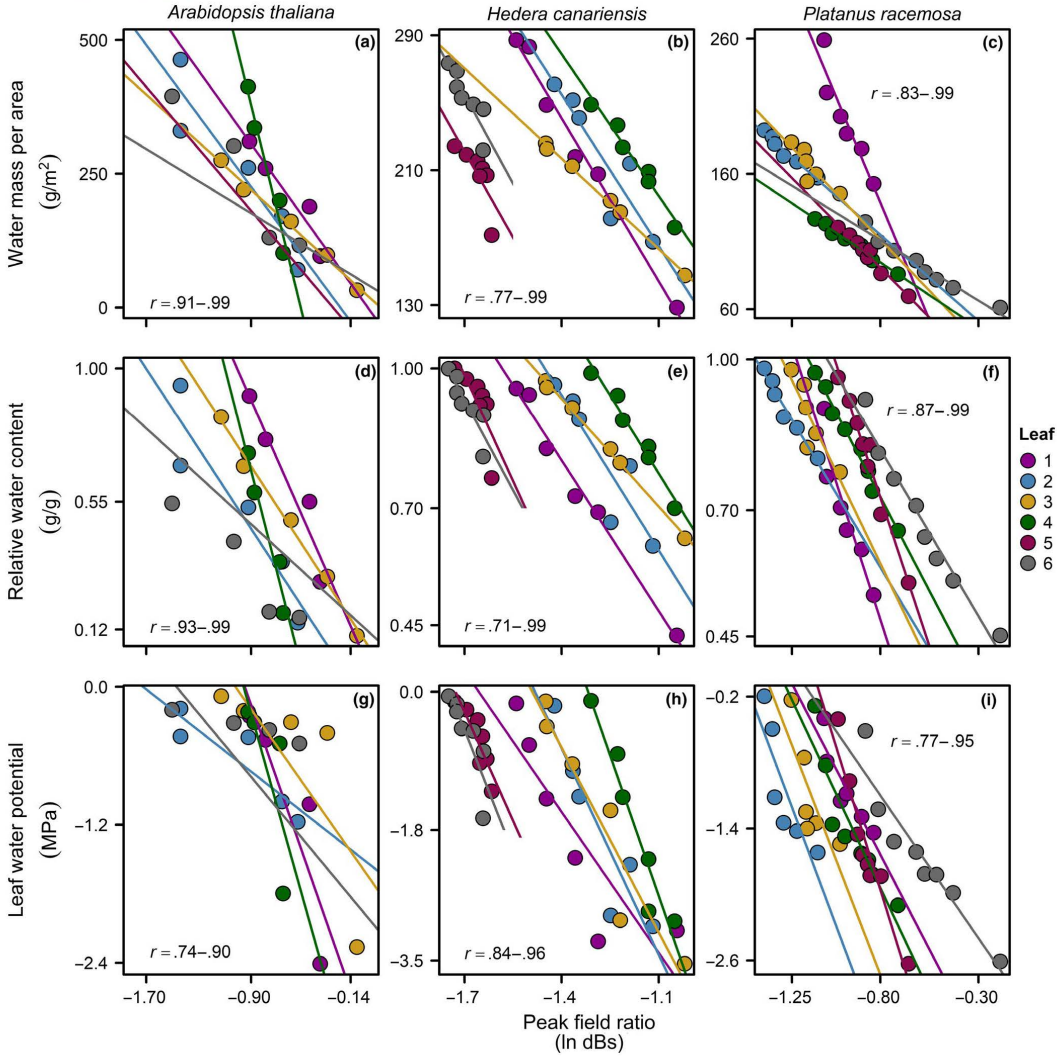

FIGURE 6 Association of water status variables with the terahertz transmission peak field ratio for three species. Lines were fitted for each leaf during dehydration by ordinary least squares (OLS): water mass per area (WMA; a–c), relative water content (RWC; d–f), and leaf water potential (Ψ_{leaf}; g–i) (fitted line parameters in Table 3). *p*-values all < .05; see values in Table 3

slopes among leaves of each species in the relationships of ln (PFR) and WMA by performing an analysis of covariance (ANCOVA) (using SMATR; Warton, Wright, Falster, Westoby, 2006). Further, we tested for the similarity of slopes across species, considering all leaves of each species together.

In applying the hierarchical approach to prediction, from $\widehat{WMA}$ to $\widehat{RWC}$ to $\widehat{\Psi_{leaf}}$, outlier points that represented impossible values were removed for higher-level predictions (Riazoshams, Midi, & Ghilagaber, 2019). Thus, when high outliers for $\widehat{WMA}$ from the fitted relationship of WMA to ln (PFR) led, when scaled by SWMA, to $\widehat{RWC}$ values that exceeded 1.0 g g^{-1}, and to $\widehat{\Psi_{leaf}}$ values that exceeded 0 MPa, or when extremely negative $\widehat{\Psi_{leaf}}$ were predicted from $\widehat{RWC}$ values far below the range of values in the PV curve, these $\widehat{RWC}$ and $\widehat{\Psi_{leaf}}$ values were removed for the estimation of predictive capacity. Altogether, for estimation of predictive capacity at the individual leaf level, values for 3 of 38 leaves were removed for *H. canariensis* and 1 of 42 leaves for *P. racemosa*; at the species level, 7 of 42 leaves for *P. racemosa*; and at the all-species level, 8 of 38 leaves for *H. canariensis*, and 21 of 42 leaves for *P. racemosa* (Table S2).

We tested model predictions of leaf water status at leaf scale, at species scale and at all species scale, by plotting estimated against observed values, and calculating R^2 and root mean square error (RMSE, in the same units as the predicted variable) as:

$$\text{RMSE} = \sqrt{\overline{(\text{observed} - \text{predicted})^2}} \quad (17)$$

To compare the error in predicting different water status variables across scales, we also calculated a normalized RMSE (i.e., NRMSE; Botchkarev, 2018).

$$\text{NRMSE} = \frac{\text{RMSE}}{y_{max} - y_{min}} \quad (18)$$

3 | RESULTS

3.1 | Estimation of leaf water status variables using terahertz measurements

Terahertz measurements showed strong ability to predict all three leaf water status variables, supporting the physically based model for the relationship of WMA with ln (PFR). As leaf water status declined, terahertz transmission increased, and for individual leaves, the declines of WMA, RWC, and Ψ_{leaf} were associated with ln (PFR) across the range from full turgor to Ψ_{tlp} and below Ψ_{tlp} (Figure 6a–i; Table 3). Notably, the relationships for individual leaves of WMA, RWC and Ψ_{leaf} with ln (PFR) differed significantly in slopes and intercepts (Table 3). Despite the variation among leaves of given species, the relationship of WMA with ln (PFR) was strong combining leaves for given species, or even across species (Figure 7).

Given these strong relationships, leaf water status variables could be predicted across scales, from individual leaf, to species, to all-species, using our hierarchical approach to estimation (Table 4; Figure 5). Thus, for given leaves, or for a given species, or across all species, $\widehat{\text{WMA}}$ could be predicted from the relationship with ln (PFR) (Figure 8a-d), relative water content ($\widehat{\text{RWC}}$) could be predicted by additionally including leaf- or species-level means for saturated water mass per unit leaf area (SWMA) (Figure 8e-h), and $\widehat{\Psi_{leaf}}$, by additionally including pressure–volume curve parameters (Figure 8i-l). As expected, the error in predicting WMA, RWC, and Ψ_{leaf} increased across these scales of variation, that is, from individual leaf to species (Figure 8a–l). Further, the error increased from the prediction of $\widehat{\text{WMA}}$ and $\widehat{\text{RWC}}$ to $\widehat{\Psi_{leaf}}$, as indicated by higher NRMSE values (Table 5; Figure 8a–l). The goodness of fit (i.e., significant R^2 values) and predictive power (i.e., relatively low RMSE and NRMSE values; Table 5) signified strong potential for estimation of all three water status variables using the physically based model and hierarchical prediction approach within and across species (Table 4; Figure 5).

4 | DISCUSSION

We present strong relationships of leaf water status variables (WMA, RWC, and Ψ_{leaf}) to the transmission of terahertz radiation for three diverse species. Our work extends from previous studies that compared terahertz measurements to leaf water status variables for very well-hydrated and strongly dehydrated leaves; we here show the strong association of terahertz absorption with water status within the range of operating leaf water status, that is, between full turgor and turgor loss point, and below. Further, previous work using terahertz radiation, and other parts of the electromagnetic spectrum, has tended to focus on the prediction of WMA (or "equivalent water thickness") and RWC, and we show the extension of this prediction to Ψ_{leaf}. Our approach to hierarchical estimation using a physically based model enables the translation of terahertz measured PFR to all three water status variables, and this approach could be extended to the detection of leaf water status using other ranges of wavelengths.

Although many species have been previously studied for the association of spectroscopic variables with leaf water status, previous studies have tended to focus on individual dehydrating leaves (Table S1). Our findings indicate the potential to extend prediction across multiple leaves of given species, and even across multiple species, assuming knowledge of additional leaf traits, such as leaf mass per area (LMA), saturated water content (SWC), and pressure–volume parameters. This finding highlights the great potential for the expansion of the use of terahertz transmission to determine water status noninvasively for individual leaves, and also across canopies and indeed, mixed canopy ecosystems.

Despite this evident predictive power, we also noted outstanding challenges. We found that leaves varied in the slopes and intercepts of the relationship of WMA to ln (PFR), which reduced the predictive power for the general relationship for given species

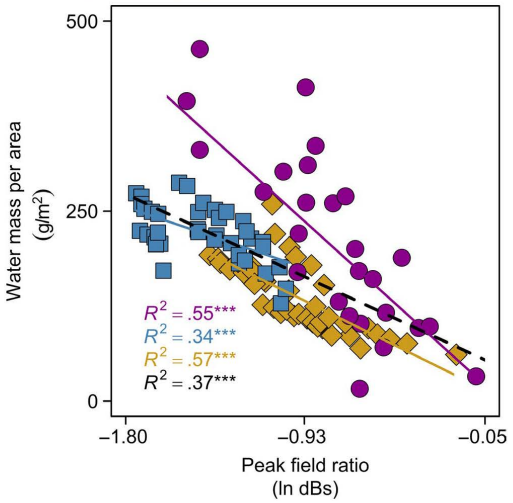

FIGURE 7 Association of water mass per area with the terahertz transmission peak field ratio, generalizing across leaves within and across three species. Each species' measurement points, regression line, and ordinary least squares R^2 values are presented: *Arabidopsis thaliana*, purple; *Hedera canariensis*, blue; *Platanus racemosa*, yellow; all species together, black. Statistical significance: *, $p < .05$; **, $p < .01$; ***, $p < .001$

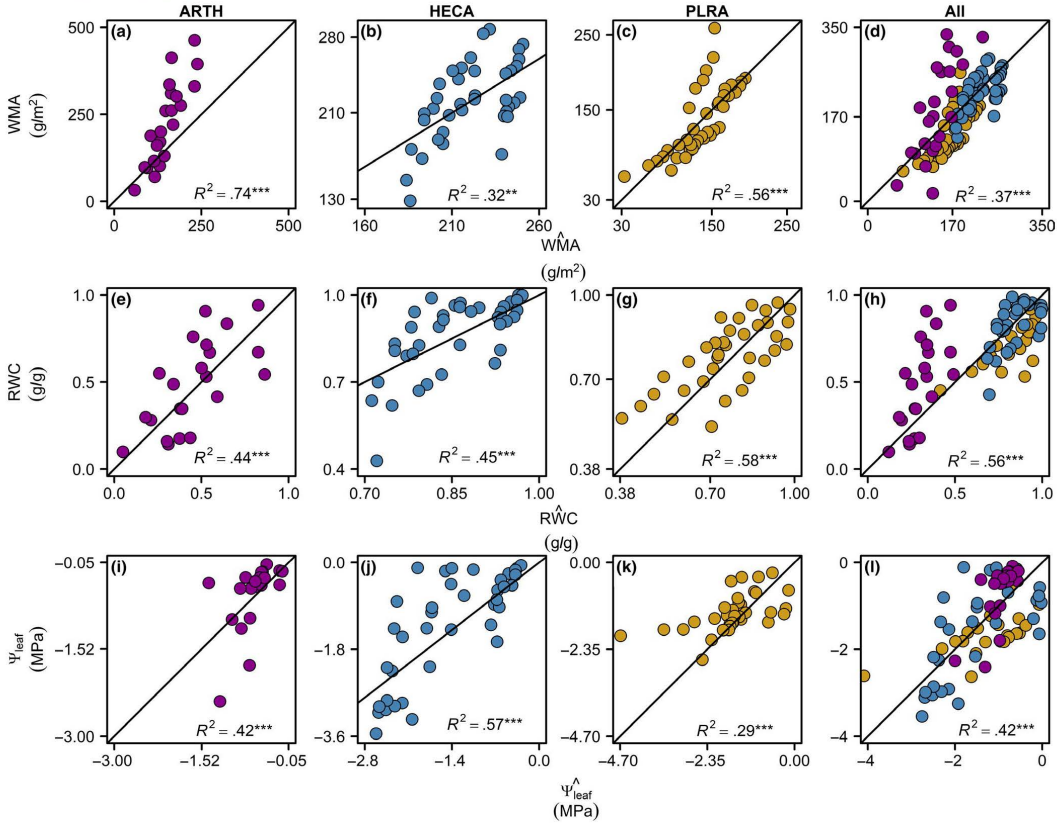

FIGURE 8 Species-specific predictions of leaf water status using terahertz spectroscopy. Plots of observed values against predicted values for leaf water mass per area (WMA), relative water content (RWC), and leaf water potential (Ψ_{leaf}). Species-level and all-species-level WMA were predicted for each measurement of PFR using species-specific and all species regression parameters, respectively (Table S2). Statistical significance: not significant, ns; **, $p < .01$; ***, $p < .001$

and the relationships across species. Indeed, due to this variation among leaves in their relationships, a number of impossible values were predicted for RWC and Ψ_{leaf} from the generalized relationships of WMA to ln (PFR) (see Methods, "*Statistics*"; Table S2). The variation in slopes indicates the potential for improving the physically based model. In the current formulation, the slopes of WMA versus ln (PFR) should simply represent the absorption coefficient of liquid water, expected to be constant. At least five effects might lead to variation in slopes. First, we did not account for the shrinkage of leaves during dehydration (Scoffoni et al., 2014), and such correction would likely slightly improve predictions. Second, we assumed that liquid water absorbs radiation as a single uniform layer, but it is unclear whether cellular structure would influence the effective absorption of water, especially given airspace shrinkage or expansion during dehydration. Third, in Equation 9 we assumed that the absorption of the "solid fraction" (i.e., absorption coefficient × thickness of solid fraction) was invariant with leaf dehydration, and, in applying Equation 11 across multiple leaves of given species and across leaves of different species, that this absorption is equivalent across leaves. This assumption would be moot if the solid fraction absorbs minimally, and, indeed, our tests have shown negligible absorption in completely dried leaves (data not shown). However, the absorption of pigments and other molecules may depend on leaf hydration state, as previous studies found that in hydrated leaves the chlorophyll and carotenoids also absorb substantially within the terahertz range of wavelengths (Qu, Zhang, Lian, & Kuang, 2017), and this absorption by pigments or other biomolecules or tissues (such as cuticle or leaf venation) could account for variation in relationships among leaves (Cotrozzi et al., 2017; Ollinger, 2011; Sims & Gamon, 2002), especially if it changes with leaf water status. Fourth, in generalizing Equation 11 we assumed that the reflectivity of the leaf (R) was constant. Previous work has shown comparatively minimal variation in reflectivity during leaf dehydration (Hadjiloucas et al., 1999; Sun et al., 2011), but no tests have been made comparing R for terahertz wavelengths among leaves of given species or across

American Society of Plant Biologists — SEB — WILEY

TABLE 5 Predictive power for the determination of water mass per area (WMA), relative water content (RWC), and leaf water potential (Ψ_{leaf}), from terahertz spectroscopy, including the root mean square error (RMSE), the R^2, and the normalized RMSE (NRMSE), for individual leaves of each species (with minimum, mean [bold type], and maximum values reported), and using species-specific relationships, and the all-species relationship (Table 4; Figure 8)

Species code	Variable	RMSE (min-mean-max)	R^2 (min-mean-max)	NRMSE (min-mean-max)
Individual leaf-level prediction				
Arabidopsis thaliana	WMA	8.43–**28.0**–48.2	0.80–**0.89**–0.99	0.347–**0.0942**–0.123
	RWC	0.0254–**0.0597**–0.0981	0.80–**0.89**–0.99	0.0344–**0.0940**–0.123
	Ψ_{leaf}	0.0223–**0.200**–0.371	0.49–**0.76**–0.92	0.0762–**0.130**–0.235
Hedera canariensis	WMA	1.55–**7.57**–15.0	0.80–**0.80**–0.80	0.0199–**0.104**–0.193
	RWC	0.00670–**0.0284**–0.0553	0.80–**0.80**–0.80	0.0199–**0.101**–0.185
	Ψ_{leaf}	0.174–**0.256**–0.339	0.70–**0.70**–0.70	0.0665–**0.112**–0.170
Platanus racemosa	WMA	1.67–**4.71**–11.4	0.80–**0.80**–0.80	0.0410–**0.0828**–0.173
	RWC	0.0122–**0.0246**–0.0398	0.80–**0.80**–0.80	0.0411–**0.0829**–0.173
	Ψ_{leaf}	0.0680–**0.170**–0.225	0.70–**0.70**–0.70	0.0305–**0.115**–0.176
Species-level prediction				
Arabidopsis thaliana	WMA	58.7	0.74	0.136
	RWC	0.184	0.44	0.218
	Ψ_{leaf}	0.487	0.42	0.209
Hedera canariensis	WMA	28.9	0.32	0.182
	RWC	0.0935	0.45	0.164
	Ψ_{leaf}	0.703	0.57	0.202
Platanus racemosa	WMA	29.8	0.56	0.151
	RWC	0.0841	0.58	0.159
	Ψ_{leaf}	0.425	0.29	0.175
All-species-level prediction				
All species	WMA	61.6	0.37	0.138
All species	RWC	0.151	0.56	0.159
All species	Ψ_{leaf}	0.700	0.42	0.201

species. Thus, future work to clarify terahertz absorption in relation to variation in leaf structure and composition is ongoing in our laboratory and others (e.g., Born et al., 2014; Gente et al., 2018). Further technical improvements in the terahertz radiation technology might also increase precision, especially in the improvement of alignment of the terahertz beam spot on the leaf during measurements at different dehydration stages.

The ability to measure leaf water status nondestructively will engender numerous applications. Notably, the THz-TDS system we used is a table-top system containing large optical components in a laboratory setting. While such a system can be deployed in the field (Gente et al., 2018), the development of compact field-ready systems have enormous potential, for example, as handheld devices or drone-mounted instruments, for greenhouse and agricultural analyses, as have been developed for other applications in terahertz spectrometry such as tissue and chemical analyses (Humphreys et al., 2004; Sun et al., 2011). Under field settings, a system incorporating terahertz reflection measurements will be even more applicable to remote determination of leaf water status, for example, pinpointing when natural or crop canopies are approaching dangerous levels of drought, and enabling "need-based" irrigation systems within crops and urban ecosystems for efficient water application (Jepsen, Cooke, & Koch, 2011). Recently, vegetation optical depth (VOD) as derived from microwave reflectance determined from airborne platforms has been used to estimate landscape-scale relative water content or leaf area index (Momen et al., 2017; Rao et al., 2019). Given its ability to resolve Ψ_{leaf} across the leaf operating range, the application of terahertz spectroscopy in reflection mode would complement and enhance those remote sensing applications. Beyond the estimation of leaf water status, measurement of Ψ_{leaf} in addition to water flux rates enables the determination of hydraulic conductance, that is, the efficiency of water transport. If Ψ_{leaf} can be estimated nondestructively for leaves at predawn (as a proxy for soil water potential; Rao et al., 2019) and at mid-day, alongside transpiration rates using gas exchange, thermal imagery, or sapflow systems (Lu & Zhuang, 2010), nondestructive measurements can be made of whole-plant hydraulic conductance, enabling insights to address numerous unknowns and controversies in the field, for example, the strength of drought at which hydraulic decline occurs at plant scale (Delzon & Cochard,

2014). The opportunities that terahertz spectroscopy offers thus extend from the resolution of drought impacts and the design of systems for their mitigation, to the remote resolution of the dynamics of plant transport capacity.

ACKNOWLEDGMENTS

We are grateful to A. Baird, C. Medeiros, and J. Zailaa for discussion. This work was supported by the U.S. National Science Foundation (IOS-145727; and NRT-INFEWS: DGE-1735325), the California NanoSystems Institute, and the UCLA Sustainable LA Grand Challenge and the Anthony and Jeanne Pritzker Family Foundation.

CONFLICT OF INTEREST

The authors declare no conflict of interest associated with the work described in this manuscript.

AUTHOR CONTRIBUTIONS

All authors contributed to the design of the study. M.B., N.T.Y., and C.S. conducted data collection and analyses. M.B., N.T.Y., M.J., and L.S. wrote the manuscript with input from all authors.

REFERENCES

Allen, C. D., Macalady, A. K., Chenchouni, H., Bachelet, D., McDowell, N., Vennetier, M., … Cobb, N. (2010). A global overview of drought and heat-induced tree mortality reveals emerging climate change risks for forests. *Forest Ecology and Management*, *259*, 660–684. https://doi.org/10.1016/j.foreco.2009.09.001

Asner, G. P., Brodrick, P. G., Anderson, C. B., Vaughn, N., Knapp, D. E., & Martin, R. E. (2016). Progressive forest canopy water loss during the 2012–2015 California drought. *Proceedings of the National Academy of Sciences*, *113*, E249–E255. https://doi.org/10.1073/pnas.1523397113

Baldacci, L., Pagano, M., Masini, L., Toncelli, A., Carelli, G., Storchi, P., & Tredicucci, A. (2017). Non-invasive absolute measurement of leaf water content using terahertz quantum cascade lasers. *Plant Methods*, *13*(1), https://doi.org/10.1186/s13007-017-0197-z.

Bartlett, M. K., Klein, T., Jansen, S., Choat, B., & Sack, L. (2016). The correlations and sequence of plant stomatal, hydraulic, and wilting responses to drought. *Proceedings of the National Academy of Sciences*, *113*, 13098–13103. https://doi.org/10.1073/pnas.1604088113

Bartlett, M. K., Scoffoni, C., & Sack, L. (2012). The determinants of leaf turgor loss point and prediction of drought tolerance of species and biomes: A global meta-analysis: Drivers of plant drought tolerance. *Ecology Letters*, *15*, 393–405. https://doi.org/10.1111/j.1461-0248.2012.01751.x

Born, N., Behringer, D., Liepelt, S., Beyer, S., Schwerdtfeger, M., Ziegenhagen, B., & Koch, M. (2014). Monitoring plant drought stress response using terahertz time-domain spectroscopy. *Plant Physiology*, *164*, 1571–1577. https://doi.org/10.1104/pp.113.233601

Botchkarev, A. (2018) Performance metrics (error measures) in machine learning regression, forecasting and prognostics: properties and typology. arXiv preprint arXiv:1809.03006.

Castro-Camus, E., Palomar, M., & Covarrubias, A. A. (2013). Leaf water dynamics of *Arabidopsis thaliana* monitored in-vivo using terahertz time-domain spectroscopy. *Scientific Reports*, *3*. https://doi.org/10.1038/srep02910

Claudio, H., Cheng, Y., Fuentes, D., Gamon, J., Luo, H., Oechel, W., … Sims, D. (2006). Monitoring drought effects on vegetation water content and fluxes in chaparral with the 970 nm water band index. *Remote Sensing of Environment*, *103*, 304–311.

Cotrozzi, L., Couture, J. J., Cavender-Bares, J., Kingdon, C. C., Fallon, B., Pilz, G., … Townsend, P. A. (2017). Using foliar spectral properties to assess the effects of drought on plant water potential. *Tree Physiology*, *37*, 1582–1591. https://doi.org/10.1093/treephys/tpx106

Danson, F. M., Steven, M. D., Malthus, T. J., & Clark, J. A. (1992). High-spectral resolution data for determining leaf water content. *International Journal of Remote Sensing*, *13*, 461–470. https://doi.org/10.1080/01431169208904049

Delzon, S., & Cochard, H. (2014). Recent advances in tree hydraulics highlight the ecological significance of the hydraulic safety margin. *New Phytologist*, *203*, 355–358. https://doi.org/10.1111/nph.12798

Gente, R., Born, N., Voß, N., Sannemann, W., Léon, J., Koch, M., & Castro-Camus, E. (2013). Determination of leaf water content from terahertz time-domain spectroscopic data. *Journal of Infrared, Millimeter, and Terahertz Waves*, *34*, 316–323. https://doi.org/10.1007/s10762-013-9972-8

Gente, R., Rehn, A., & Koch, M. (2015). Contactless water measurements on plants at 35 GHz. *Journal of Infrared, Millimeter, and Terahertz Waves*, *36*, 312–317.

Gente, R., Rehn, A., Probst, T., Stübling, E.-M., Camus, E. C., Covarrubias, A. A., … Koch, M. (2018). Outdoor measurements of leaf water content using THz quasi time-domain spectroscopy. *Journal of Infrared, Millimeter, and Terahertz Waves*, *39*, 943–948. https://doi.org/10.1007/s10762-018-0520-4

Hadjiloucas, S., Karatzas, L. S., & Bowen, J. W. (1999). Measurements of leaf water content using terahertz radiation. *IEEE Transactions on Microwave Theory and Techniques*, *47*, 142–149. https://doi.org/10.1109/22.744288

Hecht, E. (2002). *Optics*. Reading, Mass: Addison-Wesley.

Hu, B. B., & Nuss, M. C. (1995). Imaging with terahertz waves. *Optics Letters*, *20*, 1716–1718. https://doi.org/10.1364/OL.20.001716

Humphreys, K., Loughran, J. P., Gradziel, M., Lanigan, W., Ward, T., Murphy, J. A., & O'Sullivan,C. (2004) Medical applications of terahertz imaging: a review of current technology and potential applications in biomedical engineering. In The 26th Annual International Conference of the IEEE Engineering in Medicine and Biology Society, Vol 1, pp 1302–1305.

Hunt, E., & Rock, B. (1989). Detection of changes in leaf water content using near-and middle-Infrared reflectances. *Remote Sensing of Environment*, *30*, 43–54. https://doi.org/10.1016/0034-4257(89)90046-1

Hunt, E. R., Rock, B. N., & Nobel, P. S. (1987). Measurement of leaf relative water content by infrared reflectance. *Remote Sensing of Environment*, *22*, 429–435. https://doi.org/10.1016/0034-4257(87)90094-0

IPCC (2014) Climate change 2014: synthesis report. Contribution of working groups I, II and III to the fifth assessment report of the intergovernmental panel on climate change, Ed 5. IPCC, Geneva, Switzerland.

Jepsen, P. U., Cooke, D. G., & Koch, M. (2011). Terahertz spectroscopy and imaging : Modern techniques and applications. *Laser & Photonics Reviews*, *5*, 124–166. https://doi.org/10.1002/lpor.201000011

Jones, H. G. (2014). *Plants and Microclimate*, 3rd ed. Cambridge, UK: Cambridge University Press.

Jördens, C., Scheller, M., Breitenstein, B., Selmar, D., & Koch, M. (2009). Evaluation of leaf water status by means of permittivity at terahertz frequencies. *Journal of Biological Physics*, *35*, 255–264. https://doi.org/10.1007/s10867-009-9161-0

Kindt, J. T., & Schmuttenmaer, C. A. (1996). Far-infrared dielectric properties of polar liquids probed by femtosecond terahertz pulse spectroscopy. *The Journal of Physical Chemistry*, *24*, 10373–10379.

Knipling, E. B. (1970). Physical and physiological basis for the reflectance of visible and near-infrared radiation from vegetation. *Remote Sensing of Environment*, *1*, 155–159. https://doi.org/10.1016/S0034-4257(70)80021-9

Kubiske, M. E., & Abrams, M. D. (1990). Pressure-volume relationships in non-rehydrated tissue at various water deficits. *Plant, Cell & Environment*, *13*, 995–1000. https://doi.org/10.1111/j.1365-3040.1990.tb01992.x

Li, B., Long, Y., & Yang, H. (2018). Measurements and analysis of water content in winter wheat leaf based on terahertz spectroscopy. *International Journal of Agricultural and Biological Engineering*, *11*, 178–182. https://doi.org/10.25165/j.ijabe.20181103.3520

Lu, X., & Zhuang, Q. (2010). Evaluating evapotranspiration and water-use efficiency of terrestrial ecosystems in the conterminous United States using MODIS and AmeriFlux data. *Remote Sensing of Environment*, *114*, 1924–1939. https://doi.org/10.1016/j.rse.2010.04.001

Mittleman, D. M., Jacobsen, R. H., Neelamani, R., Baraniuk, R. G., & Nuss, M. C. (1998). Gas sensing using terahertz time-domain spectroscopy. *Applied Physics B*, *67*, 379–390. https://doi.org/10.1007/s003400050520

Mittleman, D. M., Jacobsen, R. H., & Nuss, M. C. (1996). T-ray imaging. *IEEE Journal of Selected Topics in Quantum Electronics*, *2*, 679–692. https://doi.org/10.1109/2944.571768

Momen, M., Wood, J. D., Novick, K. A., Pangle, R., Pockman, W. T., McDowell, N. G., & Konings, A. G. (2017). Interacting effects of leaf water potential and biomass on vegetation optical depth: Effects of LWP and biomass on VOD. *Journal of Geophysical Research: Biogeosciences*, *122*, 3031–3046. https://doi.org/10.1002/2017JG004145

Ollinger, S. V. (2011). Sources of variability in canopy reflectance and the convergent properties of plants: Tansley review. *New Phytologist*, *189*, 375–394. https://doi.org/10.1111/j.1469-8137.2010.03536.x

Peñuelas, J., Filella, I., Biel, C., Serrano, L., & Savé, R. (1993). The reflectance at the 950–970 nm region as an indicator of plant water status. *International Journal of Remote Sensing*, *14*, 1887–1905. https://doi.org/10.1080/01431169308954010

Peñuelas, J., & Inoue, Y. (1999). Reflectance indices indicative of changes in water and pigment contents of peanut and wheat leaves. *Photosynthetica*, *36*, 355–360.

Qu, Y., Zhang, S., Lian, Y., & Kuang, T. (2017). Function of terahertz spectra in monitoring the decomposing process of biological macromolecules and in investigating the causes of photoinhibition. *Science China Life Sciences*, *60*, 307–312. https://doi.org/10.1007/s11427-016-0057-9

R Core Team (2019). *R: A language and environment for statistical computing*. Ed 3.6.1. Vienna, Austria: R Foundation for Statistical Computing.

Rao, K., Anderegg, W. R. L., Sala, A., Martínez-Vilalta, J., & Konings, A. G. (2019). Satellite-based vegetation optical depth as an indicator of drought-driven tree mortality. *Remote Sensing of Environment*, *227*, 125–136. https://doi.org/10.1016/j.rse.2019.03.026

Rapaport, T., Hochberg, U., Cochavi, A., Karnieli, A., & Rachmilevitch, S. (2017). The potential of the spectral 'water balance index' (WABI) for crop irrigation scheduling. *New Phytologist*, *216*, 741–757. https://doi.org/10.1111/nph.14718

Rapaport, T., Hochberg, U., Shoshany, M., Karnieli, A., & Rachmilevitch, S. (2015). Combining leaf physiology, hyperspectral imaging and partial least squares-regression (PLS-R) for grapevine water status assessment. *ISPRS Journal of Photogrammetry and Remote Sensing*, *109*, 88–97. https://doi.org/10.1016/j.isprsjprs.2015.09.003

Riazoshams, H., Midi, H., & Ghilagaber, G. (2019). *Robust Nonlinear Regression*. Hoboken, NJ, USA: Wiley.

Rønne, C., Åstrand, P.-O., & Keiding, S. R. (1999). THz spectroscopy of liquid H_2O and D_2O. *Physical Review Letters*, *82*, 2888–2891.

Sack, L., John, G. P., & Buckley, T. N. (2018). ABA accumulation in dehydrating leaves is associated with decline in cell volume, not turgor pressure. *Plant Physiology*, *176*, 489–495. https://doi.org/10.1104/pp.17.01097

Sack, L., & Pasquet-kok, J. (2011) Leaf pressure-volume curve parameters. PromethusWiki.

Sancho-Knapik, D., Gismero, J., Asensio, A., Peguero-Pina, J. J., Fernández, V., Álvarez-Arenas, T. G., & Gil-Pelegrín, E. (2011). Microwave I-band (1730MHz) accurately estimates the relative water content in poplar leaves. A comparison with a near infrared water index (R1300/R1450). *Agricultural and Forest Meteorology*, *151*, 827–832. https://doi.org/10.1016/j.agrformet.2011.01.016

Santesteban, L. G., Palacios, I., Miranda, C., Iriarte, J. C., Royo, J., & Gonzalo, R. (2015). Terahertz time domain spectroscopy allows contactless monitoring of grapevine water status. Frontiers. *Plant Science*, *6*. https://doi.org/10.3389/fpls.2015.00404

Schindelin, J., Arganda-Carreras, I., Frise, E., Kaynig, V., Longair, M., Pietzsch, T., … Cardona, A. (2012). Fiji: An open-source platform for biological-image analysis. *Nature Methods*, *9*, 676. https://doi.org/10.1038/nmeth.2019

Scoffoni, C., Albuquerque, C., Cochard, H., Buckley, T. N., Fletcher, L. R., Caringella, M. A., … Sack, L. (2018). The causes of leaf hydraulic vulnerability and its influence on gas exchange in *Arabidopsis thaliana*. *Plant Physiology*, *178*, 1584–1601.

Scoffoni, C., McKown, A. D., Rawls, M., & Sack, L. (2012). Dynamics of leaf hydraulic conductance with water status: Quantification and analysis of species differences under steady state. *Journal of Experimental Botany*, *63*, 643–658. https://doi.org/10.1093/jxb/err270

Scoffoni, C., Vuong, C., Diep, S., Cochard, H., & Sack, L. (2014). Leaf shrinkage with dehydration: Coordination with hydraulic vulnerability and drought tolerance. *Plant Physiology*, *164*, 1772–1788. https://doi.org/10.1104/pp.113.221424

Sims, D. A., & Gamon, J. A. (2002). Relationships between leaf pigment content and spectral reflectance across a wide range of species, leaf structures and developmental stages. *Remote Sensing of Environment*, *81*, 337–354. https://doi.org/10.1016/S0034-4257(02)00010-X

Skoog, D. A., Holler, F. J., & Crouch, S. R. (2017). *Principles of instrumental analysis*. Cengage learning.

Sokal, R. R., & Rohlf, F. J. (1995). *Biometry: the principles and practice of statistics in biological research*, 3rd ed. New York, NY: W. H. Freeman & Co.

Sun, Y., Sy, M. Y., Wang, Y.-X.- J., Ahuja, A. T., Zhang, Y.-T., & Pickwell-Macpherson, E. (2011). A promising diagnostic method: Terahertz pulsed imaging and spectroscopy. *World Journal of Radiology*, *3*, 55–65. https://doi.org/10.4329/wjr.v3.i3.55

Thrane, L., Jacobsen, R. H., Uhd Jepsen, P., & Keiding, S. R. (1995). THz reflection spectroscopy of liquid water. *Chemical Physics Letters*, *240*, 330–333. https://doi.org/10.1016/0009-2614(95)00543-D

Trueba, S., Pan, R., Scoffoni, C., John, G. P., Davis, S. D., & Sack, L. (2019). Thresholds for leaf damage due to dehydration: Declines of hydraulic function, stomatal conductance and cellular integrity precede those for photochemistry. *New Phytologist*, *223*(1), 134–149. https://doi.org/10.1111/nph.15779

Tucker, C. J. (1980). Remote sensing of leaf water content in the near infrared. *Remote Sensing of Environment*, *10*, 23–32. https://doi.org/10.1016/0034-4257(80)90096-6

Warton, D. I., Wright, I. J., Falster, D. S., & Westoby, M. (2006). Bivariate line-fitting methods for allometry. *Biological Reviews*, *81*, 259–291.

Yang, Y., Shutler, A., & Grischkowsky, D. (2011). Measurement of the transmission of the atmosphere from 0.2 to 2 THz. *Optics Express*, *19*, 8830–8838.

Yardimci, N. T., Cakmakyapan, S., Hemmati, S., & Jarrahi, M. (2017). A high-power broadband terahertz source enabled by three-dimensional light confinement in a plasmonic nanocavity. *Scientific Reports*, *7*, 4166. https://doi.org/10.1038/s41598-017-04553-4

Yardimci, N. T., & Jarrahi, M. (2017). High sensitivity terahertz detection through large-area plasmonic nano-antenna arrays. *Scientific Reports*, *7*, 42667. https://doi.org/10.1038/srep42667

Yardimci, N. T., Yang, S. H., Berry, C. W., & Jarrahi, M. (2015). High-power terahertz generation using large-area plasmonic photoconductive emitters. *IEEE Transactions on Terahertz Science and Technology*, *5*, 223–229. https://doi.org/10.1109/TTHZ.2015.2395417

SUPPORTING INFORMATION

Additional supporting information may be found online in the Supporting Information section.

How to cite this article: Browne M, Yardimci NT, Scoffoni C, Jarrahi M, Sack L. Prediction of leaf water potential and relative water content using terahertz radiation spectroscopy. *Plant Direct*. 2020;4:1–16. https://doi.org/10.1002/pld3.197

Supplementary Materials

Supplementary Data Captions (see attached Excel Workbook)

Table S2.1. Previous studies assessing leaf water status using electromagnetic radiation, presenting species; organ and scale tested; wavelengths used; index of water status and range tested, with goodness of fit of correlation of water status with spectroscopy variable; and method to establish the relationship between spectroscopy variables and leaf water status. Relative water content values (RWC) are noted as percentages, leaf water potential in -MPa, and water mass per area (WMA) in grams per meter squared unless otherwise noted. When individual species' water status variable ranges were not reported, either the maximum value (extracted from tables) or a range across all species studied is presented. Canopy-scale indicates that measurements were made across many leaves of the same individuals at once.

Table S2.2. Terahertz spectroscopy variables, leaf traits and model estimates for the prediction of leaf water status from terahertz spectroscopy (see variable key below rows of data). Data are presented for each dehydration stage for each tested leaf of each of the three study species. Measured values are presented for peak field ratio (PFR), ln-transformed values, and leaf water potential (Ψ_{leaf}); leaf-specific values of lamina dry mass, leaf area, leaf mass per area (LMA); saturated water mass (SWM), saturated water content (SWC), water mass per area (WMA) and saturated water mass per area (SWMA). Estimation of leaf water status variables were made for individual leaves, and combining leaves of all species, and across species (Table 2.5, Figure 2.6

and 2.7). Values highlighted in brown are impossible values estimated from the fitted relationships (see Methods)

Chapter 3: Low baseline intraspecific variation in leaf pressure-volume traits: Biophysical basis and implications for spectroscopic sensing

Received: 18 April 2023 | Revised: 23 June 2023 | Accepted: 2 July 2023

DOI: 10.1111/ppl.13974

ORIGINAL RESEARCH

Physiologia Plantarum

Low baseline intraspecific variation in leaf pressure-volume traits: Biophysical basis and implications for spectroscopic sensing

Marvin Browne[1] | Megan K. Bartlett[2] | Christian Henry[1] | Mona Jarrahi[3] | Grace John[4] | Christine Scoffoni[5] | Nezih Tolga Yardimci[3] | Lawren Sack[1]

[1]Department of Ecology and Evolutionary Biology, University of California Los Angeles, Los Angeles, California, USA

[2]Department of Viticulture and Enology, University of California, Davis, California, USA

[3]Department of Electrical and Computer Engineering, University of California Los Angeles, Los Angeles, California, USA

[4]Department of Biology, University of Florida, Gainesville, Florida, USA

[5]Department of Biological Sciences, California State University, California, Los Angeles, USA

Correspondence
Marvin Browne, Department of Ecology and Evolutionary Biology, University of California Los Angeles, 621 Charles E. Young Drive South, Los Angeles, CA 90095, USA.
Email: mgbrowne@ucla.edu

Funding information
Anthony and Jeanne Pritzker Family Foundation; National Science Foundation, Grant/Award Numbers: 1735325, 1951244, 2017949

Edited by J.M. Torres-Ruiz

Abstract

Intra-specific trait variation (ITV) plays a role in processes at a wide range of scales from organs to ecosystems across climate gradients. Yet, ITV remains rarely quantified for many ecophysiological traits typically assessed for species means, such as pressure volume (PV) curve parameters including osmotic potential at full turgor and modulus of elasticity, which are important in plant water relations. We defined a baseline "reference ITV" (ITV_{ref}) as the variation among fully exposed, mature sun leaves of replicate individuals of a given species grown in similar, well-watered conditions, representing the conservative sampling design commonly used for species-level ecophysiological traits. We hypothesized that PV parameters would show low ITV_{ref} relative to other leaf morphological traits, and that their intraspecific relationships would be similar to those previously established across species and proposed to arise from biophysical constraints. In a database of novel and published PV curves and additional leaf structural traits for 50 diverse species, we found low ITV_{ref} for PV parameters relative to other morphological traits, and strong intraspecific relationships among PV traits. Simulation modeling showed that conservative ITV_{ref} enables the use of species-mean PV parameters for scaling up from spectroscopic measurements of leaf water content to enable sensing of leaf water potential.

1 | INTRODUCTION

Functional traits are widely used to discern and explain patterns and processes across scales from organ and species-level physiology to ecosystem function (Albert et al., 2011; Bartlett et al., 2014; Medeiros et al., 2019; Violle et al., 2007). Plant-water relations traits are critical for determining species' responses across aridity gradients, including, for example, pressure-volume (PV) curve traits estimated from the relationship between water potential and relative water content: turgor loss (wilting) point (π_{tlp}), osmotic potential at full turgor (π_o), modulus of elasticity (ε), relative water content at turgor loss point (RWC_{tlp}) and capacitances at full turgor (C_{ft}) and at turgor loss (C_{tlp}; see Table 1 for terms, symbols, and definitions; Bartlett et al., 2016; Bartlett, Scoffoni, & Sack, 2012; Brodribb et al., 2020; de Bello et al., 2011; Rosas et al., 2019; Sack & Pasquet-Kok, 2011). Species mean values for these traits are becoming increasingly available (Kattge et al., 2020), yet there has been little consideration of intraspecific trait variation (ITV) in most PV parameters. PV parameters influence drought responses: π_{tlp} and RWC_{tlp} correspond closely on average to the threshold for stomatal closure during dehydration (Henry et al., 2019; Trueba et al., 2019) and that for incipient cell damage (John et al., 2018); the ε and π_o are underlying cellular traits quantifying wall stiffness and osmotic concentration; and C_{ft} and C_{tlp} are water storage parameters (Bartlett, Scoffoni, & Sack, 2012). Further, PV parameters can be applied to the prediction of leaf water status based on electromagnetic radiation, an increasingly popular approach (Cotrozzi et al., 2017; Rapaport et al., 2017; Sapes et al., 2022; reviewed in Browne et al., 2020 Table S1). Thus,

TABLE 1 Leaf water status, structural composition and pressure-volume curve parameter symbols, units, and definitions.

Variable	Symbol	Unit	Definitions
Leaf water status			
Leaf water potential	Ψ_{leaf}	MPa	Water status variable indicating the bulk leaf average chemical potential of water within leaf cells
Osmotic potential	Ψ_S	MPa	Component of leaf water potential relating to the concentration of cell solutes
Pressure potential	Ψ_P	MPa	Turgor pressure against the cell walls
Relative water content	RWC	$g \cdot g^{-1}$	Water status index, the ratio of the mass of water in the leaf to that in the saturated leaf
Water mass per area	WMA	$g \cdot m^{-2}$	Water status index, the ratio of the mass of water in the leaf to the leaf area, also known as the "equivalent water thickness"
Structural composition			
Saturated water content	SWC	$g \cdot g^{-1}$	Mass of water in fully saturated leaves relative to dry mass
Leaf thickness	LT	cm	Thickness of leaf lamina
Leaf mass per area	LMA	$g \cdot m^{-2}$	Ratio of mass of dry leaf lamina to leaf area
Saturated water mass per area	SWMA	$g \cdot m^{-2}$	Mass of water in fully saturated leaves relative to leaf area; equivalent to the product of leaf mass per area and saturated water content
Leaf dry matter content	LDMC	$mg \cdot g^{-1}$	Ratio of dry mass to leaf fresh mass at full saturation
Leaf density	ρ_{leaf}	$g \cdot cm^{-3}$	Leaf dry mass per saturated volume; equivalent to the quotient of LMA and leaf thickness
Pressure-volume curve parameters (symplastic basis denoted by an "s" in the subscript)			
Water potential at turgor loss point	π_{tlp}	MPa	Bulk chemical potential of water within leaf cells at "wilting point", equivalent to the solute potential of cells at the point of turgor loss
Osmotic potential at full turgor	π_o	MPa	Bulk component of water potential relating to the solute concentration in cells (Ψ_S) at full turgor (i.e., at saturation)
Modulus of elasticity	ε; ε_s	MPa	Bulk stiffness of leaf cell walls as quantified by slope of the relationship between Ψ_P and relative water content above Ψ_{tlp}
Relative water content at turgor loss point	RWC_{tlp}; $RWC_{tlp,s}$	$g \cdot g^{-1}$	Leaf hydration at which cells lose turgor
Capacitance at full turgor, relative	C_{ft}; $C_{ft,s}$	MPa^{-1}	Relative water storage capacity at full turgor
Capacitance at Ψ_{tlp}, relative	C_{tlp}; $C_{tlp,s}$	MPa^{-1}	Relative water storage capacity for leaves dehydrated beyond turgor loss point
Absolute capacitance at full turgor	$C_{ft,abs}$	$mol\ m^{-2}\ MPa^{-1}$	Symplastic absolute water mass capacitance at full turgor normalized by leaf area
Apoplastic fraction	a_f	unitless	Extracellular fraction of water content. This is equivalent to $g^* g^{-1}$.
Terahertz spectroscopy			
Terahertz time-domain spectroscopy	THz-TDS	–	System of generating and detecting terahertz wavelength pulses interacting with a sample
Peak field ratio	PFR	$dBs \cdot dBs^{-1}$	Ratio of transmitted radiation through sample to radiation transmitted through an empty system

Note: Empirically estimated parameters are presented with hats within the text.

measurements of water mass per unit leaf area (WMA) derived from spectroscopy can be scaled up to Ψ_{leaf}, based on inputs of species mean π_o, ε, π_{tlp}, RWC_{tlp} and saturated water mass per area (the product of leaf mass per area and saturated water content; Figure 1). The aim of this study is to consider the ITV and inter-relationships of PV parameters at the scale of most measurements in the literature, and its importance for upscaling for the spectroscopic estimation of leaf water potential.

Quantifying ITV is crucial to effectively predict many population, community, and ecosystem-scale processes (Kraft et al., 2014). Theory holds that ITV especially benefits resource capture under patchy spatial and temporal availability (Bolnick et al., 2011; Funk, 2008; Nicotra et al., 2010). Yet, ITV can be a "fuzzy" concept: its definition and functional importance depend on scale and environmental conditions (synthesized in Table 2; Albert et al., 2010; Dawson et al., 2021; Reich et al., 2003). Thus, ITV can be assessed within or among co-existing individuals of a species or among populations and may reflect genetic variation and phenotypic plasticity, arising from ontogeny and environmental differences, including climate, soil and/or microclimate. Indeed, ITV can arise even among adjacent leaves on a given plant

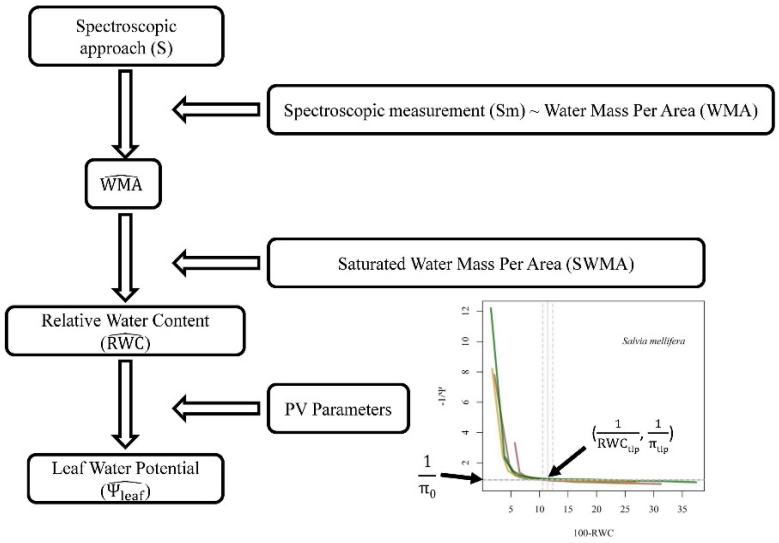

FIGURE 1 Diagram of inputs used to predict of leaf water status variables from spectroscopy-based measurements and leaf traits from spectroscopy approaches (S) (extended from Browne et al. (2020)). Energy transmitted from leaf tissue is indicative of the tissue "equivalent water thickness" or water mass per area (WMA). A function relating WMA to the spectroscopic measurement (Sm) across leaves varying in hydration state enables prediction of WMA. Relative water content (RWC) is then estimated by including the saturated water mass per area (i.e., the product of leaf mass per area and saturated water content). Last, leaf water potential is determined using species-mean pressure-volume (PV) curve parameters.

TABLE 2 Intraspecific variation can arise from multiple sources and across multiple temporal, spatial and conceptual scales, each reflecting multiple underlying processes. Traits vary among individuals of the same species due to three sources, that is, genomic variation, developmental and ontogenetic variation, and environmental variation, and can vary within an individual, across individuals of a community, and across populations, with examples provided for each; as noted, typically, the sources and scales cannot be fully disentangled.

	Scales		
Source	Within a canopy	Across individuals of a given ecotype	Across populations/ecotypes
Genomic variation	Among leaves of different heights in a tree, separated by long mitotic history (e.g., within long-lived trees such as oaks (Plomion et al., 2018, Scholes & Paige, 2015)	Among individuals of annual plant species from a given community (Fridley & Grime, 2010)	Across ecotypes of *Arabidopsis thaliana* grown in a common garden (Sartori et al., 2019)
Developmental and ontogenetic variation	**Among sun leaves on a given tree branch (e.g., variation due to hydraulic sectoriality** (Orians et al., 2005)	Between trees of different ages in a community (Nicotra et al., 2010); also includes genomic variation	Between trees of different ages of different communities; also includes genomic variation, and possibly environmental variation
Environmental variation	Between sun and shade leaves (Niinemets et al., 2004, Sack et al., 2006)	Among individuals of a species in different microsites within a community (Williams et al., 2020); also includes genomic variation and possibly ontogenetic variation	Among individuals of different populations; also includes genomic variation and possibly ontogenetic variation

Note: The cell in **bold-face** represents the types of variation involved in the baseline, "reference" intraspecific trait variation (ITV_{ref}) considered in this study, that is, variation across individuals in "typical" sun leaves.

shoot, reflecting developmental plasticity arising from gene expression variation and subtle differences in microclimate (Table 2). In many contexts, ITV can account for important trait variation even relative to interspecific differences, most notably among sun and shade leaves (Albert et al., 2011; Baird et al., 2017; Delagrange et al., 2004; Givnish, 1988; Siefert et al., 2015; Valladares et al., 2000). One reason that many leaf-level ecophysiological traits have not been assessed for ITV is that the typical determination of species mean trait values

involves selecting "typical" sunlit, fully exposed and mature leaves sampled from replicate plants of given species, often growing in close proximity. This approach is justified to achieve accuracy and precision in the determination of species trait means for exposed leaves with the highest level of photosynthetic activity (e.g., Albert et al., 2011; González-Villagra et al., 2022; Jones & Turner, 1980; Novoplansky et al., 1989; Watson & Casper, 1984). Here, we defined a "reference" ITV (ITV_{ref}) at this scale of typical measurement, that is, representing the variation among sun leaves of replicate plants in similar growing conditions. The ITV_{ref} is expected to be low relative to other scales of ITV, such as comparison of sun versus shade leaves, or of populations across soil or climatic gradients (Rosas et al., 2019). Our intention in clarifying the ITV_{ref} of PV parameters is two-fold. First, the understanding of the relative variation of different traits provides key insights into mechanisms of adaptation, that is, indicating the constraints on traits and their correlations within and across environments. Second, the variation among sun leaves of given species in PV parameters has urgent implications for spectroscopic sensing of water potential that relies on species mean PV parameters.

We hypothesized conservative ITV_{ref} in PV parameters relative to other leaf traits. Notably, plants typically photosynthesize and grow within a narrow range of cell hydration, and PV parameters either directly represent thresholds below which functions decline and damage may occur (π_{tlp} and RWC_{tlp}), or contribute to the determination of these thresholds (π_o, ε, C_{ft}, C_{tlp}). Thus, PV curves for sun leaves of given species should be conservative to preserve hydration during short-term but often extreme changes in canopy microclimates. By contrast, other leaf traits related to light capture, such as leaf area, leaf mass per area, leaf thickness, leaf dry matter content, and leaf density, may be more variable as light conditions may vary greatly within a canopy to optimize irradiance capture, nitrogen allocation, and/or carbon gain relative to water loss. Indeed, our hypothesis for the conservative ITV of PV traits for sun leaves is analogous to theory at the whole plant scale considering ITV across spatial resource gradients. Thus, optimization hypotheses predict that organ level traits may show lower ITV than whole-plant traits, such as growth rate and water use efficiency, which relate to stronger environmental variation (Marks, 2007; Siefert et al., 2015; Zhou et al., 2022; but see Herrera, 2017). One study of species populations across an aridity gradient reported a conservative ITV for π_{tlp} (Rosas et al., 2019), that is, coefficient of variation of 15% relative to leaf mass per area, which had a value of 46% across that aridity gradient.

We also examined the trait–trait relationships among PV parameters and other leaf structural traits. Notably, trait–trait relationships observed across species may not hold within given species and vice versa (Messier et al., 2018; Rosas et al., 2019). Yet, theory developed across species proposed that PV parameters are intrinsically related, with "higher-level" traits π_{tlp}, RWC_{tlp}, and C_{ft} arising as biophysical functions of underlying traits: ε, π_o, and apoplastic fraction (a_f) (Bartlett, Scoffoni, & Sack, 2012). Thus, we hypothesized that relationships for replicate sun leaves of given species would follow the biophysical relationships established across species. Indeed, these strong relationships would provide an explanation for why certain PV parameters would be conservative; if π_{tlp} needs to be conservative to maintain hydration above a given threshold for leaf function, and π_{tlp} is biophysically determined by π_o and ε, then these parameters too would need to be conservative. Further, we tested whether, as expected from the inter-relationship of PV parameters, the variation in the PV parameters would be correlated across species, such that species with high ITV_{ref} in one trait would show high ITV_{ref} in other traits.

Finally, we tested whether ITV_{ref} in PV traits is typically sufficiently conservative such that species mean PV parameters can enable accuracy and precision in the spectroscopic estimation of Ψ_{leaf} from leaf water content, using as an example terahertz (THz) radiation (Figure 1; Table 1). Such sensing is an urgent priority for climate-forward irrigation system design and, potentially, for in-situ gas exchange systems that would estimate water potential simultaneously (Jepsen et al., 2011; Li et al., 2018; Lu & Zhuang, 2010).

Thus, overall, we hypothesized that ITV_{ref} of PV parameters would be lower than for other morphological traits, that PV parameters (and their variation) would show strong inter-relationships within species, and that the low ITV_{ref} for PV parameters would enable robust predictions of leaf water potential from spectroscopic data using species-mean parameters. To test these hypotheses, we compiled a database for ITV_{ref} of PV parameters for 50 species and additional leaf traits for 39 species based on new data and published studies (Bartlett, Scoffoni, Ardy, et al., 2012; John et al., 2018; Maréchaux et al., 2015; Pivovaroff et al., 2014; Scoffoni et al., 2011; Scoffoni et al., 2014).

2 | MATERIALS AND METHODS

2.1 | Data collection and compilation, and pressure volume curve construction

We constructed PV curves for 12 native California woody shrub species within six genera, selected for variation in native habitat (Table S1). Juveniles of each species were acquired in 1 L pots in April 2019 (Rancho Santa Ana Botanic Garden, Claremont, CA) and grown for 11 months to heights of 1–2.5 m in the Plant Growth Center at the University of California, Los Angeles (minimum, mean and maximum values for sunny days during a representative 2 week period between 1000 and 1400 h for temperature, 20.4°C, 22.0°C, 23.8°C; for relative humidity 30.1%, 35.6%, 43.1%; and for irradiance 64.2, 283, 1090 μmol photons m^{-2} s^{-1}). Leaf pressure volume curves were constructed in March–May 2020 using the bench drying method (Sack & Pasquet-Kok, 2011). Shoots with fully developed sun leaves from six individuals were harvested in the afternoon of the day prior to measurements and transported to the lab in dark plastic bags with wet paper towels. From each shoot, two nodes were recut under deionized water, and shoots were rehydrated overnight under plastic. Leaves were repeatedly weighted with an analytical balance (0.01 mg; MS205DU Mettler Toledo) and Ψ_{leaf} was determined using a pressure

chamber (0.001 MPa resolution, Plant Moisture Stress Model 1000; PMS Instruments Co). When "plateau effects" were detected during early dehydration, these measurements were excluded before estimation of pressure-volume parameters (Kubiske & Abrams, 1990). We constructed PV curves for one leaf from each of five to six individuals, except for *Clematis lasiantha*, for which we measured two leaves of each of three individuals due to limited availability.

Additionally, we compiled a dataset of PV curves from six previously published studies (Bartlett, Scoffoni, Ardy, et al., 2012; John et al., 2018; Maréchaux et al., 2015; Pivovaroff et al., 2014; Scoffoni et al., 2011; Scoffoni et al., 2014), for a total of 50 unique species diverse in phylogeny, habitat type, and drought tolerance parameters (Table S2). Data were for adult plants growing in urban or wild forests. For five species (*Cercocarpus betuloides*, *Comarostaphylis diversifolia*, *Encelia farinosa*, *Platanus racemosa*, and *Quercus agrifolia*), PV curve data were collected from two studies and were included as independent records. In each study, mature sun leaves were sampled from 3 to 6 replicate individuals, grown in similar conditions and in close proximity. For uniformity, the original data were acquired and re-analyzed by constructing PV curves and extracting parameters (Sack & Pasquet-Kok, 2011). For the PV parameters that can be expressed in relation to either the total or the symplastic water content (i.e., RWC, ε, C_{ft} and C_{tlp}; Koide et al., 2000; Tyree & Hammel, 1972), we analyzed both versions. Symplastic parameters rely on the accurate determination of the apoplastic fraction, which is not always possible (e.g., Lenz et al., 2006; Sack et al., 2003). We determined the apoplastic fraction as the *x*-intercept of the linear relationship between the negative inverse of Ψ_{leaf} and 100-RWC; that is, the RWC at which declining leaf water potential (and solute potential) tends to negative infinity (Bartlett, Scoffoni, & Sack, 2012). We calculated the symplastic RWC (RWC_s), symplastic modulus of elasticity (ε_s), and symplastic capacitance at full turgor ($C_{ft,s}$) and turgor loss point ($C_{tlp,s}$) as:

$$RWC_s = \frac{RWC - \frac{a_f}{100}}{1 - \frac{a_f}{100}} \quad (1)$$

$$\varepsilon_s = \frac{\Delta\Psi_P}{\Delta RWC_s} \quad (2)$$

$$C_{ft,s} = \frac{\Delta RWC_s}{\Delta\Psi_{leaf}} = \frac{SD(RWC_s)}{SD(\Psi_{leaf})}, \Psi_{leaf} > \pi_{tlp} \quad (3)$$

$$C_{tlp,s} = \frac{\Delta RWC_s}{\Delta\Psi_{leaf}} = \frac{SD(RWC_s)}{SD(\Psi_{leaf})}, \Psi_{leaf} < \pi_{tlp} \quad (4)$$

Notably, for capacitances, which are defined as the slope of RWC versus Ψ_{leaf}, we used the quotient of standard deviations, which represents the slope of the standard major axis, which has the advantage of symmetry in *y* and *x* (Warton et al., 2011). Absolute leaf area specific capacitance at full turgor ($C_{ft,abs}$) was determined as:

$$C_{ft,abs} = C_{ft} \bullet \frac{SWMA}{18} \quad (5)$$

where SWMA is the saturated water mass per leaf area (=leaf mass per area × saturated water content per leaf mass; g m^{-2}) and 18 g mol^{-1} is the molar mass of water.

We included data for species for which there were ≥5 individual leaf values after statistical outliers were removed to improve the estimation of PV parameters. We tested for outliers in each species' PV parameter dataset, when traits differed by more than two-fold in their values across the sun leaves, by applying the Dixon Q outlier test (*dixon.test* function in R 4.2.1; *outliers* package version 0.14; Komsta, 2011; R Core Team, 2022; Table S3). The typical cause of outlier PV parameter values was a paucity of points (1) above the turgor loss point, leading to uncertainty in the estimation of saturated water content and, thereby, of leaf relative water content, or (2) below turgor loss point, leading to uncertainty in the estimation of water potential and relative water content at turgor loss point. When an outlier was found in a parameter, the raw pressure volume curve values were checked for any errors, and if errors could not be corrected, given leaves were removed; 1/6 leaves were removed for *Betula occidentalis*, *Camellia sasanqua*, *Fraxinus dipetala*, *Helianthus annuus and Qualea rosea* and data for 24 species records were removed due to no longer being represented by ≥5 individual leaf values. The parameters for which outliers were most frequent were bulk modulus of elasticity (9/383 leaves), capacitance at full turgor (8/383 leaves), and their symplastic counterparts (symplastic modulus and symplastic capacitance at full turgor; 6/383 each). Unrealistic negative apoplastic fraction estimates were also removed from the data set; 23/53 species had ≥5 non-negative a_f values and were analyzed for a_f and symplastic PV parameters. We also tested the effect of excluding outliers (see subsequent section).

For 39 species that were measured in this study and in the published literature, data for means and standard deviations for leaf mass per area (LMA), leaf area (LA), leaf dry matter content (LDMC), and leaf thickness (LT) were compiled for sun leaves from the same individuals as those sampled for the pressure volume curve parameters (Table S4). We estimated leaf density (ρ_{leaf}) from mean LMA and LT as:

$$\rho_{leaf} = \frac{LMA}{LT} \quad (6)$$

Standard deviation for ρ_{leaf} was calculated based on those of LMA and LT by propagation of error (Beers, 1957). We did not remove outliers from morphological traits because raw individual data were not available from some studies, and thus coefficients of variation were determined from mean, standard errors, and sample number.

2.2 | Statistics: Within-species trait variability

As a measure of ITV_{ref} for PV parameters, we used the coefficient of variation (CV; Albert et al., 2010):

$$ITV_{ref} = \frac{SD\left(trait_{species}\right)}{mean\left(trait_{species}\right)} \bullet 100 \quad (7)$$

Where $trait_{species}$ represents the measured values for the sun leaves of a given trait for a given species. To compare differences in ITV_{ref} between trait types (i.e., morphological and pressure volume parameters), we performed a nested ANOVA with species' ITV_{ref} values for traits nested within trait type using *aov* from the stats package in R (R Core Team, 2022). We also conducted this test while including the outlier leaves in the calculation of ITV_{ref} for PV parameters π_o, π_{tlp}, ε, RWC_{tlp}, C_{ft}, and C_{tlp}.

2.3 | Statistics: Testing theory for the basis of intraspecific relationships among PV parameters and additional morphological traits

We tested the relationships among PV traits across sun leaves of given species (using the *cor.test* function for R software; version 4.2.1; R Core Team, 2022). We used absolute values for negative PV parameters (i.e., π_o and π_{tlp}). We considered relationships significant if $p < 0.05$ for both Spearman and Pearson correlation tests, with Pearson tests conducted on untransformed or log-transformed data, that is, respectively testing linear and nonlinear (power law) relationships; we report in the text the strongest correlation coefficient (Table S5) and present relationships among PV parameters with correlation coefficient fitted with standard major axes using the *smatr* R package (Warton et al., 2011).

To determine whether the theory for trait relationships previously established across leaves of diverse species would apply within species, we tested whether π_{tlp} and RWC_{tlp} and leaf capacitance at full turgor (C_{ft}) are biophysical functions of π_o and ε. According to Bartlett, Scoffoni, and Sack (2012),

$$\widehat{\pi_{tlp}} = \frac{\pi_o \varepsilon_s}{\pi_o + \varepsilon_s} \quad (8)$$

$$\widehat{RWC_{tlp,s}} = \frac{\pi_o + \varepsilon_s}{\varepsilon_s} \quad (9)$$

$$\widehat{C_{ft}} = \frac{\left(100 - RWC_{tlp}\right)}{0 - \Psi_{tlp}} \quad (10)$$

Combined with Equations 8 and 9 and simplified:

$$\widehat{C_{ft}} = \frac{(100 - a_f)(\pi_o + \varepsilon)}{\varepsilon^2} \quad (11)$$

where π_o is the osmotic potential at full turgor, ε is the symplastic modulus of elasticity, and a_f is the apoplastic fraction.

We tested the application of these relationships intraspecifically for π_{tlp}, RWC_{tlp}, and C_{ft} using ordinary least squares (OLS) regressions of observed values versus values predicted based on Equations (8–10), respectively (Table S6).

2.4 | Statistics: Testing for correlations across species in the ITV_{ref} of the PV parameters

To test whether species with high ITV_{ref} in a given trait show high ITV_{ref} in other traits, we analyzed correlations of ITV_{ref} among PV parameters across all species using *cor.test* function for R software (version 4.2.1; R Core Team, 2022; Table S7).

2.5 | Testing the impact of intraspecific variation in PV parameters on remotely sensed leaf water potential

We considered the influence of intraspecific variation in PV parameters on the accuracy and precision of scaling up from spectroscopic determination of leaf water content to the estimation of Ψ_{leaf} (Figure 1). We conducted a sensitivity analysis of the impact of error in each variable relative to other sources of error on the estimation of Ψ_{leaf} for the illustrative case of scaling up from THz time-domain spectroscopy based on previously published data (Browne et al., 2020). THz radiation falls within the 100 GHz–10 THz frequency range or 10–1000 μm wavelength range (Mittleman et al., 1996), and its transmission through a sample is very sensitive to liquid water (Hecht, 2002; Rønne et al., 1999; Thrane et al., 1995), such that the peak field ratio (PFR), the ratio of transmitted radiation through a sample to total propagated radiation, can predict leaf water mass per area (WMA) (Baldacci et al., 2017; Gente et al., 2018), which can be upscaled to Ψ_{leaf} using saturated leaf water content per leaf area (SWMA, itself a function of SWC and LMA) and PV parameters (Figure 1; Browne et al., 2020).

First, to determine how variation in input parameters would limit the prediction of leaf water potential, we tested the intrinsic sensitivity of Ψ_{leaf} to increases in pressure volume curve parameters (both π_{tlp} and ε) and saturated water mass per area. We estimated a base model using species mean parameters and sampled values of PV parameters and SWMA. Then, we increased each of the input parameters by 5%–100%.

We estimated the root mean square error (RMSE) as:

$$RMSE = \sqrt{\overline{(observed - fitted)^2}} \quad (12)$$

Where the observed values are the estimated Ψ_{leaf} from the base model and the fitted values are estimated Ψ_{leaf} when increasing input parameters in the intrinsic sensitivity analysis.

Next, we used previously published data for the estimation of Ψ_{leaf} based on ln (PFR) for two species, *Hedera canariensis* and *Platanus racemosa* (Browne et al., 2020). We chose five ln (PFR) values representing a range of leaf hydration, i.e., 95%, 80%, 75%, 70%, and 65% of the saturated water mass per area (−1.69, −1.27, −1.13, −0.99, −0.85 dBs dBs^{-1} for *H. canariensis* and − 1.14, −0.95, −0.89, −0.83 and − 0.76 dBs dBs^{-1} for *P. racemosa*). We conducted three types of simulations to estimate the influence of error in specific input variables on the precision of Ψ_{leaf} estimates, that is, by sampling with replacement from a normal distribution with the mean and standard

TABLE 3 Simulations testing the influence of error in variables on the prediction of leaf water potential scaling up from the log transformed peak field ratio, ln (PFR), which relates to water mass per area (WMA; Figure 1). For each bootstrapping simulation we used either the mean value of each parameter or values sampled from a constructed distribution with the same mean and standard deviation from published data (Browne et al., 2020), or using our own database of traits.

Simulation	lnPFR ~ WMA	PV parameters	SWMA
A	Species mean	Sampled distribution	Species mean
B	Species mean	Species mean	Sampled distribution
C	Species mean	Sampled distribution	Sampled distribution

deviation of the sample data while keeping other variables constant at their mean value (Table 3). In simulation A, we added error to the PV parameters, that is, the modulus of elasticity and osmotic potential at full turgor. In simulation B, we added error to the saturated water mass per area (SWMA) based on its mean and standard deviation (Browne et al., 2020; Table S2). In simulation C, we added error to both the PV parameters and SWMA. For each set of simulations (A–C), we estimated 1000 relationships of PFR to Ψ_{leaf} (Figure 1). In detail, for simulating each relationship of ln PFR to WMA, for each of the five PFR values, we first made predictions of WMA ($\widehat{WMA}$) using species-specific WMA ~ ln PFR relationships:

$$\widehat{WMA} = a \cdot \ln PFR + b \tag{13}$$

Where a and b are a species-specific slope and intercept, respectively, determined empirically by Browne et al. (2020). Next, we predicted the relative water content ($\widehat{RWC}$) as:

$$\widehat{RWC} = \frac{\widehat{WMA}}{SWMA}, \tag{14}$$

where saturated water mass per area is:

$$SWMA = LMA \cdot SWC \tag{15}$$

To scale up from $\widehat{RWC}$ to Ψ_{leaf}, we estimated π_{tlp} and RWC_{tlp} (Equations 8 and 9, respectively). For simulations (A) and (C), we randomly sampled species-specific values of π_o and ε with replacement from normal distributions based on the mean and standard deviations of measured leaves of each species. Using calculated values of π_{tlp} and RWC_{tlp}, based on Equations (8) and (9), we then determined leaf osmotic potential (Ψ_S), leaf pressure potential (Ψ_P) and leaf water potential (Browne et al., 2020; Sack et al., 2018):

$$\widehat{\Psi_S} = \frac{\pi_o \cdot \pi_{tlp}\left(1 - RWC_{tlp}\right)}{\pi_o\left(1 - \widehat{RWC}\right) + \pi_{tlp}\left(\widehat{RWC} - RWC_{tlp}\right)} \tag{16}$$

and,

$$\widehat{\Psi_P} = \begin{cases} \pi_o \cdot \left(\dfrac{\widehat{RWC} - RWC_{tlp}}{1 - RWC_{tlp}}\right), & \text{if } \widehat{RWC} > RWC_{tlp} \\ 0, & \text{if } \widehat{RWC} < RWC_{tlp} \end{cases} \tag{17}$$

and,

$$\widehat{\Psi_{leaf}} = \Psi_S + \Psi_P \tag{18}$$

For simulation types B and C, we randomly sampled species-specific values of SWMA with replacement from normal distributions based on the mean and standard deviations of measured leaves of each species. When samples of SWMA were less than WMA, which would be impossible in reality, we resampled from the same distribution. We compared RMSE for the estimates of Ψ_{leaf} for each of these simulation types to determine the role of error in each input variable, in particular the role of uncertainty PV parameters relative to that of other input variables.

3 | RESULTS

3.1 | Assessing intraspecific variation in PV parameters

The ITV_{ref}, that is, the variation among sun leaves of different individuals of given species, quantified as a coefficient of variation, varied across measured PV parameters from 6.87 ± 0.84% to 34.1 ± 2.1% (mean ± SE) for RWC_{tlp} and C_{ft}, respectively, and was on average 22.0 ± 0.7%. The ITV_{ref} for PV parameters was on average significantly lower than those for other leaf structural traits, which varied from 12.3 ± 1.4 to 112 ± 7.34% for LT and LDMC, respectively, and on average 42.9 ± 3.3% (Nested ANOVA; $p < 0.001$; Figure 2; Table S8). This analysis was robust to the inclusion of outlier leaves in the calculation of ITV_{ref} for PV parameters π_o, π_{tlp}, ε, RWC_{tlp}, C_{ft}, and C_{tlp}, which increased the across-species mean ITV_{ref} values for these traits by 2.6%–5.4% (Nested ANOVA; $p < 0.001$; Table S8).

3.2 | Intraspecific correlations among PV parameters

Across leaves of given species, PV parameters were strongly correlated (Table S5), with relationships consistent with those previously reported across species, and the mechanistic linkages in Equations (8–11). Thus, relationships of π_{tlp} with π_o were found for 41/53 species (77% of species; mean $r = 0.81$), C_{ft} with ε for 50/53 species (94%; mean $r = -0.93$), RWC_{tlp} with ε for 24/53 species (45%; mean $r = 0.67$), RWC_{tlp} with C_{ft} for 32/53 species (60%: mean $r = -0.71$), and C_{tlp} with a_f for 14/23 species (57%; mean $r = -0.73$).

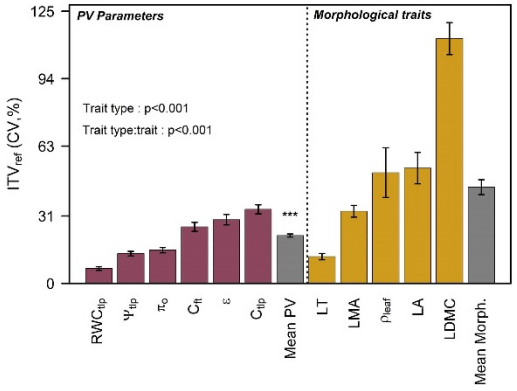

FIGURE 2 Mean intraspecific variation among sun leaves of plants growing in similar conditions (ITV_{ref}) for pressure volume curve parameters of 50 species and other morphological and compositional leaf traits for 39 species, separated by the dotted line and in each category ordered by increasing median coefficient of variation ($n = 12–50$ species). Error bars indicate the standard error of the mean and asterisks denote the significant difference between mean of pressure volume curve and morphological and compositional leaf traits (***$p < 0.001$; Nested ANOVA).

3.3 | Testing theory for the relationships among PV parameters within species

Our findings were consistent with theory established among species for biophysical relationships among PV parameters across sun leaves of given species, that is, the mechanistic determination of π_{tlp}, RWC_{tlp}, and C_{ft} based on ε, π_o, and a_f (Equations 8–11). Thus, we found strong relationships within species between the observed PV parameter values and those estimated based on theoretical formulae previously shown to hold across species (Bartlett, Scoffoni, & Sack, 2012; $r = 0.76–0.999$; Figure 3; Table S6).

3.4 | Correlations of ITV_{ref} of PV parameters across species

We found strong across-species correlations among the ITV_{ref} values for different traits. Species with high intraspecific variation in one PV parameter also tended to have high variation in other PV parameters. The correlations of ITV_{ref} among variables that were biophysically related (Equations 8–11) were particularly strong, that is, for π_{tlp} and π_o ($r = 0.87$), RWC_{tlp} and ε ($r = 0.79$), C_{ft} and ε ($r = 0.85$; Figure 4), RWC_{tlp} (bulk) and apoplastic fraction (RWC_{tlp} $r = 0.56$), a_f and bulk capacitance at full turgor and at turgor loss point (C_{ft} $r = 0.38$; C_{tlp} $r = 0.51$) and symplastic capacitance at full turgor and π_o ($r = 0.56$; Table S7). Further, the ITV_{ref} for saturated water content correlated with those for ε and capacitance at full turgor ($r = 0.44$ and 0.48, respectively; Table S7).

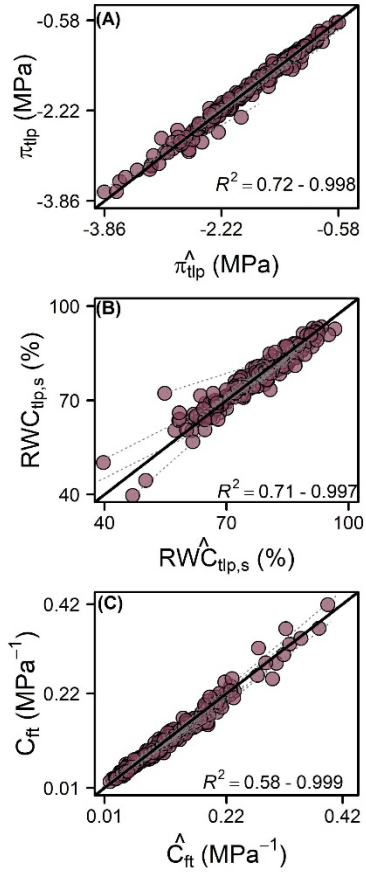

FIGURE 3 Tests of observed versus predicted values of leaf water potential at turgor loss point (π_{tlp} and $\widehat{\pi_{tlp}}$, respectively), relative water content at turgor loss point (RWC_{tlp} and $\widehat{RWC_{tlp}}$, respectively) and capacitance at full turgor (C_{ft} and $\widehat{C_{ft}}$, respectively) for 5–6 leaves of 40–44 species. Each point represents a leaf, and lines are plotted for all significant within-species regressions (gray dashed lines), with 1:1 line (solid black line). Values were predicted using Equations (8), (9) and (10) for $\widehat{\pi_{tlp}}$, $\widehat{RWC_{tlp}}$, and $\widehat{C_{ft}}$, respectively.

3.5 | Testing the influence of intraspecific variation in PV parameters in in-situ remote sensing of leaf water status

We tested whether ITV_{ref} for PV parameters is sufficiently conservative to enable precise predictions of leaf water potential from in-situ spectroscopic measurements of leaf water mass per area (WMA, a.k.a., "equivalent water thickness"), exemplified by the use of peak field ratio (PFR) based on THz transmission. Thus, we tested simulations differing in the variation (noise) in predicted Ψ_{leaf} values given the error added to different inputs. In our test of the intrinsic sensitivity

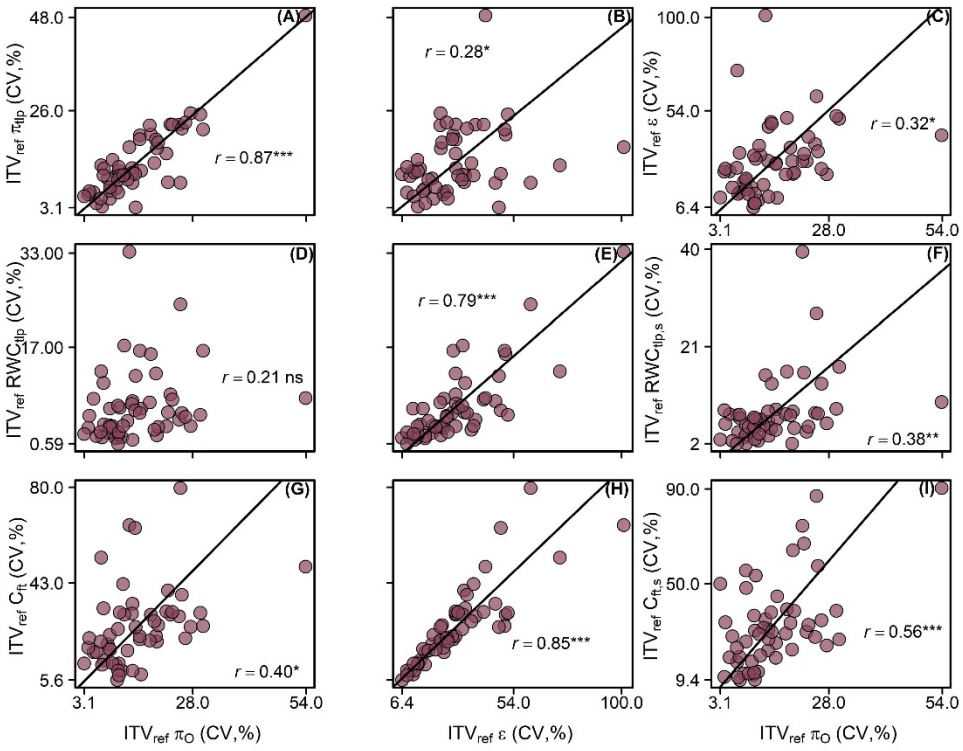

FIGURE 4 Correlations across species of the coefficient of variation (CV) across individual sun leaves of plants grown in similar, well-watered conditions (a measure of ITV_{ref}) for total (C_{ft}) and symplastic ($C_{ft,s}$) capacitance, total and symplastic relative water content at turgor loss point (RWC_{tlp} and $RWC_{tlp,s}$, respectively), and leaf water potential at turgor loss point (π_{tlp}) with their mechanistic drivers according to biophysical theory, the leaf osmotic potential at full turgor (π_o) and modulus of elasticity (ε) for 53 species records. Statistical significance; $^*p < 0.05$; $^{**}p < 0.01$; $^{***}p < 0.001$). There is a strong relationship among variation in "higher level" parameters and their constituents. Black solid lines were drawn with standard major axis.

of the increase in variation in predicted Ψ_{leaf} in relation to increasing each input variable by a given percentage of the mean, all else being equal, we found similar sensitivity to PV parameters and SWMA (Figure 5). The error in predicted Ψ_{leaf} increased gradually by ~0.05 MPa (RMSE) when 30% error was added to either the PV parameters or to SWMA, and then much more steeply thereafter, especially when error was added to both PV and SWMA (Figure 5). We also estimated the noise that would reduce predictive power using the RMSE for simulations based on sampling from the observed distributions of input parameters at each hydration level (i.e., at each input peak field ratio). For both *Hedera canariensis* and *Platanus racemosa*, there was similar noise in the prediction of Ψ_{leaf} due to error added to PV parameters and SWMA (Figure 6); however, when adding both together we saw compounding error for *H. canariensis* and compensation for *P. racemosa* (mean ± SE for RMSE for simulations A, B, and C; 0.29 ± 0.01, 0.24 ± 0.01, and 0.35 ± 0.01 MPa for *H. canariensis*; 0.51 ± 0.03 MPa, 0.34 ± 0.02 MPa, and 0.34 ± 0.02 MPa for *P. racemosa*; $p < 0.001$ and $p = 0.003$ for differences between species and among simulations, respectively; two-way ANOVA). Furthermore, across hydration states, the error in Ψ_{leaf} for *H. canariensis* declined slightly while RMSE increased with dehydration for *P. racemosa*. Overall, these results highlight the feasibility of predicting Ψ_{leaf} from PFR for sun leaves using species mean values for PV parameters and SWMA, with a RMSE resolution typically at <0.5 MPa.

4 | DISCUSSION

Our analyses showed that PV parameters had low ITV_{ref} relative to other leaf morphological traits consistent with their importance as variables with strong influence on thresholds for dehydration responses. Further, the relationships among PV parameters and their variation supported biophysical hypotheses that were previously formulated across species. Our simulation modeling demonstrated that conservative ITV_{ref} for PV parameters validates the use of species-

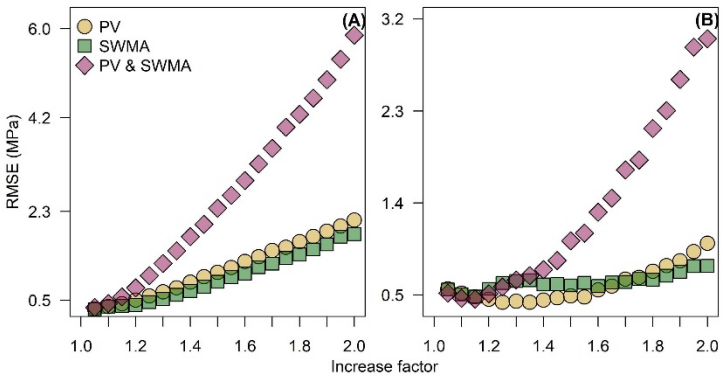

FIGURE 5 Test of model sensitivity to increasing parameters values for *Hedera canariensis* (A) and *Platanus racemosa* (B). We estimated the error in predicted leaf water potential (Ψ_{leaf}) using the root mean square error (RMSE; MPa) by increasing the sampled parameters, that is, for pressure volume curve (PV) parameters (π_{tlp} and ε); for saturated water mass per area (SWMA); and for PV parameters and SWMA together, in our model (Figure 1). We increased sampled parameters by 5%–100%, represented here as multiplying parameters by 1.05–2.0.

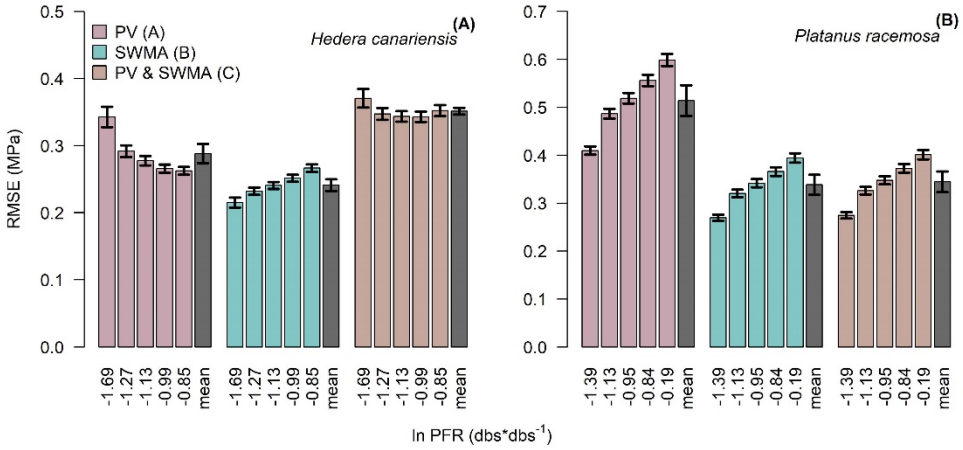

FIGURE 6 Root mean squared error of predictions (RMSE $\widehat{\Psi_{leaf}}$) for five values across the typical measured range of the log transformed peak field ratio, ln (PFR), which relates to water mass per area (WMA) and can thus be scaled up to give $\widehat{\Psi_{leaf}}$ for *Hedera canariensis* (A) and *Platanus racemosa* (B) (analysis using PFR data from (Browne et al., 2020)). For each ln (PFR), we predicted 1000 $\widehat{\Psi_{leaf}}$ values based on the approach presented in Figure 1, and for each term either using the mean value, or adding error by sampling from a normal distribution based on the measured mean and standard deviation (Table 3) to: (simulation A) the pressure volume (PV) curve parameters; (simulation B) the saturated water mass per area (SWMA); and (simulation C) both the PV parameters and SWMA.

mean values for scaling up from spectroscopic measurements for remote sensing from leaves to canopies.

4.1 | Variation in ITV_{ref} among pressure volume curve parameters and other leaf traits

The ITV_{ref}, estimated based on sun-exposed, mature leaves of plants grown under similar conditions, enables the use of ecophysiological and structural composition data collected using typical sampling for comparison of within-species variation in PV parameters relative to other traits. Notably, ITV at this scale provides a "baseline" ITV that minimizes environmental variation and ecotypic variation that would arise among populations, and emphasizes the developmental plasticity, genetic variation and microclimate disparity (e.g., in irradiance and water status) that arises among sun leaves (Sack et al., 2006). An avenue for future study is the variation in ITV_{ref} for given traits of given species that may arise under different growing conditions.

We found relatively low ITV_{ref} in PV parameters compared to other leaf morphological traits. PV parameters such as π_o, ε, and π_{tlp} are theoretically expected to be conservative for individuals of a given species as they either contribute to or directly represent thresholds of dehydration responses (Bartlett et al., 2014; Bartlett, Scoffoni, & Sack, 2012). By contrast, other leaf morphological traits may vary to optimize competitive ability across more axes of performance, including light capture and water and nutrient use efficiencies (Bolnick

et al., 2011; Funk, 2008; Givnish, 1988; Novick et al., 2022). Another explanation of the conservative variation in the PV parameters is that it arises from bulk cell-level traits such as protoplast osmotic concentration and cell wall thickness, which may be more conservative within a species than organ-level morphological traits with higher ITV_{ref} such as LDMC and ρ_{leaf}, which depend on not only cell properties, but also are strongly influenced by variation in cell numbers and sizes in the different tissues (John et al., 2017).

4.2 | Theoretical implications of variation among PV parameters and with leaf traits

In support of established biophysical hypotheses for PV parameters, we confirmed intraspecifically the relationships for the determination of "higher level" traits based on underlying traits, i.e., of π_{tlp}, RWC_{tlp}, and C_{ft} from ε, π_o, and a_f (Figure 3). The π_{tlp} and RWC_{tlp} could be predicted as explicit functions of π_o, ε, and C_{ft} as previously reported across species (Bartlett, Scoffoni, & Sack, 2012). These findings thus supported the causal role of the π_o and ε as drivers of π_{tlp}, capacitance at full turgor, and the RWC at turgor loss point. For example, the accumulation of solutes within the symplast (i.e., more negative osmotic potential at full turgor) allows for the maintenance of turgor at more negative water potentials, and additionally variation in the extensibility of cell walls (ε) influences the water storage of cells, impacting the variation in RWC_{tlp} and C_{ft}.

Additionally, we found correlations among traits in their ITV_{ref} across species, such that species with high variation in one trait also varied strongly in others (Figure 4). This pattern is expected given the relationships among PV parameters, and highlights the inter-related functionality of these traits. We note that the correlation of ITV across traits would not necessarily be expected to hold across other sets of traits, contexts or scales of variation generally. Theory for trait plasticity holds that traits may differ in their variation according to species and function (Grime et al., 1986; Grime & Mackey, 2002) such that species specialized in resource-rich environments may show high ITV in organ-level morphological traits that confer competitive ability (e.g., leaf size and leaf density), whereas species of resource-poor conditions may show high ITV in physiological traits that could enable high resource capture during periods of high availability within the lifetime of the organ (e.g., photosynthetic rate; Grubb, 1998). Further, previous studies of intracanopy plasticity in leaf morphological traits (i.e., leaf mass per area, leaf perimeter^2/area, sapwood to leaf area ratio and stomatal density) including sun and shade leaves found that trait variation was not correlated across species as was found here for ITV_{ref} for PV traits (Sack et al., 2006). An important avenue for future study is the question of whether the ITV of PV parameters would be correlated across species for other scales of ITV, that is, for plasticity across light or nutrient gradients. Notably, in this study, we focused on the relationships between ITV_{ref} of PV parameters, but not among morphological parameters given the lack of raw individual data for some of the studies; future studies could test the relationship of ITV_{ref} across functional traits more commonly measured (such as, e.g., leaf mass per area and leaf thickness) would benefit from available large global datasets.

4.3 | Implications of low ITV_{ref} for PV parameters for scaling up from leaf to plant to landscape

Our findings indicate the viability of scaling up spectroscopic measurements of WMA to Ψ_{leaf} using species mean PV curve parameters (Figure 6). The narrow ITV_{ref} of PV parameters results in relatively low error, generally <0.5 MPa in RMSE, such that Ψ_{leaf} estimation is not rendered imprecise by the baseline plasticity of sun leaves. The error in predicting Ψ_{leaf} was greater for both species when varying pressure volume curve parameters (simulation A) than SWMA (simulation B), given our randomly sampling error for two PV parameters simultaneously (π_o and ε). The increasing error for *P. racemosa* at more dehydrated states corresponds to the effects of lamina shrinkage during leaf dehydration in an already relative thin-leaved species (Browne et al., 2020; Scoffoni et al., 2014). Our demonstration of the utility of species-mean PV parameters in the estimation of Ψ_{leaf} from ln (PFR) indicates that analyses utilizing species-means for SWMA and PV-parameters can be feasible for estimating Ψ_{leaf} and provides a first estimate of the error expected from this approach.

We recommend that this approach to testing the importance of ITV_{ref} in the prediction of scaled up leaf water status from spectroscopic measurements be applied to studies of other species and spectroscopic approaches, to enable the application of mean PV parameters in these applications. Spectroscopic assessment of leaf water content can be applied at leaf, canopy, or landscape scale (Asner et al., 2016; Hunt et al., 1987; Li et al., 2018; reviewed by Browne et al. (2020)). Notably, the application tested here was for the prediction of Ψ_{leaf} at the scale of individual sun leaves using transmittance spectroscopy. Indeed, several studies matching Ψ_{leaf} for sun leaves with airborne spectroscopic reflectance measurements indicate strong predictive power in estimated Ψ_{leaf} among sun leaves (Momen et al., 2017). Yet, for other spectroscopic measurements at canopy and landscape scales, such as using vegetative optical depth for the estimation of WMA, involves disentangling the effects of shade leaves and branches, which will have different PV parameters than sun leaves. For instance, X-band microwave detection represents attenuation from water in leaves and tissues at the top of the canopy whereas L-band microwave detection may include water throughout a canopy (Konings et al., 2021). Thus, these approaches to scale to whole canopies may need to account for ITV that includes environmental-driven trait variation within canopies to achieve strong predictive power for estimates of landscape Ψ_{leaf} (Holtzman et al., 2021; Konings et al., 2021).

Approaches to the sensing of Ψ_{leaf} based on estimates of WMA have great urgency and importance across scales. At leaf scale, Ψ_{leaf} measurements that can be made in vivo, in situ within a gas exchange system, would contribute strongly to the determination of photosynthetic drought responses, and our findings indicate that species-mean PV parameters could be used for such an application. At larger scales,

measurements from a mounted in situ or remote system will improve estimates of drought-induced physiological responses at ecosystem scale (Konings et al., 2021; Momen et al., 2017; Rao et al., 2019), and enable the development and refinement of "need-based" irrigation systems of crops and urban ecosystems (Jepsen et al., 2011). Coupled with eddy-flux tower or spectroscopic measurements of canopy evapotranspiration and temperature (Fisher et al., 2020), remotely sensed Ψ_{leaf} measurements would enable a higher resolution of the control of canopy fluxes by leaf water status and hydraulic conductance (Anderegg et al., 2017; Novick et al., 2022). While analysis of the ITV_{ref} leads to important insights and applications at leaf scale, the range of applications at larger scales shows the increasingly need to quantify the ITV of pressure-volume parameters across a yet wider range of contexts.

AUTHOR CONTRIBUTIONS

Marvin Browne and Lawren Sack conceived and designed the study. Marvin Browne, Megan K. Bartlett, Christian Henry, Grace John, Christine Scoffoni, and Nezih Tolga Yardimci collected experimental data. Marvin Browne processed the experimental data and performed analyses. Marvin Browne and Lawren Sack interpreted the results, wrote the manuscript, and designed the figures. All authors discussed the results and commented on the manuscript.

ACKNOWLEDGMENTS

We are grateful to A. Baird, A. Ongjoco, M. Ochoa and N. Vinod for discussion. This work was supported by the U.S. National Science Foundation (grants 1951244, 2017949, and 1735325), and the Anthony and Jeanne Pritzker Family Foundation.

DATA AVAILABILITY STATEMENT

Data used in our analyses are provided within Table S2.

ORCID

Marvin Browne https://orcid.org/0000-0002-9640-0759
Christian Henry https://orcid.org/0000-0003-4805-8212
Grace John https://orcid.org/0000-0002-8045-5982
Christine Scoffoni https://orcid.org/0000-0002-2680-3608
Nezih Tolga Yardimci https://orcid.org/0000-0002-3623-5835
Lawren Sack https://orcid.org/0000-0002-7009-7202

REFERENCES

Albert, C.H., Grassein, F., Schurr, F.M., Vieilledent, G. & Violle, C. (2011) When and how should intraspecific variability be considered in trait-based plant ecology? *Perspectives in Plant Ecology, Evolution and Systematics*, 13, 217–225.

Albert, C.H., Thuiller, W., Yoccoz, N.G., Soudant, A., Boucher, F., Saccone, P. et al. (2010) Intraspecific functional variability: extent, structure and sources of variation. *Journal of Ecology*, 98, 604–613.

Anderegg, W.R., Wolf, A., Arango-Velez, A., Choat, B., Chmura, D.J., Jansen, S. et al. (2017) Plant water potential improves prediction of empirical stomatal models. *PLoS One*, 12, e0185481.

Asner, G.P., Brodrick, P.G., Anderson, C.B., Vaughn, N., Knapp, D.E. & Martin, R.E. (2016) Progressive forest canopy water loss during the 2012–2015 California drought. *Proceedings of the National Academy of Sciences*, 113, E249–E255.

Baird, A.S., Anderegg, L.D.L., Lacey, M.E., Hillerislambers, J. & Van Volkenburgh, E. (2017) Comparative leaf growth strategies in response to low-water and low-light availability: variation in leaf physiology underlies variation in leaf mass per area in Populus tremuloides. *Tree Physiology*, 37, 1140–1150.

Baldacci, L., Pagano, M., Masini, L., Toncelli, A., Carelli, G., Storchi, P. et al. (2017) Non-invasive absolute measurement of leaf water content using terahertz quantum cascade lasers. *Plant Methods*, 13, 51.

Bartlett, M.K., Klein, T., Jansen, S., Choat, B. & Sack, L. (2016) The correlations and sequence of plant stomatal, hydraulic, and wilting responses to drought. *Proceedings of the National Academy of Sciences*, 113, 13098–13103.

Bartlett, M.K., Scoffoni, C., Ardy, R., Zhang, Y., Sun, S., Cao, K. et al. (2012) Rapid determination of comparative drought tolerance traits: using an osmometer to predict turgor loss point. *Methods in Ecology and Evolution*, 3, 880–888. Available from: https://doi.org/10.1111/j.2041-210X.2012.00230.x

Bartlett, M.K., Scoffoni, C. & Sack, L. (2012) The determinants of leaf turgor loss point and prediction of drought tolerance of species and biomes: a global meta-analysis: drivers of plant drought tolerance. *Ecology Letters*, 15, 393–405.

Bartlett, M.K., Zhang, Y., Kreidler, N., Sun, S., Ardy, R., Cao, K. et al. (2014) Global analysis of plasticity in turgor loss point, a key drought tolerance trait. *Ecology Letters*, 17, 1580–1590.

Beers, Y. (1957) *Introduction to the theory of error*. Redding, MA: Addison-Wesley Publishing Company.

Bolnick, D.I., Amarasekare, P., Araújo, M.S., Bürger, R., Levine, J.M., Novak, M. et al. (2011) Why intraspecific trait variation matters in community ecology. *Trends in Ecology & Evolution*, 26, 183–192.

Brodribb, T.J., Powers, J., Cochard, H. & Choat, B. (2020) Hanging by a thread? Forests and drought. *Science*, 368, 261–266.

Browne, M., Yardimci, N.T., Scoffoni, C., Jarrahi, M. & Sack, L. (2020) Prediction of leaf water potential and relative water content using terahertz radiation spectroscopy. *Plant Direct*, 4, e00197.

Cotrozzi, L., Couture, J.J., Cavender-Bares, J., Kingdon, C.C., Fallon, B., Pilz, G. et al. (2017) Using foliar spectral properties to assess the effects of drought on plant water potential. *Tree Physiology*, 37, 1582–1591.

Dawson, S.K., Carmona, C.P., González-Suárez, M., Jönsson, M., Chichorro, F., Mallen-Cooper, M. et al. (2021) The traits of "trait ecologists": an analysis of the use of trait and functional trait terminology. *Ecology and Evolution*, 11, 16434–16445.

De Bello, F., Lavorel, S., Albert, C.H., Thuiller, W., Grigulis, K., Dolezal, J. et al. (2011) Quantifying the relevance of intraspecific trait variability for functional diversity. *Methods in Ecology and Evolution*, 2, 163–174.

Delagrange, S., Messier, C., Lechowicz, M.J. & Dizengremel, P. (2004) Physiological, morphological and allocational plasticity in understory deciduous trees: importance of plant size and light availability. *Tree Physiology*, 24, 775–784.

Fisher, J.B., Lee, B., Purdy, A.J., Halverson, G.H., Dohlen, M.B., Cawse-Nicholson, K. et al. (2020) Ecostress: Nasa's next generation mission to measure evapotranspiration from the international Space Station. *Water Resources Research*, 56, e2019WR026058.

Fridley, J.D. & Grime, J.P. (2010) Community and ecosystem effects of intraspecific genetic diversity in grassland microcosms of varying species diversity. *Ecology*, 91, 2272–2283.

Funk, J.L. (2008) Differences in plasticity between invasive and native plants from a low resource environment. *Journal of Ecology*, 96, 1162–1173.

Gente, R., Rehn, A., Probst, T., Stübling, E.-M., Camus, E.C., Covarrubias, A.A. et al. (2018) Outdoor measurements of leaf water content using THz quasi time-domain spectroscopy. *Journal of Infrared, Millimeter, and Terahertz Waves*, 39, 943–948.

Givnish, T. (1988) Adaptation to sun and shade: a whole-plant perspective. *Functional Plant Biology*, 15, 63–92.

González-Villagra, J., Omena-Garcia, R.P., Rodrigues-Salvador, A., Nunes-Nesi, A., Cohen, J.D. & Reyes-Díaz, M.M. (2022) Differential physiological and metabolic responses in young and fully expanded leaves of Aristotelia chilensis plants subjected to drought stress. *Environmental and Experimental Botany*, 196, 104814.

Grime, J., Crick, J. & Rincon, J. (1986) *The ecological significance of plasticity*. Cambridge: Published for the Society for Experimental Biology by the Company of Biologists Limited.

Grime, J.P. & Mackey, J. (2002) The role of plasticity in resource capture by plants. *Evolutionary Ecology*, 16, 299–307.

Grubb, P.J. (1998) A reassessment of the strategies of plants which cope with shortages of resources. *Perspectives in Plant Ecology, Evolution and Systematics*, 1, 3–31.

Hecht, E. (2002) *Optics, Reading Mass*. Reading, MA: Addison-Wesley.

Henry, C., John, G.P., Pan, R., Bartlett, M.K., Fletcher, L.R., Scoffoni, C. et al. (2019) A stomatal safety-efficiency trade-off constrains responses to leaf dehydration. *Nature Communications*, 10, 3398.

Herrera, C.M. (2017) The ecology of subindividual variability in plants: patterns, processes, and prospects. *Web Ecology*, 17, 51–64. Available from: https://doi.org/10.5194/we-17-51-2017

Holtzman, N.M., Anderegg, L.D.L., Kraatz, S., Mavrovic, A., Sonnentag, O., Pappas, C. et al. (2021) L-band vegetation optical depth as an indicator of plant water potential in a temperate deciduous forest stand. *Biogeosciences*, 18, 739–753.

Hunt, E.R., Rock, B.N. & Nobel, P.S. (1987) Measurement of leaf relative water content by infrared reflectance. *Remote Sensing of Environment*, 22, 429–435.

Jepsen, P.U., Cooke, D.G. & Koch, M. (2011) Terahertz spectroscopy and imaging: modern techniques and applications. *Laser & Photonics Reviews*, 5, 124–166.

John, G.P., Henry, C. & Sack, L. (2018) Leaf rehydration capacity: associations with other indices of drought tolerance and environment: loss of leaf rehydration capacity. *Plant, Cell & Environment*. Available from: https://doi.org/10.1111/pce.13390

John, G.P., Scoffoni, C., Buckley, T.N., Villar, R., Poorter, H. & Sack, L. (2017) The anatomical and compositional basis of leaf mass per area. *Ecology Letters*, 20, 412–425.

Jones, M.M. & Turner, N.C. (1980) Osmotic adjustment in expanding and fully expanded leaves of sunflower in response to water deficits. *Australian Journal of Plant Physiology*, 7, 181–192.

Kattge, J., Bönisch, G., Díaz, S., Lavorel, S., Prentice, I.C., Leadley, P. et al. (2020) TRY plant trait database—enhanced coverage and open access. *Global Change Biology*, 26, 119–188.

Koide, R. T., Robichaux, R. H., Morse, S. R. & Smith, C. M. (2000). Plant water status, hydraulic resistance and capacitance. In: *Plant physiological ecology: field methods and instrumentation*. Dordrecht, Netherlands: Kluwer, 161–183. https://doi.org/10.1007/978-94-010-9013-1_9

Komsta, L. (2011) Outliers: tests for outliers.

Konings, A.G., Saatchi, S.S., Frankenberg, C., Keller, M., Leshyk, V., Anderegg, W.R.L. et al. (2021) Detecting forest response to droughts with global observations of vegetation water content. *Global Change Biology*, 27, 6005–6024.

Kraft, N.J.B., Crutsinger, G.M., Forrestel, E.J. & Emery, N.C. (2014) Functional trait differences and the outcome of community assembly: an experimental test with vernal pool annual plants. *Oikos*, 123, 1391–1399.

Kubiske, M.E. & Abrams, M.D. (1990) Pressure-volume relationships in non-rehydrated tissue at various water deficits. *Plant, Cell & Environment*, 13, 995–1000.

Lenz, T.I., Wright, I.J. & Westoby, M. (2006) Interrelations among pressure-volume curve traits across species and water availability gradients. *Physiologia Plantarum*, 127, 423–433.

Li, B., Long, Y. & Yang, H. (2018). Measurements and analysis of water content in winter wheat leaf based on terahertz spectroscopy. *International Journal of Agricultural and Biological Engineering*, 3, 178–182. https://doi.org/10.25165/j.ijabe.20181103.3520

Lu, X. & Zhuang, Q. (2010) Evaluating evapotranspiration and water-use efficiency of terrestrial ecosystems in the conterminous United States using MODIS and AmeriFlux data. *Remote Sensing of Environment*, 114, 1924–1939. Available from: https://doi.org/10.1016/j.rse.2010.04.001

Maréchaux, I., Bartlett, M.K., Sack, L., Baraloto, C., Engel, J., Joetzjer, E. et al. (2015) Drought tolerance as predicted by leaf water potential at turgor loss point varies strongly across species within an Amazonian forest. *Functional Ecology*, 29, 1268–1277.

Marks, C.O. (2007) The causes of variation in tree seedling traits: the roles of environmental selection versus chance. *Evolution*, 61, 455–469.

Medeiros, C.D., Scoffoni, C., John, G.P., Bartlett, M.K., Inman-Narahari, F., Ostertag, R. et al. (2019) An extensive suite of functional traits distinguishes Hawaiian wet and dry forests and enables prediction of species vital rates. *Functional Ecology*, 33, 712–734.

Messier, J., Violle, C., Enquist, B.J., Lechowicz, M.J. & McGill, B.J. (2018) Similarities and differences in intrapopulation trait correlations of co-occurring tree species: consistent water-use relationships amid widely different correlation patterns. *American Journal of Botany.*, 105, 1477–1490.

Mittleman, D.M., Jacobsen, R.H. & Nuss, M.C. (1996) T-ray imaging. *IEEE Journal of Selected Topics in Quantum Electronics*, 2, 679–692.

Momen, M., Wood, J.D., Novick, K.A., Pangle, R., Pockman, W.T., Mcdowell, N.G. et al. (2017) Interacting effects of leaf water potential and biomass on vegetation optical depth: effects of LWP and biomass on VOD. *Journal of Geophysical Research: Biogeosciences*, 122, 3031–3046.

Nicotra, A.B., Atkin, O.K., Bonser, S.P., Davidson, A.M., Finnegan, E.J., Mathesius, U. et al. (2010) Plant phenotypic plasticity in a changing climate. *Trends in Plant Science*, 15, 684–692.

Niinemets, Ü., Kull, O. & Tenhunen, J.D. (2004) Within-canopy variation in the rate of development of photosynthetic capacity is proportional to integrated quantum flux density in temperate deciduous trees. *Plant, Cell & Environment*, 27, 293–313.

Novick, K.A., Ficklin, D.L., Baldocchi, D., Davis, K.J., Ghezzehei, T.A., Konings, A.G. et al. (2022) Confronting the water potential information gap. *Nature Geoscience*, 15, 158–164.

Novoplansky, A., Cohen, D. & Sachs, T. (1989) Ecological implications of correlative inhibition between plant shoots. *Physiologia Plantarum*, 77, 136–140.

Orians, C.M., Smith, S.D.P. & Sack, L. (2005) How are leaves plumbed inside a branch? Differences in leaf-to-leaf hydraulic sectoriality among six temperate tree species. *Journal of Experimental Botany*, 56, 2267–2273.

Pivovaroff, A., Sharifi, R., Scoffoni, C., Sack, L. & Rundel, P. (2014) Making the best of the worst of times: traits underlying combined shade and drought tolerance of Ruscus aculeatus and Ruscus microglossum (Asparagaceae). *Functional Plant Biol.*, 41, 11–24. Available from: https://doi.org/10.1071/FP13047

Plomion, C., Aury, J.-M., Amselem, J., Leroy, T., Murat, F., Duplessis, S. et al. (2018) Oak genome reveals facets of long lifespan. *Nature Plants*, 4, 440–452.

R Core Team. (2022) *R: a language and environment for statistical computing*. 4.2.1 ed. Vienna, Austria: R Foundation for Statistical Computing.

Rao, K., Anderegg, W.R.L., Sala, A., Martínez-Vilalta, J. & Konings, A.G. (2019) Satellite-based vegetation optical depth as an indicator of drought-driven tree mortality. *Remote Sensing of Environment*, 227, 125–136.

Rapaport, T., Hochberg, U., Cochavi, A., Karnieli, A. & Rachmilevitch, S. (2017) The potential of the spectral 'water balance index' (WABI) for crop irrigation scheduling. *New Phytologist*, 216, 741–757.

Reich, P.B., Wright, I.J., Cavender-Bares, J., Craine, J.M., Oleksyn, J., Westoby, M. et al. (2003) The evolution of plant functional variation: traits, spectra, and strategies. *International Journal of Plant Sciences*, 164, S143–S164. Available from: https://doi.org/10.1086/374368

Rønne, C., Åstrand, P.-O. & Keiding, S.R. (1999) THz spectroscopy of liquid H_2O and D2O. *Physical Review Letters*, 82, 2888–2891.

Rosas, T., Mencuccini, M., Barba, J., Cochard, H., Saura-Mas, S. & Martínez-Vilalta, J. (2019) Adjustments and coordination of hydraulic, leaf and stem traits along a water availability gradient. *New Phytologist*, 223, 632–646.

Sack, L., Cowan, P.D., Jaikumar, N. & Holbrook, N.M. (2003) The 'hydrology' of leaves: co-ordination of structure and function in temperate woody species. *Plant, Cell & Environment*, 26, 1343–1356.

Sack, L., John, G.P. & Buckley, T.N. (2018) ABA accumulation in dehydrating leaves is associated with decline in cell volume, not turgor pressure. *Plant Physiology*, 176, 489–495.

Sack, L., Melcher, P.J., Liu, W.H., Middleton, E. & Pardee, T. (2006) How strong is intracanopy leaf plasticity in temperate deciduous trees? *American Journal of Botany*, 93, 829–839.

Sack, L. & Pasquet-Kok, J. (2011) *Leaf pressure-volume curve parameters*. PrometheusWiki. Available from: https://prometheusprotocols.net/function/water-relations/pressure-volume-curves/leaf-pressure-volume-curve-parameters/. [Accessed 20th January 2020]

Sapes, G., Lapadat, C., Schweiger, A.K., Juzwik, J., Montgomery, R., Gholizadeh, H. et al. (2022) Canopy spectral reflectance detects oak wilt at the landscape scale using phylogenetic discrimination. *Remote Sensing of Environment*, 273, 112961.

Sartori, K., Vasseur, F., Violle, C., Baron, E., Gerard, M., Rowe, N. et al. (2019) Leaf economics and slow-fast adaptation across the geographic range of *Arabidopsis thaliana*. *Scientific Reports*, 9, 10758.

Scholes, D.R. & Paige, K.N. (2015) Plasticity in ploidy: a generalized response to stress. *Trends in Plant Science*, 20, 165–175.

Scoffoni, C., Pou, A., Aasamaaa, K. & Sack, L. (2008) The rapid light response of leaf hydraulic conductance: new evidence from two experimental methods. *Plant, Cell & Environment*, 31, 1803–1812.

Scoffoni, C., Rawls, M., Mckown, A., Cochard, H. & Sack, L. (2011) Decline of leaf hydraulic conductance with dehydration: relationship to leaf size and venation architecture. *Plant Physiology*, 156, 832–843.

Scoffoni, C., Vuong, C., Diep, S., Cochard, H. & Sack, L. (2014) Leaf shrinkage with dehydration: coordination with hydraulic vulnerability and drought tolerance. *Plant Physiology*, 164, 1772–1788.

Siefert, A., Violle, C., Chalmandrier, L., Albert, C.H., Taudiere, A., Fajardo, A. et al. (2015) A global meta-analysis of the relative extent of intraspecific trait variation in plant communities. *Ecology Letters*, 18, 1406–1419.

Thrane, L., Jacobsen, R.H., Uhd Jepsen, P. & Keiding, S.R. (1995) THz reflection spectroscopy of liquid water. *Chemical Physics Letters*, 240, 330–333.

Trueba, S., Pan, R., Scoffoni, C., John, G.P., Davis, S.D. & Sack, L. (2019) Thresholds for leaf damage due to dehydration: declines of hydraulic function, stomatal conductance and cellular integrity precede those for photochemistry. *New Phytologist*, 0, 134–149.

Tyree, M.T. & Hammel, H.T. (1972) The measurement of the turgor pressure and the water relations of plants by the pressure-bomb technique. *Journal of Experimental Botany*, 23, 267–282.

Valladares, F., Wright, S.J., Lasso, E., Kitajima, K. & Pearcy, R.W. (2000) Plastic phenotypic response to light of 16 congeneric shrubs from a panamanian rainforest. *Ecology*, 81, 1925–1936.

Violle, C., Navas, M.-L., Vile, D., Kazakou, E., Fortunel, C., Hummel, I. et al. (2007) Let the concept of trait be functional! *Oikos*, 116, 882–892.

Warton, D.I., Duursma, R.A., Falster, D.S. & Taskinen, S. (2011) Smatr 3– an R package for estimation and inference about allometric lines. *Methods in Ecology and Evolution*, 3, 257–259. Available from: https://doi.org/10.1111/j.2041-210X.2011.00153.x

Watson, M. & Casper, B. (1984) Morphogenetic constraints on patterns of carbon distribution in plants. *Annual Review of Ecology and Systematics*, 15, 233–258.

Williams, L.J., Cavender-Bares, J., Paquette, A., Messier, C. & Reich, P.B. (2020) Light mediates the relationship between community diversity and trait plasticity in functionally and phylogenetically diverse tree mixtures. *Journal of Ecology*, 108, 1617–1634.

Zhou, J., Cieraad, E. & Van Bodegom, P.M. (2022) Global analysis of trait–trait relationships within and between species. *New Phytologist*, 233, 1643–1656.

SUPPORTING INFORMATION

Additional supporting information can be found online in the Supporting Information section at the end of this article.

How to cite this article: Browne, M., Bartlett, M.K., Henry, C., Jarrahi, M., John, G., Scoffoni, C. et al. (2023) Low baseline intraspecific variation in leaf pressure-volume traits: Biophysical basis and implications for spectroscopic sensing. *Physiologia Plantarum*, 175(4), e13974. Available from: https://doi.org/10.1111/ppl.13974

Supplementary Materials

Supplementary Data Captions (see attached Excel Workbook)

Table S3.1. Pressure volume parameters (mean and standard error) for 12 California native species. List of variables, units and definitions are tabulated below. See Table S2 for species names associated with the species codes tabled.

Table S3.2. Pressure volume curve parameters, structural variables, and predicted values of pressure volume curve parameters from relationships presented in Bartlett et al., 2012 (see variable key below rows of data). Values are included for at least five individuals of 50 species and their source citation. "_a" indicates pressure volume curves made sun exposed fully developed leaves in a second study.

Table S3.3. Outlier test for each pressure volume curve parameter for each study species. I performed Dixon Q tests when greater than two-fold variation existed for a given trait. Legend of variables and their meanings are tabled below the rows of data.

Table S3.4. Species mean, standard error, and sample count for leaf morphological traits for 39 species in my database along with their sources. Standard deviations for leaf density were estimated by propagation of error (Beers, 1957). Legend of symbols provided below as well as the source references.

Table S3.5. Intraspecific correlation matrices for traits for each species and their significance (*p<0.05; **p<0.01; ***p<0.001) for raw, log and rank transformed data in that order separated by semicolons across all study species as well as mean untransformed correlation and count of significant correlations. Mean correlations are summarized by species matrices with and without apoplastic fraction (a_f).

Table S3.6. Ordinary least squares regression parameters for the plots of observed versus predicted values of pressure volume curve parameters (i.e., Ψ_{tlp}, $RWC_{tlp,s}$, C_{ft}), using prediction equations 8, 9 and 10; I provide the slope and intercept of the ordinary least squares regression line, R^2 and the associated p value for each species (indicated by their species code; see Table S3.2 for the associated species and genus names). I presented only the lines which were significant (i.e., p<0.05).

Table S3.7. Correlation matrices of species' coefficient of variation (CV) for pressure volume curve parameters and leaf traits. I include correlation coefficients and their significance (*p<0.05; **p<0.01; ***p<0.001) for raw, log and rank transformed data in that order separated by semicolons. Significant correlations are highlighted in yellow, i.e., if p<0.05 for both Spearman and Pearson correlation tests, with Pearson tests conducted on untransformed or log transformed data.

Table S3.8. Coefficients of variation (mean and standard error) for pressure volume curve parameters, morphological and compositional traits. Legend of variables and their meanings are tabled below.

Table S3.9. Estimated variation in the simulated leaf water potential based on scaling up from spectroscopy. I provide the root mean square error (RMSE), RMSE standard error, simulation mean RMSE, and simulation RMSE standard error for 1000 estimated of leaf water potential at five hydration states (ln PFR) for each for the simulations (A-C) of my bootstrapping analysis.

Supplemental Figures

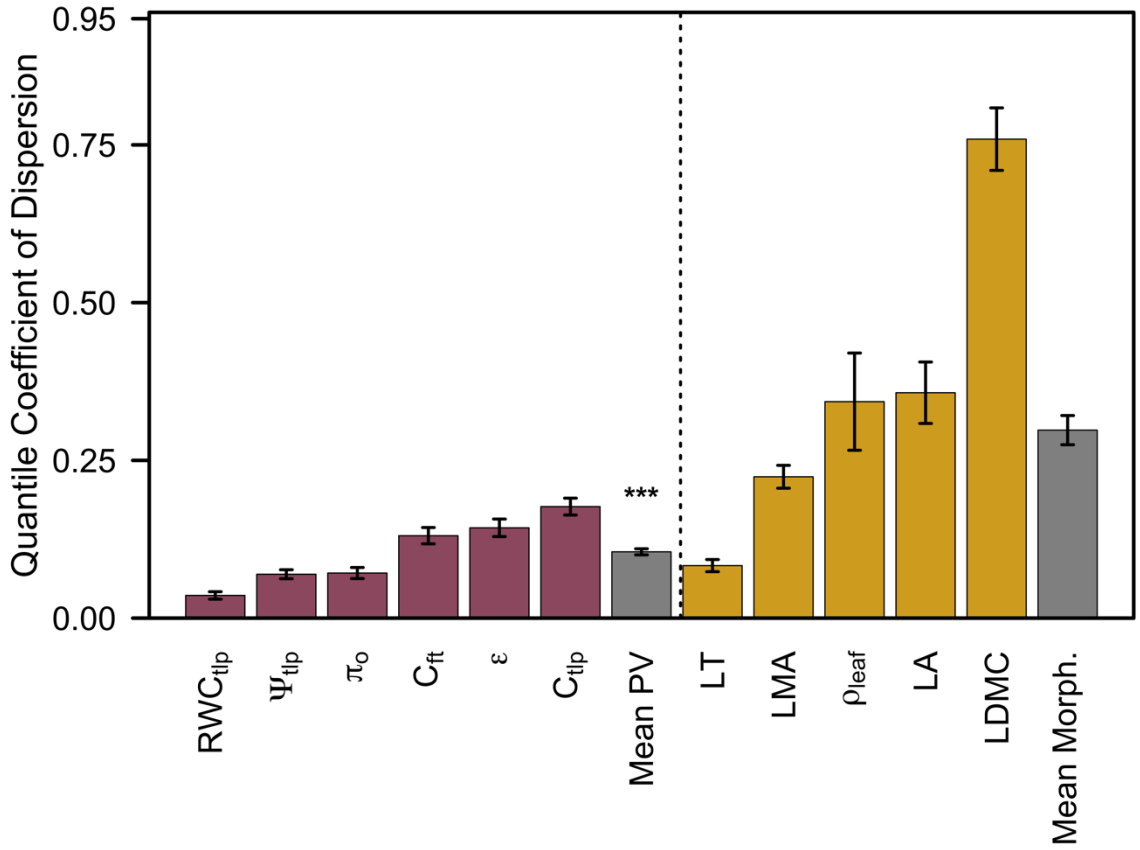

Supplemental Figure 3.1. Mean intraspecific variation among sun leaves of plants growing in similar conditions (ITV_{ref}) for pressure volume curve parameters and other morphological and compositional leaf traits for 39 species, separated by the dotted line and in each category ordered by increasing median quantile coefficient of dispersion (n=12-50 species). Error bars indicate the standard error of the mean and asterisks denote the significant difference between mean of pressure volume curve and morphological and compositional leaf traits (***p<0.001; Welch's Two Sample t-test).

Chapter 4: The contribution of osmotic adjustment to drought adaptation in *Arabidopsis thaliana*

Abstract

Traits that confer plant drought tolerance are increasingly prominent foci for studies of plant and ecosystem responses to climate change. Leaf osmotic potential at full turgor (π_o) is the main determinant of turgor loss (i.e., wilting) point, a threshold for stomatal closure and decline of photosynthetic function during drought. Intraspecific variation in π_o may thus influence the adaptation of populations along gradients of climatic aridity. Yet, the contribution of plasticity (adjustment) in π_o during drought to tolerance and its potential costs in relative growth rate (RGR) have not been quantified. For 29 ecotypes of *Arabidopsis thaliana* native to a wide range of climatic aridity and grown in a common garden, I tested the associations across ecotypes among the π_o of well-watered plants ($\pi_{o,w}$) and plants after drought ($\pi_{o,d}$), and osmotic adjustment ($\Delta\pi$), biomass allocation and structural traits, relative growth rate (RGR), and survival time under extreme drought, and with climatic aridity in ecotypes' native ranges. Among the 29 ecotypes, 65% showed adjustment to more negative π_o during the drought; and across those ecotypes, osmotic adjustment contributed strongly to post-drought π_o. Drought survival time was associated with lower $\pi_{o,w}$ and $\pi_{o,d}$ across all genotypes, and with $\Delta\pi$ for those ecotypes that adjusted. Ecotypes exhibited responses from drought avoidance (e.g., faster growth, greater alignment with climate) and resistant (e.g., slower growth, greater association between $\Delta\pi$ and $\pi_{o,d}$) strategies under dehydration. My findings among ecotypes of a given species exhibits the need to account for variation in response to stress across populations with distinct drought strategies.

Introduction

As droughts become increasingly prevalent in many locations globally, clarifying the traits that contribute to drought resilience becomes urgent. Variation in these traits among agricultural cultivars or across populations could explain reduction in productivity and mortality in crop and wild ecosystems worldwide (Allen et al., 2010; IPCC, 2014). For example, a lower osmotic potential at full turgor (π_o; see Table 4.1 for variables, units and definitions) drives a lower leaf water potential at turgor loss (π_{tlp}), and contributes to drought resistance, being associated with the maintenance of hydraulic and stomatal conductance, and photosynthetic gas exchange later into drought (Bartlett et al., 2016; Trueba et al., 2019). Theory maintains that greater plasticity in turgor loss point, known as osmotic adjustment (Bartlett et al., 2014; Blum, 2017), would enable drying plants to maintain greater stomatal opening (Henry et al., 2019), and hydraulic conductance (Scoffoni et al., 2008), and thereby greater drought resilience (de Bello et al., 2011) and contribute to the distribution of species in more arid climates (Bartlett et al., 2019; Brodribb et al., 2020; Rosas et al., 2019). Notably, plasticity in these traits may contribute to drought tolerance in two ways: resistance to drought stress would be associated with a greater plasticity and thus a more negative $\pi_{o,d,}$ whereas "avoidance" response may be associated with a lower plasticity in osmotic potential, and faster growth and allocation to reproductive structures such that a given population would set seed sooner to avoid future extremes (Fletcher et al., 2022). My aim was to quantify intraspecific plasticity in π_o ($\Delta\pi$ or osmotic adjustment) among ecotypes of a single species with a very widespread range in the temperate zone, *Arabidopsis thaliana,* and test for associations among osmotic adjustment, growth, and climate.

Osmotic adjustment ($\Delta\pi$) regulates tissue stress under drought and can shape responses to water deficit. $\Delta\pi$ is characterized by the accumulation of organic (e.g. proline) and/or inorganic

(e.g., K^+, Na^+, Cl^- or Ca^{2+}) solutes within the cell in response to dehydration or increased soil salinity and has been linked with resilience to drought across crop species (Blum, 2017; Girma and Krieg, 1992; González et al., 1999; Morgan, 1977). Among cultivated or wild species, even those with high $\pi_{o,w}$ may have greater $\Delta\pi$ under drought and thereby achieve relatively strong performance under drought. In a review of 26 studies of osmotic adjustment in crop varieties (e.g., *Helianthus annus, Glycine max* and *Pisum sativum*), species' varieties in 24/26 studies increased in yield with greater $\Delta\pi$ under drought (Blum, 2017). Among wild species, lianas have stronger osmotic adjustment than trees due to seasonal dehydration ($\Delta\pi$ =-0.43 MPa versus -0.12 MPa, for lianas and trees respectively), which may enable greater resilience in drought (Maréchaux et al., 2017). Among species of eastern Amazon rainforest, more drought resistant species were more likely to osmotically adjust under induced drought conditions (Binks et al., 2016). Notably, a global meta-analysis of seasonal osmotic adjustment in woody species found that $\Delta\pi$ was relatively conservative across species (mean $\Delta\pi$ = -0.29 ± 0.03 MPa; n = 240 species) and the well-hydrated osmotic potential at full turgor ($\pi_{o,w}$) was a greater predictor of the final post-drought osmotic potential at full turgor ($\pi_{o,d}$) and of the turgor loss point, but for herbaceous crops, $\Delta\pi$ made a strong contribution to $\pi_{o,d}$ (Bartlett et al., 2014). I hypothesized that across Arabidopsis ecotypes, $\Delta\pi$ would contribute strongly to $\pi_{o,d}$.

Given the strong association between $\pi_{o,w}$ and ecosystem aridity (Bartlett et al., 2014; Fletcher et al., 2018), the capacity for osmotic adjustment may support resistance and survival under drought. Yet, plants with a drought avoidance strategy might show a decoupling of osmotic adjustment and growth from climate. Across 15 ecotypes of *A. thaliana* native across an aridity gradient (Fletcher et al., 2022), three types of strategies were distinguished: resistance, i.e., the maintenance of function under stress; avoidance, i.e., the ability to grow rapidly under ideal

conditions; and ambivalence, i.e., strong stress sensitivity for ecotypes adapted to moist conditions (Table 4.2). Resistant ecotypes may have more negative $\pi_{o,w}$ and $\pi_{o,d}$, which would allow for maintenance of turgor during drought (Bartlett et al. 2012). This may be paired with slower growth overall and greater allocation towards roots (Reich, 2014). Alternatively, avoidant and ambivalent ecotypes may have higher values of $\pi_{o,w}$ and $\pi_{o,d}$ along with rapid and moderate growth, respectively. The ecotypes less intrinsically adapted to dehydration will allocate growth to leaves over roots, where avoidant ecotypes will utilize that greater photosynthetic capacity to produce flowers and seeds sooner. Across all ecotypes measured in Fletcher et al. (2022), a less negative $\pi_{o,w}$ was associated with moister native climate, while relative growth rate (RGR) was independent of climatic aridity (i.e., aridity index, mean annual temperature, and annual precipitation). The lack of association between growth and drought tolerance was evidence of a mixture of avoidant, resistant and ambivalent strategies, which would contribute to the species' wide overall ecological range. Yet, there have been no studies on the potential association of $\Delta\pi$ and $\pi_{o,d}$ (i.e., osmotic potential at full turgor for plants after drought) with climate and growth. I hypothesized that ecotypes specialized for water-abundant ecosystems (i.e., with less negative $\pi_{o,w}$) would show lower $\Delta\pi$ due to their lack of adaptation to water stressed conditions.

Thus, for 29 ecotypes of *A.thaliana*, I tested for relationships among osmotic potential variables (i.e., $\pi_{o,w}$ and $\pi_{o,d}$, and $\Delta\pi$), native climate variables, and relative growth rate and its components (including leaf mass per area (LMA), unit leaf rate (ULR) and leaf area ratio (LAR)), other biomass allocation variables (leaf mass fraction (LMF), root mass fraction (RMF), and reproductive mass fraction (ReMF)) and flowering time and survival under drought (i.e., time until death under lethal drought). I hypothesized that (1) $\Delta\pi$ would contribute to the osmotic potential at full turgor for droughted plants ($\pi_{o,d}$); (2) lower $\pi_{o,w}$ and $\pi_{o,d}$ and greater $\Delta\pi$ would be positively

coordinated with greater climatic aridity of the genotypes' native ranges, (3) with other drought tolerance traits (i.e., low SLA and high RMF), and with (4) survival time during drought, but (5) independent of RGR. Further, I tested these hypotheses among groups of ecotypes (i.e., those that osmotically adjusted in response to drought and those that not).

Materials and Methods

Plant material

Twenty-nine ecotypes of *Arabidopsis thaliana* cataloged for the 1001 Genome Project were grown to test the associations of leaf osmotic adjustment, climate, and growth (Figure 4.1, Table 4.3). The selected *A. thaliana* ecotypes represent populations from wide diversity of climatic aridity (estimated by aridity index and mean annual temperature) and from 10 "origin groups" as described in The Arabidopsis Information Resource (TAIR; Huala et al., 2001). Thus, the ecotypes represented a range of native climates from dry to mesic (total growing season precipitation from 29 mm to 1829 mm) and cold to warm (mean growing season temperature from 11.8°C to 27°C). Seeds were first cold-acclimated at 4°C for three days and sown in pots (7.95 cm width × 12.4 cm length × 5.87 cm deep) in soil (1:1:2:1:1 mixture of washed plaster sand, loam, peat moss, perlite, vermiculite). Individuals were grown in a climate-controlled glasshouse (minimum, mean and maximum values for temperature, 16.4°C, 22.3°C and 29.0°C; for relative humidity 18.6%, 46.5%, and 72.6%; and for irradiance 1.2, 95.1, 1128 μmol photons m^{-2} s^{-1}) at the University of California, Los Angeles, from February to March 2019. After approximately a week, I thinned plants to one individual per pot. Single individuals of each ecotype were randomized into blocks (each block consisting of two nursery trays of potted individuals). Blocks for control and drought-treatment plants (n=12 individuals per treatment) were then placed across three greenhouse benches.

Before the start of the drought period, all plants were drought-hardened for seven days, during which water was withheld. This pre-treatment was imposed such that the subsequent strong drought treatment would not be the first experienced by the experimental plants, and thus to better mimic natural plants facing successive escalating drought events (Ding et al., 2014; Hsiao et al., 1976). Following drought-hardening, all blocks were watered until the soil was fully saturated, and osmotic potential at full turgor ($\pi_{o,w}$) was determined for five individuals of each ecotype using an osmometer (see subsequent section). Plants under control conditions were kept well hydrated by watering all pots at least once per week to saturation. Drought-treated plants were allowed to dehydrate until 5 of 12 individuals of a given ecotype exhibited extreme stress, indicated by a distinctive change in leaf color from green to purple or brown, which often corresponded to complete plant collapse, indicating death. Plants were checked for these signs of extreme stress daily at 1100 h. When an ecotype had reached this stage, trays of stressed and well-watered individuals were brought to lab and leaves were excised (one leaf from each of five individuals from each treatment) and placed into a bag (Whirl-Pak, Nasco, Fort Atkinson, WI, USA), which had been exhaled into to equilibrate. Then, I measured leaf water potential with a pressure chamber (0.001 MPa resolution, Plant Moisture Stress Model 1000; PMS Instruments Co). All the droughted and control individuals of the ecotype were subsequently rehydrated overnight in dark, moist containers. The next day, individuals that became moldy at the end of the rehydration process or exhibited other deterioration (e.g., leaf drop or deeper color change) were excluded from leaf or whole individual measurements. In total, 26 of 29 ecotypes survived the drought experiment with at least 5 individuals for measurement of $\pi_{o,d}$ and $\Delta\pi$ (see following section). Five individuals of the control treatment for each ecotype (29 ecotypes) were harvested for growth measurements (i.e., leaf mass per area (LMA), unit leaf rate (ULR) and leaf area ratio (LAR); see section *Plant biomass*

and trait measurement). From each individual, five leaves were scanned (using an Epson Perfection 4490 Photo flatbed scanner, Seiko Epson Corporation), leaf area was determined using Image J (version 2.3.0; National Institutes of Health, USA), measured for mass using an analytical balance (0.01 mg; MS205DU Mettler Toledo, Toledo, OH), enabling calculation of leaf dry mass per unit area (Schindelin et al., 2012). Plants were separated into roots, remaining leaves, and reproductive parts (i.e., inflorescences), and mass values were determined for each compartment.

Determination of osmotic potential at full turgor, and the contribution of osmotic adjustment to post drought resilience

After harvest, the remaining plants from both treatments (droughted and control) were watered to saturation and rehydrated overnight in dark, moist containers. Then, osmotic potential at full hydration was estimated using the osmometer method for one disk from one leaf for five individuals from each ecotypes in each treatment (Bartlett et al., 2012a). Disks (4 mm diameter) were taken from leaves, and immediately submerged in liquid nitrogen. Once frozen for at least 2 minutes, disks were quickly punctured 10-15 times, and the osmolality of the cell sap was measured using osmometers (VAPRO 5520 and 5600 vapor pressure osmometers; Wescor, Logan, UT). Osmotic potential at full turgor then estimated using the osmolality of the disk.

I calculated osmotic adjustment as the difference between post-drought osmotic potential at full turgor ($\pi_{o,d}$) and well-watered osmotic potential at full turgor ($\pi_{o,w}$)

$$\Delta\pi = \pi_{o,d} - \pi_{o,w} \quad (1)$$

Standard deviations were determined for $\Delta\pi$ by propagation of error (Beers, 1957): Then, I calculated the percent relative contribution of $\Delta\pi$ and $\pi_{o,w}$ to $\pi_{o,d}$ as:

$$\text{Osmotic adjustment } (\Delta\pi) \text{ contribution} = \frac{\Delta\pi}{\pi_{o,d}} \cdot 100 \quad (2)$$

$$\text{Well} - \text{watered } \pi_O \text{ contribution} = \frac{\pi_{o,w}}{\pi_{o,d}} \cdot 100 \text{ (3)}$$

Plant biomass and trait measurement

Relative growth rate (RGR) was calculated for well-watered control individuals of each ecotype as:

$$\text{RGR} = \frac{\ln(M_2) - \ln(M_1)}{t_2 - t_1} \text{ (4)}$$

Where M_2 and M_1 are the total final and initial mass, respectively, and t_2 and t_1 are the days of the final and initial harvest, respectively. Leaf mass per area (LMA), unit leaf rate (ULR) and leaf area ratio (LAR) were calculated from control individuals of all ecotypes as follows:

$$\text{LMA} = \frac{\text{Leaf dry mass}}{\text{Leaf area}} \text{ (5)}$$

$$\text{LAR} = \frac{\frac{\text{Total leaf mass}}{\text{LMA}}}{\text{Total plant mass}} \text{ (6)}$$

$$\text{ULR} = \frac{\text{RGR}}{\text{LAR}} \text{ (7)}$$

LAR was calculated from the mean leaf mass per area for each ecotype (n = 5 individuals). Final leaf mass and total plant mass of control individuals were used for calculation of RGR and LAR. Growth of organs compared to total plant mass were also calculated for leaves (LMF), roots (RMF) and reproductive organs (ReMF), where each represented the quotient of the respective organ mass and total plant mass (Table S4.1).

Climate and flowering time data

Occurrence coordinates for each ecotype were obtained from information provided by the 1001 Genomes Consortium 2016 (https://1001genomes.org/accessions.html) (Alonso-Blanco et al., 2016a). Nineteen annual climate variables were downloaded from WorldClim Global Climate Data (BioClim), and twenty-two monthly variables from CRU-TS-4.03 from the Climatic Research Unit, University of East Anglia (Harris et al., 2014), which was downscaled and

downloaded from WorldClim's historical climate database (Fick and Hijmans, 2017) (Table S4.1; all climate terms and abbreviations summarized in Table S4.2). Additionally, aridity index and potential evapotranspiration (PET) were obtained from the Consultative Group for International Agriculture Research (CGIAR) Consortium for Spatial Information (CSI) database (Ferrero-Serrano and Assmann, 2019; Monroe et al., 2018). PET was estimated by the Penman-Monteith equation. Climate information was extracted at each coordinate for each ecotype using ArcMap (version 10.0). Growing season variables were calculated with historical climate data using data for the months with ≥4°C mean temperature and precipitation ≥ 2mm x mean temperature (Lasky et al., 2012). Lastly, flowering time at 10°C and 16°C for each of the 29 ecotypes was obtained from the 1001 Genomes Consortium (Alonso-Blanco et al., 2016b).

Statistical and phylogenetic analyses

I performed statistical analyses across all genotypes, as well as among adjusters and non-adjusters (i.e., ecotypes which had $\Delta\pi < 0$ and $\Delta\pi \geq 0$, respectively). I estimated the associations of traits and climate variables accounting phylogenetic relatedness, i.e., with kinship. I tested for correlations among osmotic adjustment variables (i.e., $\pi_{o,w}$, $\pi_{o,d}$, and $\Delta\pi$), climate variables (e.g., mean annual precipitation, mean annual temperature, length of growing season) and growth and biomass allocation variables (i.e., RGR, ULR, LAR, LMF, RMF, and ReMF) across 29 ecotypes of *A. thaliana*. All 29 ecotypes were only used to test relationships among growth and climate, otherwise 26/29 ecotypes were used for testing correlations among osmotic, climate, and growth variables. To test these correlations, I implemented linear mixed effects models with kinship using the *lmekin* function in the coxme package (Therneau, 2020). Kinship matrices were derived from the 1001 Genomes Project data release v3.1 (Alonso-Blanco et al., 2016a). My models were fit with both untransformed and log-transformed data, to test for both linear and nonlinear (power

law) relationships. I used absolute values for traits which were negative (i.e., π_o, $\pi_{o,w}$, $\pi_{o,d}$) and transformed traits represented by both negative and positive values (i.e., temperature associated variables: mean annual temperature (MAT), growing season minimum and maximum temperatures, minimum temperature of the coldest month (bioclimatic variable 6), mean temperature of the wettest quarter (bioclimatic variable 8), mean temperature of the driest quarter (bioclimatic variable 9), mean temperature of the coldest month (bioclimatic variable 11); as well as osmotic adjustment traits, i.e., $\Delta\pi$, and the contributions of $\Delta\pi$ and $\pi_{o,w}$ to $\pi_{o,d}$) by adding the absolute value of the lowest value of the dataset minus 1. I report in the main text the most significant relationship (i.e., lowest corrected AIC) for untransformed or log-transformed data and all relationships are presented in Table S3.

I performed a repeated measures analysis of variance (ANOVA) to test for associations among individuals differences within genotypes, from well-watered to droughted estimates of osmotic potential at full turgor, and treatment using *aov* function in the stats package (R Core Team, 2023) (Table S4.4).

To determine the causal contribution of the components of RGR (i.e., ULR and LAR), I applied a causal partitioning analysis (Buckley and Diaz-Espejo, 2015; Fletcher et al., 2022; John et al., 2017), which considers the function of RGR and estimates to infinitesimal change in RGR caused by ULR and LAR, integrated across all my genotypes, to provide the total contribution of each variable to the difference among genotypes. This approach avoids the influence of covariation among RGR components in correlations among those variables (John et al., 2017). Statistical analyses were performed using the R Statistical Software (v. 4.2.3; (R Core Team, 2023)).

Results

Variation across ecotypes in osmotic adjustment and growth and biomass allocation

The 29 ecotypes of *A. thaliana* varied in their adaptation to aridity based on their range in native climate (Table 4.3), and well hydrated osmotic potential at full turgor ($\pi_{o,w}$) was on average -0.84 $\pm$ 0.02 MPa and ranged across ecotypes from -0.72 MPa to -1.01 MPa (Table S4.1). Further, response to drought varied strongly among ecotypes. In the drought experiment, the leaf water potential declined on average across ecotypes to -1.51 ± 0.12 MPa (Figure S4.1). For 17/26 (65%) of ecotypes, osmotic adjustment to a more negative π_o occurred, with average post-drought osmotic potential at full turgor ($\pi_{o,d}$) of -0.94 $\pm$ 0.05 MPa, varying across ecotypes from -0.61 MPa to -1.71 MPa, significantly different from the control individuals (p=0.003) (Figure 4.2a). In 9/26 ecotypes, there was no negative osmotic adjustment ($\Delta\pi \geq 0$). Across all genotypes, osmotic adjustment ($\Delta\pi$) ranged from -0.91 to 0.17 MPa, on average -0.11 ± 0.05 MPa, a significantly greater shift than occurred on average for my control well-watered plants for the duration of the study ($\Delta\pi$ = 0.06 $\pm$0.02 MPa; Welch's Two Sample test, p=0.006) (Figure 4.2b). Among the ecotypes that adjusted, the average $\Delta\pi$ was -0.21 $\pm$ 0.06 MPa. The leaf water potential at harvest was not correlated with $\pi_{o,d}$ or $\Delta\pi$ for drought treatment plants.

If the contribution of $\Delta\pi$ or $\pi_{o,w}$ to $\pi_{o,d}$ for a given ecotype exceeded 50%, that variable was determined to be the more important determinant of the magnitude of $\pi_{o,d}$. Across ecotypes of *A. thaliana*, $\pi_{o,w}$ was the primary determinant of $\pi_{o,d}$. Well-watered osmotic potential at full turgor ($\pi_{o,w}$) contributed to 97.0% of $\pi_{o,d}$ (ranging from 46.6-124%) for 25/26 genotypes. By contrast, $\Delta\pi$ contributed to $\pi_{o,d}$ on average 15.3% (ranging from 1.83-53.4%); indeed, $\Delta\pi$ contributed > 50% to the $\pi_{o,d}$ for only 1/26 of ecotypes (CS76774) (Figure S4.2).

The ecotypes also varied substantially in drought survival, and in relative growth rate (RGR) and other functional traits for well-watered plants. Ecotypes survived 26-35 days under the drought treatment. Relative growth rate (RGR) varied 1.66-fold from 0.15 to 0.24 g g^{-1} day^{-1}, and ecotypes varied seven-fold in leaf mass per area (LMA), eight-fold in leaf area ratio (LAR) and unit leaf rate (ULR) respectively, ten-fold in LMF and in RMF, and seven-fold in ReMF (Table S4.1).

Correlations among osmotic adjustment variables

I found strong correlations across ecotypes among osmotic adjustment variables (i.e., $\pi_{o,w}$, $\pi_{o,d}$ and $\Delta\pi$) for drought treated individuals (regression analyses accounting for kinship). Despite $\Delta\pi$ accounting for the minority of variation in $\pi_{o,d}$ (and $\pi_{o,w}$ accounting for the majority) across ecotypes, $\pi_{o,d}$ was strongly related to $\Delta\pi$ (r= -0.87; p<0.001) and independent of $\pi_{o,w}$ (r= 0.25; p=0.27), which in turn was independent of $\Delta\pi$ (r = 0.17; p=0.38) (Figure 4.3; Table S4.3). This pattern was due to the existence of adjusters and non-adjusters. When considering adjuster and non-adjuster ecotypes separately, among adjusters, $\pi_{o,d}$ was related to strength of adjustment (r=-0.87; p<0.001; Figure 4.3B), whereas among non-adjusters, $\pi_{o,d}$ was related to $\pi_{o,w}$ (r=0.71; p=0.002) (Figure 4.3C; Table S4.3). $\Delta\pi$ was unrelated to $\pi_{o,w}$ for both the adjusters and non-adjusters (Figure 4.3a; Table S4.3).

Correlations among osmotic adjustment and growth with survival of extreme drought

Among drought treated plants, ecotypes with more negative $\pi_{o,w}$ and $\pi_{o,d}$ survived longer into the drought treatment (i.e., longer "time until death", in days) (r = 0.52-0.55; p=0.001; Figure 4.4A & B; Table S4.3). While among the non-adjusters those with more negative $\pi_{o,w}$ survived

longer (r=0.91, p<0.001), among the ecotypes that did adjust, those with more negative $\pi_{o,d}$ survived longer (r=0.69, p<0.001). Across all ecotypes, there was no significant relationship between $\Delta\pi$ and survival time, though this association was found considering only the adjusters; those with stronger adjustment survived longer (r=-0.48, p=0.03). Drought individuals' harvest leaf water potential was not associated with the survival time throughout the drought among the drought treated plants.

Functional traits that mechanistically contribute to drought adaptation were related to drought survival time. For adjusters alone, those with greater a greater LMA survived longer (r = 0.68; p <0.001; Figure 4.4D). Across all ecotypes, and for adjusters and non-adjusters separately, those with greater allocation to root tissue survived longer (r=0.55-0.64; p = 0.01 - <0.001) (Figure 4.4E; Table S4.3). I also found strong relationships among other growth and biomass allocation traits and survival in response to drought. Across all ecotypes and the non-adjusters, those with longer time until flowering survived longer (r = 0.60 and 0.79, respectively; p < 0.001; Figure 4.5A and Table S4.3). Further, for all ecotypes and the adjusters considered separately, faster relative growth rate (RGR) was associated with a shorter survival time (r = -0.52 and -0.74, respectively; p = 0.002 and <0.001, respectively; Figure 4.5B). Across all ecotypes, a higher LAR, higher LMF and lower ULR and ReMF were linked with longer survival (r = 0.40-0.62; p = 0.003- <0.001; Figure 4.5C-F), and similarly for LAR, LMF and ReMF for the adjusters considered separately (r = 0.50-0.69; p = 0.04- <0.001; Figure 4.5C, E & F).

Correlations among osmotic adjustment variables and growth

I tested for the relationships among osmotic adjustment growth and biomass allocation traits of well-watered plants (i.e., RGR, LMA, LAR, ULR, LMF, RMF, ReMF). The adjusters showed

positive associations of $\pi_{o,w}$ and $\pi_{o,d}$ with RGR (r = 0.56 and 0.56, respectively; p = 0.007 and 0.007; Figure 4.6A and E, and Figure S4.4). Across all ecotypes, $\pi_{o,d}$ and $\Delta\pi$ were negatively related to LAR (r = -0.56 and -0.51; p <0.001 and p=0.003; Figure 4.6F and J, also see Figure S4.5 and S4.6), and positively related to ULR (r = 0.56 and 0.56, respectively; p =0.02 and p=0.01; Figure 4.6G and K, also see Figure S4.5 and S4.6), and the same trend was also found for adjusters alone (LAR r = -0.62 and -0.51, ULR r = 0.62 and 0.44; p = 0.001-0.02; Figure 4.6F, G, J and K, also see Figure S4.5 and S4.6). Lastly, ecotypes (i.e., across all ecotypes and the non-adjusters specifically) with higher $\pi_{o,w}$ showed lower leaf mass per area (all ecotypes r = 0.37, p=0.047; non-adjuster r = 0.56; p=0.04) (Figure 4.6D and Figure S4.4; Table S4.3).

There were no significant correlations of RGR with biomass allocation variables (Figure S4.3). Nonetheless, my causal analysis indicated that across all ecotypes and adjusters, ULR was the strongest determinant of RGR on average (95.4% for all and 250% among adjusters), whereas for the non-adjuster ecotypes, LAR also contributed strongly to RGR (69.6%) compared to ULR (30.4%) (Figure S4.7).

Correlations among osmotic adjustment, growth, survival and native climate

I assessed whether $\pi_{o,w}$, $\pi_{o,d}$ and $\Delta\pi$ were associated with the native climates of *A. thaliana* ecotypes, including average growing season aridity index, total growing season precipitation, average growing season temperature, maximum growing season temperature, potential evapotranspiration, plant extractable water capacity of soil, and flowering time at 10°C and 16°C) (Table S4.1). There were no significant relationships of $\pi_{o,w}$, $\pi_{o,d}$ or $\Delta\pi$ with mean annual precipitation, mean annual temperature, or aridity index across all ecotypes or within adjusters and non-adjuster ecotypes (Tables S4.3). Indeed, across all ecotypes there were few associations among climate and osmotic variables. Well-watered osmotic potential at full turgor was negatively

associated with mean diurnal range in temperature (r = -0.52; p = 0.002), elevation (r=-0.60; p<0.001), and spring rainfall (r=-0.40; p=0.03), and positively associated with the minimum temperature and wind speed of the growing season (r=0.44 and 0.47, respectively; p = 0.008 and 0.02), wind speed from January and April (r = 0.45; p = 0.01) (Figure S4.8I, G, B,D, and E). Both the adjusters and non-adjusters showed the same trends between $\pi_{o,w}$ and mean diurnal range and elevation as across all ecotypes (r= -0.49 and -0.59, respectively) (Figure S4.8I and F). However, $\pi_{o,w}$ among the adjusters was also associated with precipitation in the warmest quarter (bioclim 18; r = 0.54), annual potential evapotranspiration (r = -0.48; p=0.03), spring rainfall (r=-0.52; p=0.02), summer NDVI and solar radiation intensity through January and April (r= 0.53 and -0.51, respectively) (Figure S4.8J, G, H, K). The non-adjuster $\pi_{o,w}$ significantly correlated with the minimum and average temperature and wind speed of the growing season (r= 0.59, 0.62 and 0.60, respectively; p = 0.03, 0.02 and 0.03), wind speed from January and April (r = 0.62; p = 0.02) (Figure S4.8A, B, D, E). The post-drought osmotic potential at full turgor ($\pi_{o,d}$) was not significantly related to climate variables across all ecotypes or among the adjusters. Among the non-adjusters, $\pi_{o,d}$ was associated with mean diurnal range in temperature (r = 0.81; p < 0.001), the minimum temperature in the coldest month (r = 0.62; p=0.01), annual range in temperature (r=-0.56; p=0.04), mean temperature of the driest and coldest quarters (r = 0.56; p=0.04), the minimum temperature, PET, solar radiation and wind speed of the growing season (r=0.63, -0.72, -0.62, 0.65, respectively; p = 0.01, 0.002, 0.02, and 0.01), mean temperature, minimum temperature and wind speed from January and April (r = 0.57, 0.60, 0.75; p = 0.04, 0.02, and <0.001) (Figure S4.9A-K). $\Delta\pi$ was similarly not associated with climate across all ecotypes but showed strong relationships for both non-adjusters and adjusters. The non-adjusting ecotypes showed significant relationships with precipitation (e.g., precipitation in the driest month, quarter

and seasonality; r= -0.56, 0.63, and -0.57, respectively) (Figure S4.10A-C). Additionally, for this group, Δπ and climatic water deficit, average growing season maximum temperature, and VHI Summer were related (r=0.65, -0.60, -0.63, respectively) (Figure S4.10D-F). Adjuster Δπ was associated with wind speed variables (i.e., average growing season wind speed and wind speed between January and April; r= 0.48, and 0.46, respectively) (Table S4.3) (Figure S4.10G -H).

There were several significant relationships between survival time, growth and climate. Relative growth was associated with elevation and precipitation in the wettest quarter and month. Slower growing ecotypes were found at lower elevations (r= 0.38, p= 0.04), while faster growing ecotypes were found in climates with greater precipitation in the wettest quarter (r=-0.56, p = 0.04) and month (r = -0.58, p=0.03) (Figure S4.11A-C). Neither the adjusters nor the non-adjusters alone showed associations between growth and climate. Survival time was associated with elevation, flowering time at 10°C and 16°C, and evapotranspiration. Non-adjusting ecotypes from greater elevations survived fewer days into the drought (r=-0.81, p<0.001; Figure S4.12A) and those with longer flowering times at 10°C and 16°C survived longer (r=0.60 and 0.79, respectively, p=0.03 and <0.0001; Figure S4.12B and C). Additionally, across all ecotypes and the adjusters longer flowering times at 16°C were associated with longer survival (r=0.60 and 0.53, respectively, p<0.0001 and p = 0.01; Figure S4.12B). The adjusting ecotypes alone showed a strong association between evapotranspiration and survival where survival was greatest for those from native climates with greater evapotranspiration (r=0.48; p=0.03; Figure S4.12D).

Discussion

I tested the associations among drought resilience traits in the first drought experiment estimating both osmotic adjustment and growth for *A. thaliana*. I found modest absolute change of the osmotic

potential at full turgor from well-watered to droughted conditions. Yet, although associations of these traits with native climate across all ecotypes were few, more relationships with climate were found for the non-adjusting ecotypes. These findings provide compelling evidence among my set of ecotypes for the importance of drought avoidance and resistance in the adaptation of ecotypes across their climatic range.

Contribution of $\pi_{o,w}$ ***and*** $\Delta\pi$ ***to*** $\pi_{o,d}$

My finding of a greater contribution of $\pi_{o,w}$ to $\pi_{o,d}$ corroborates previous work on these parameters on global wild and crop species (Bartlett et al., 2014). There, the authors found that the $\pi_{o,w}$ and $\pi_{o,d}$ were strongly correlated and $\Delta\pi$ contributed 16%, compared to my 15.3%, to the magnitude of the $\pi_{o,d}$. I found strong association with a single species among $\pi_{o,w}$ and $\pi_{o,d}$; however, it was only evident among non-adjusting ecotypes. Though across all genotypes and the adjusting ecotypes, I found support for my hypothesis of a significant association between $\Delta\pi$ and $\pi_{o,d}$. Bartlett et al. (2014) found a similar predominance of the $\Delta\pi$ and $\pi_{o,d}$ relationship among cultivars within species but suggested that the relationship was driven by the lack of drought hardening. Given our conditioning of the ecotypes, this disassociation among $\pi_{o,w}$ and $\pi_{o,d}$ across all ecotypes shows a preference for a drought resistance.

Implications of variation in survival time and growth rate

I expected the growth to be independent of the osmotic variables. That was true across all ecotypes, but I found significant relationships when separating the osmotic adjusters and non-adjusters. I found evidence of a trade-off between drought resistance and drought avoidance strategies, corresponding to slower vs faster growth rate and greater vs lower allocation to reproductive

organs among the ecotypes of *A. thaliana*. This phenomenon has been characterized across species on the spectrum of "fast-slow" plant life strategy where growth is limited in stressful environments (Wright et al., 2004). However, these findings indicate support for a generalized response even within a given species and exhibit the strength of water deficit on growth rates. Ecotypes which grew slower, and often presented more drought resistant physiology (e.g., more negative $\pi_{o,w}$), survived much further into the drought.

Correlations of osmotic variables and growth with climate

Across all ecotypes, I found few associations between climate variables $\pi_{o,w}$, $\pi_{o,d}$, and $\Delta\pi$ and none with gross climate variables such as mean annual precipitation or temperature. All osmotic variables were associated with at least one precipitation (e.g., bioclim13 and bioclim14; precipitation of the wettest and driest month) and temperature variable (e.g., bioclim2, mean diurnal range, and average maximum temperature of the growing season). These relationships were primarily driven by individual groups of ecotypes, highlighting differential intraspecific responses to drought that appear to correspond to the growing conditions of a genotype's range. Fletcher et al. (2022) found strong relationship between well-watered osmotic potential at full turgor and aridity index across 15 ecotypes of *A. thaliana* but similar to this study, they also found no relationship with relative growth rate, mean annual temperature, annual precipitation across all ecotypes. Thus, the only relationships among climate and osmotic variables across all of my ecotypes were for average and minimum growing season temperature, elevation, mean diurnal range, spring rainfall, and growing season and January – April windspeed. This may be indicative of the ecotypes' phenology but also the importance of hydraulic parameters to survival. Across an aridity gradient, Rosas et al. (2019) found a predominance among hydraulic parameters (e.g.,

Huber value and π_{tlp}) driving trait variability within species. Previous work has also found lower baseline intraspecific variation in hydraulic parameters, which may be the result of the scale of the measurement (i.e., among leaves) and environment selection (Marks, 2007; Browne et al., 2023). Together the lower variation in hydraulic traits due to the strength of environmental selection could ensure survival across ecotypes and among groups of ecotypes reinforce the impact of microclimates.

Implications for intraspecific response to drought and conservation

The impacts of drought on shift in annual species community structure (Brodribb et al., 2020; Kraft, 2016). Annual species and individual responses to drought can fall into three strategies. They may be resistant to the drought, such that they are able to maintain cellular turgor, photosynthesis albeit at a lower rate, and have a relatively lower growth rate. Second, they may avoid the drought, whereby they mitigate the stress by achieving rapid growth when resources are available. Lastly, they may be ambivalent, i.e., drought sensitive. My selection of the *A. thaliana* ecotypes overall showed all three strategies, in their associations of slow growth with survival and including osmotic adjusters and non-adjusters. Conservation of the multiple populations of a species should account for the variation among them in drought strategies. Thus, there is a need to consider comprehensive estimates of the variation within Arabidopsis that accounts for strategy variation among ecotypes.

Tables

Table 4.1. Leaf water status, osmotic adjustment, climate and growth variables, symbols, units, and definitions. Full list of climate variables is available in Supplemental Table 2.

Variable	Symbol	Unit	Definitions
Leaf water status and osmotic adjustment			
Leaf water potential	Ψ_{leaf}	MPa	Water status variable indicating the bulk leaf average chemical potential of water within leaf cells
Osmotic potential	Ψ_s	MPa	Represents the concentration of cell solutes and component of leaf water potential
Osmotic potential at full turgor	π_o	MPa	Solute concentration at full turgor (i.e., Ψ_S when relative water content=100%)
Well-watered osmotic potential at full turgor	$\pi_{o,w}$	MPa	Solute potential at full turgor under well-watered conditions
Droughted osmotic potential at full turgor	$\pi_{o,d}$	MPa	Solute potential at full turgor post drought
Osmotic adjustment	$\Delta\pi$	MPa	Change in solute potential at full turgor from well-watered to post drought conditions
Osmotic potential at turgor loss point	π_{tlp}	MPa	Solute potential at turgor loss i.e., when pressure potential equals 0
Time until death	TTD	days	Days from start of experiment until 5/21 individuals had died
Climate variables (see Supplemental Table 2 for extended list of climate variables)			
Mean annual temperature	MAT	°C	

Mean annual precipitation	MAP	mm	Average precipitation in a year
Potential evapo-transpiration	PET	unitless	Estimate of atmospheric demand for water
Aridity Index	AI	unitless	Index of precipitation to PET and is indicative of climate dryness
Length of growing season	Length GS	days	Number of days of the year with ≥4°C mean temperature and precipitation ≥ 2mm x mean temperature
Flowering time	FT	days	Days until beginning of flower phenology at 10 or 16°C within text
Growth and allocation variables			
Relative growth rate	RGR	$g \cdot day^{-1}$	Change in mass per day from sowing to harvest
Leaf mass per area	LMA	$g \cdot m^{-2}$	Ratio of mass of dry leaf lamina to leaf area
Leaf area ratio	LAR	$cm^2\ g^{-1}$	Ratio of leaf area to plant dry mass. Reflects size of photosynthetic surface relative to respiratory mass
Unit leaf rate	ULR	$g \cdot day^{-1} \cdot cm^{-2}$	Reflects efficiency of the assimilatory organs to producing new growth. Can reflect light availability and leaf display.
Leaf mass fraction	LMF	$g \cdot g^{-1}$	Proportion of leaf dry mass to total individual dry mass
Reproductive mass fraction	ReMF	$g \cdot g^{-1}$	Proportion of inflorescence dry mass to total individual dry mass

Root mass fraction	RMF	$g \cdot g^{-1}$	Proportion of root dry mass to total individual dry mass

Table 4.2. In response to drought stress, three types of strategies may arise: resistance, i.e., the maintenance of function under stress; avoidance, i.e., the ability to grow rapidly under ideal conditions; and ambivalence, i.e., strong stress sensitivity for ecotypes adapted to moist conditions. Tabled are osmotic, growth and allocation traits, the expected response under resistant, avoidant and ambivalent strategies and the associated reasoning for the response.

Trait	**Resistant**	**Avoidant**	**Ambivalent**	**Reason**
Osmotic traits (i.e., $\pi_{o,w}$,$\pi_{o,d}$, $\Delta\pi$)	Low values of $\pi_{o,w}$ and $\pi_{o,d}$ and greater $\Delta\pi$	High values of $\pi_{o,w}$ and $\pi_{o,d}$	High values of $\pi_{o,w}$ and $\pi_{o,d}$	More negative $\pi_{o,w}$ or $\pi_{o,d}$ allow for maintanance of turgor during drought, thus preventing irreparable hydraulic damage (Bartlett et al. 2012)
Growth (i.e., RGR, LAR, ULR, FT)	Slow	Rapid	Moderate	These traits a predominantly associated with fast-slow continuum, such that species that are more resistant to drought are more likely to grow faster to avoid further degradation (Reich, 2014)
Allocation (LMF, RMF, REMF, LMA)	Low LMF, high RMF, high LMA, low ReMF	High LMF, low RMF, low LMA, high ReMF	High LMF, low RMF, low LMA	Ecotypes/species less susceptible to deleterious effects of drought are associated with thicker leaves, deeper roots, which

allow them to be

ambivalent to dehydration.

Table 4.3**.** Ecotypes of *Arabidopsis thaliana* grown experimental presented with their origin group, pre and post drought osmotic potential at full turgor ($\pi_{o,w}$ and $\pi_{o,d}$), leaf mass per area (LMA), time until death (TTD), flowering time, and climate variables (mean annual temperature (MAT) and mean annual precipitation (MAP)).

Genotype	**Origin group**	$\pi_{o,w}$	$\pi_{o,d}$	**LMA**	**TTD**	**FT10**	**MAT**	**MAP**
		MPa	MPa	$g*m^{-2}$	d	d	deg C	mm
CS76375	Asia	-0.74	-0.87	17.2	45	82	4.2	513
CS76382	Asia	-0.74	-0.65	18.7	41	69.8	-3.9	819
CS76411	Relict	-0.95	-0.57	22.3	48	75.8	17.8	546
CS76413	Admixed	-0.78	-0.81	18.4	45	114	10.2	544
CS76433	Asia	-0.81	-0.75	24.3	49	71.3	3.6	169
CS76441	Germany	-0.96	-0.94	27.3	47	81.5	7.6	1824
CS76498	Germany	-0.76	-0.73	11.1	42	71.0	8.1	750
CS76514	Western Europe	-0.83	-0.77	19.5	47	61.5	9.8	701
CS76519	Central Europe	-0.81	-0.73	11.9	40	57.8	9	518
CS76522	Asia	-0.72	-0.75	12.7	42	65.8	0.9	454
CS76525	Germany	-0.83	-0.86	14.9	41	74.8	9.8	610
CS76644	North Sweden	-0.80	-0.63	11.3	45	97.0	3.2	656
CS76678	South Sweden	-1.01	-0.86	25.0	48	88.0	6.8	805
CS76710	North Sweden	-0.90	-0.74	9.79	47	95.5	2.9	615
CS76740	Relict	-0.84	-0.82	35.0	46	72.3	18.3	177
CS76769	Italy/Balkan/Caucasus	-0.90	-0.96	17.3	41	71.3	13.8	485
CS76774	Spain	-0.79	-0.82	20.0	48	69.8	15.3	354
CS76789	Relict	-0.86	-0.80	12.0	45	62.8	22.2	369
CS76844	Italy/Balkan/Caucasus	-0.94	-0.82	14.1	45	61.3	15.9	587

CS76894	Spain	-0.77	-0.79	20.9	46	57.3	14.6	483
CS76944	Admixed	-1.01	-0.90	18.5	47	78.8	9.9	559
CS76994	Admixed	-0.90	-0.81	11.6	44	69.8	2.6	297
CS77062	Western Europe	-0.80	-0.68	13.2	45	67.5	13.5	455
CS77150	South Sweden	-0.92	-0.84	19.3	45	101	7.8	518
CS77156	Admixed	-0.91	-0.76	27.4	48	82.5	7.2	2190
CS77356	South Sweden	-0.91	-0.65	68.9	46	83.8	7.5	613
CS77389	Admixed	-0.78	-0.88	16.3	44	81.3	14.9	2385
CS78835	Spain	-0.76	-0.82	15.5	45	64.3	16.2	618
CS78888	Admixed	-0.86	-0.86	26.6	44	71.8	9.6	816

Figures

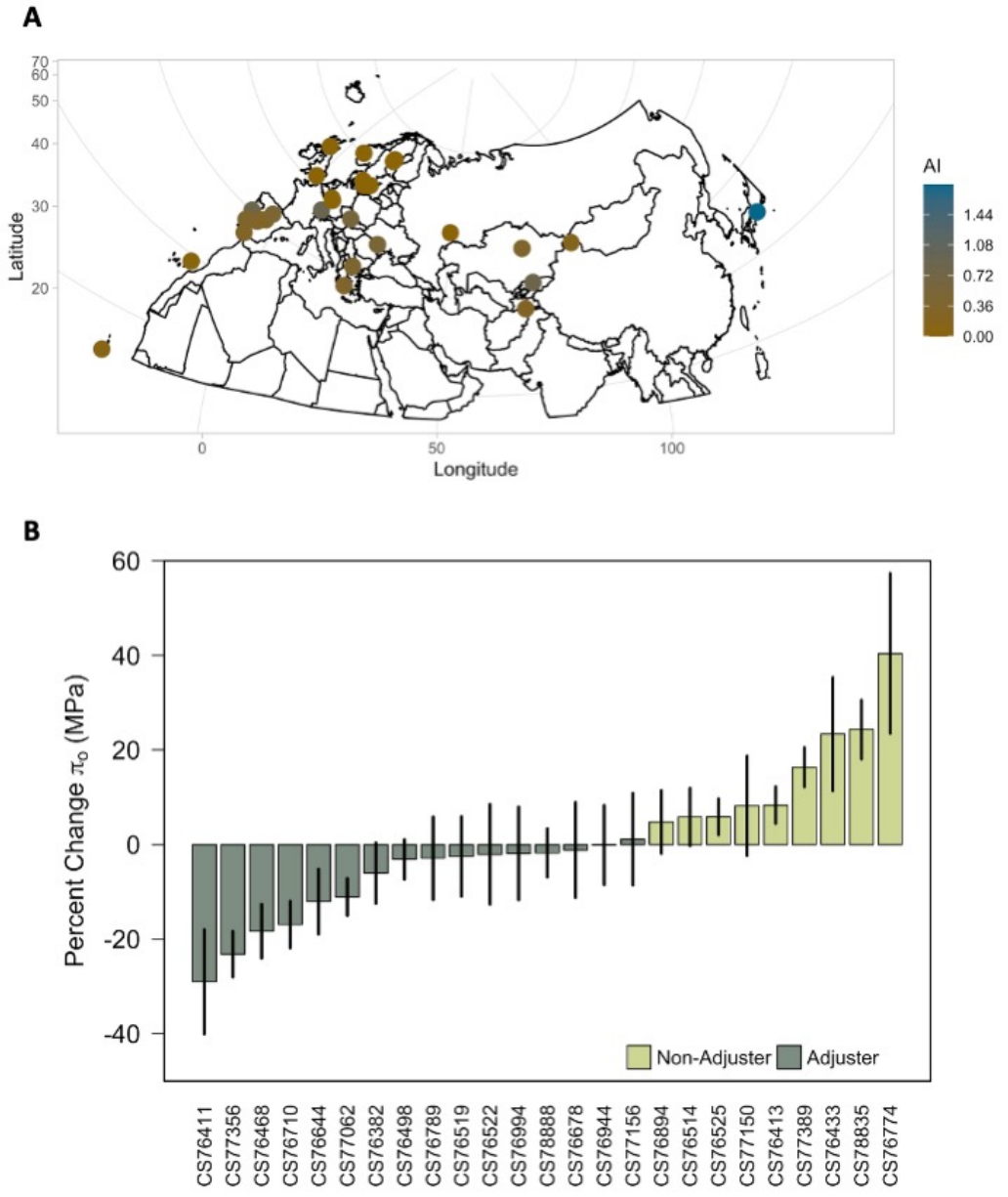

Figure 1. Map of provenance for 26 ecotypes of *Arabidopsis thaliana* catalogued in the 1001 Genome Project (A). Individuals from each provenance were grown in a climate-controlled glasshouse at the University of California, Los Angeles. Each point represents the provenance of an ecotype and each scaled color represents the aridity index (AI) of the associated climate. Individuals were allowed to dehydrate and by the end of the drought cycle, they showed a range

of change in their osmotic potential at full turgor ($\Delta\pi$) from -0.91 to 0.17 MPa (B). Negative values indicate osmotic adjustment that would provide drought resistance. Light green points and lines represent ecotypes which had not osmotically adjusted, and darker green points represent those which had adjusted. Statistical significance; *$p<0.05$; **$p<0.01$; ***$p<0.001$.

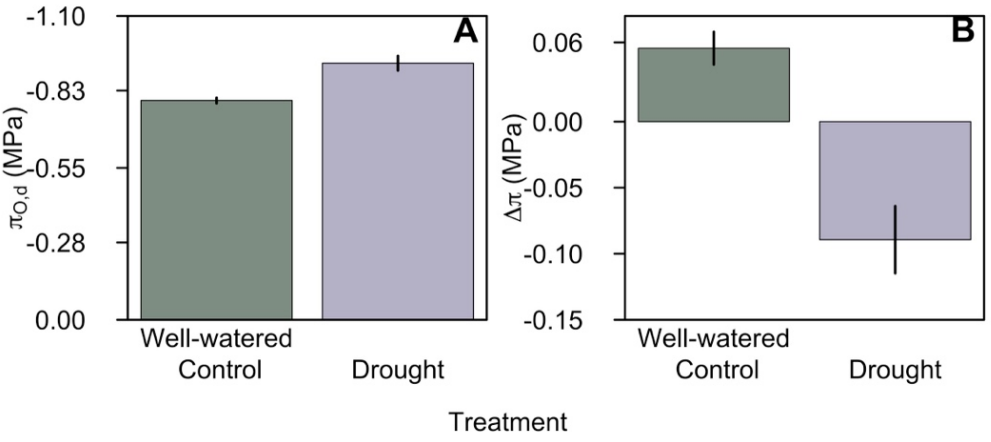

Figure 2. After five of 12 individuals of *Arabidopsis thaliana* from each ecotype exhibit strong negative signs to the drought experiment, I harvested the control and droughted individuals of 29 and 26 genotypes respectively. Before rehydration, I equilibrated and estimated leaf water potential (Ψ_{leaf}; A). Then, entire plants were rehydrated overnight and I estimated the post drought osmotic potential at full turgor ($\pi_{o,d}$; B) and the change in osmotic potential at full turgor from well-watered to post drought conditions ($\Delta\pi$; C). Light green points and lines represent ecotypes which had not osmotically adjusted, and darker green points represent those which had adjusted. Statistical significance; *p<0.05; **p<0.01; ***p<0.001.

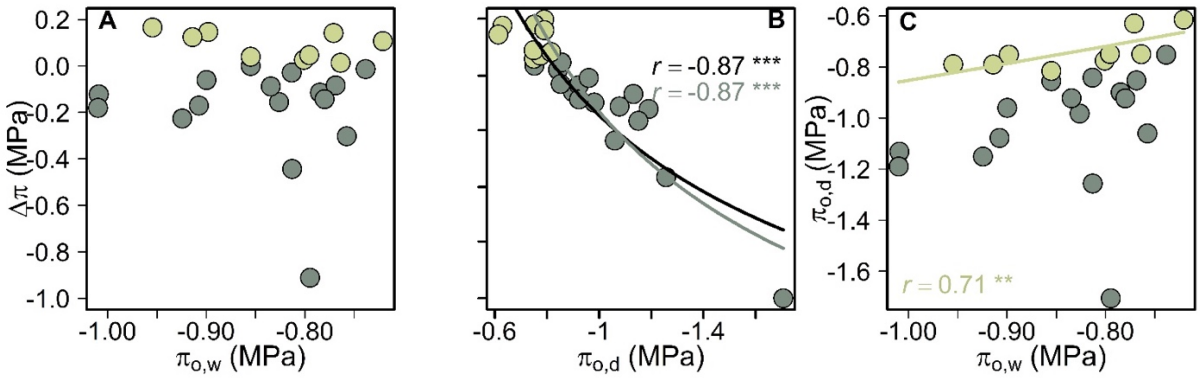

Figure 3. I estimated kinship-informed correlations among well-watered osmotic potential at full turgor ($\pi_{o,w}$) droughted osmotic potential at full turgor ($\pi_{o,d}$) and the change in osmotic potential at full turgor ($\Delta\pi$) across all my genotypes and among those that had or had not adjusted osmotically. Across ecotypes, $\pi_{o,w}$ did not predict osmotic adjustment (A) but $\pi_{o,d}$ was strong associated (B). When I considered osmotic adjustment strategies, the adjusters' $\pi_{o,d}$ strongly predicted osmotic adjustment. Further, only the non-adjusters' $\pi_{o,w}$ was significantly related to $\pi_{o,d}$ (C). Light green points and lines represent ecotypes which had not osmotically adjusted, and darker green points represent those which had adjusted. Statistical significance; *p<0.05; **p<0.01; ***p<0.001.

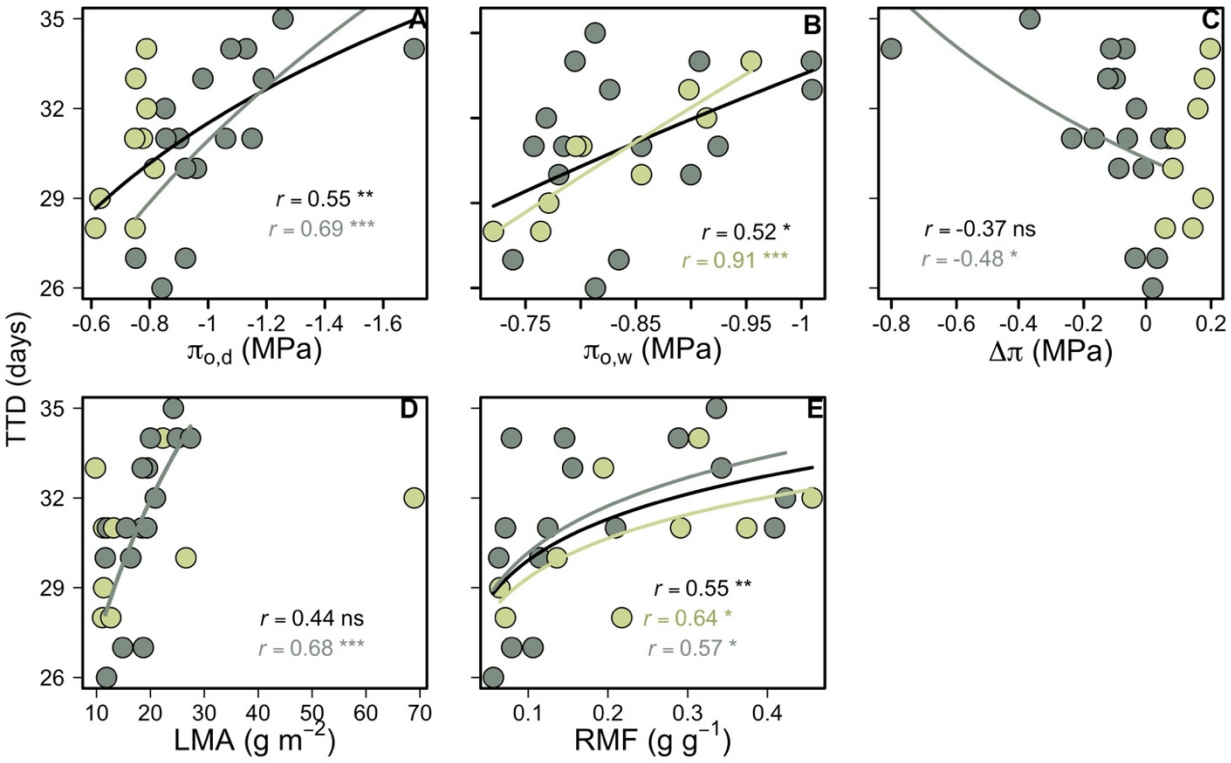

Figure 4. I tested for kinship-informed correlations among drought resilient traits, $\pi_{o,w}$, $\pi_{o,d}$, $\Delta\pi$, leaf mass per area (LMA) and root mass fraction (RMF), and drought survival time as the time until death from the beginning of the drought experiment until 5/12 individuals had died (TTD). I found significant correlations among $\pi_{O,w}$, $\pi_{O,d}$, $\Delta\pi$, LMA and RMF with survival where "less-resilient" ecotypes survived for shorter periods of the drought. Light green points and lines

represent ecotypes which had not osmotically adjusted, and darker green points represent those which had adjusted. Statistical significance; *p<0.05; **p<0.01; ***p<0.001.

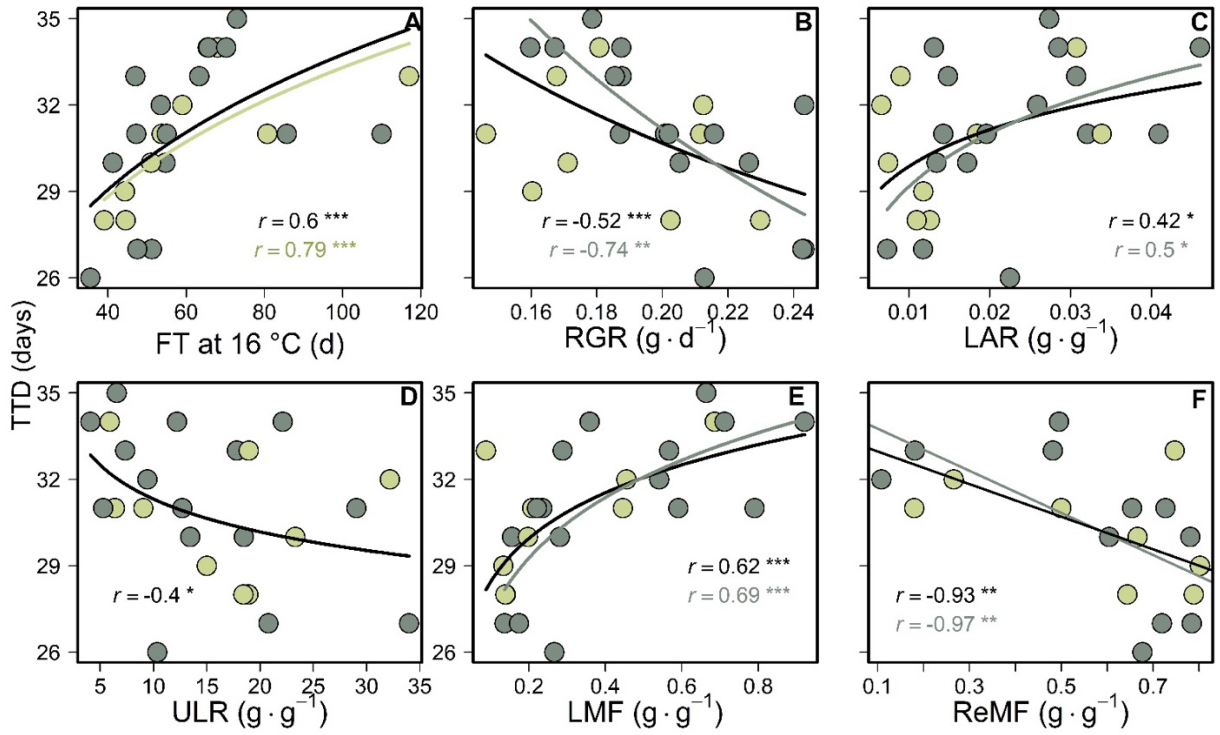

Figure 5. I tested for kinship-informed correlations among drought avoidant traits, flowering time at 16°C, relative growth rate, leaf area ratio, unit leaf rate, leaf mass fraction and reproductive mass fraction (ReMF) and drought survival time as the time until death from the beginning of the drought experiment until 5/12 individuals had died (TTD). I found significant correlations among flower time, relative growth rate, leaf area ratio, leaf mass fraction, and reproductive mass fraction with survival where longer-lived ecotypes grew less, allocate more of their biomass to leaves over flowers and flower later. Light green points and lines represent

ecotypes which had not osmotically adjusted, and darker green points represent those which had adjusted. Statistical significance; *$p<0.05$; **$p<0.01$; ***$p<0.001$.

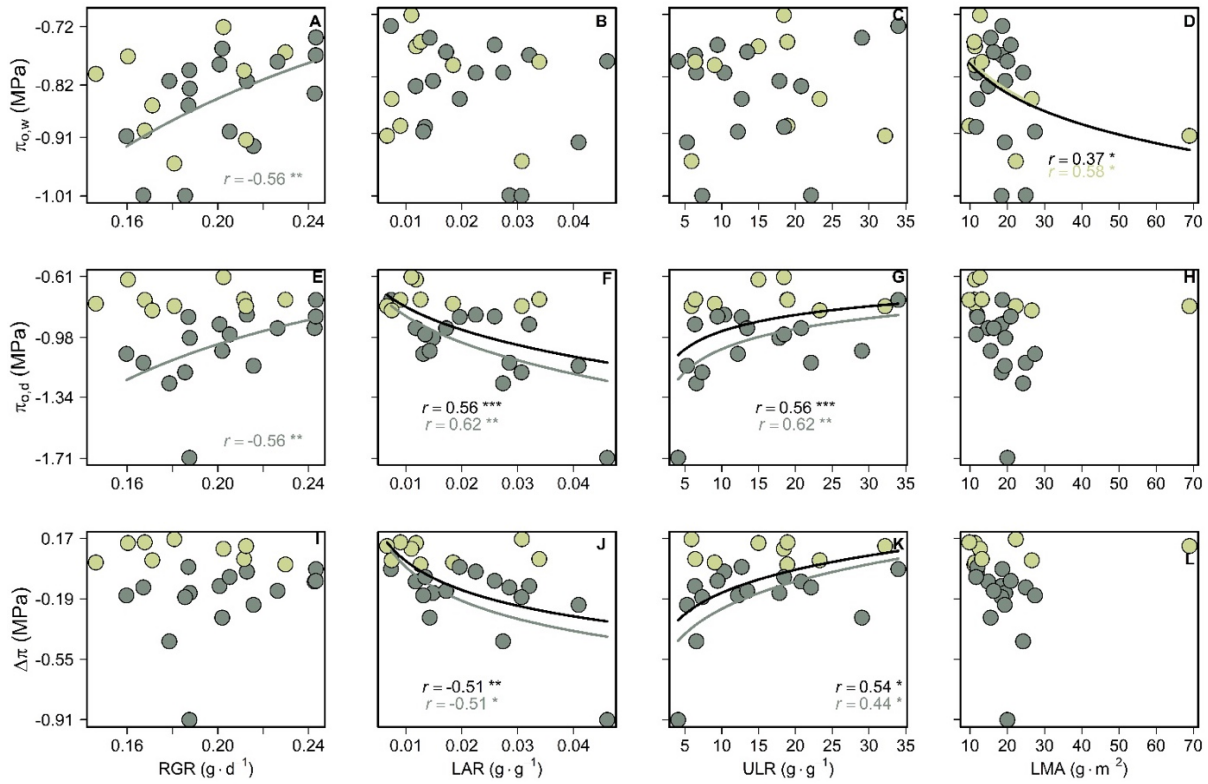

Figure 6. Kinship-informed correlations among osmotic variables relative growth (RGR) and its component traits (unit leaf rate (ULR), leaf area ratio (LAR), and leaf mass per area (LMA)). Many strong relationships among osmotic and growth traits were significant for the ecotypes which had osmotically adjusted. The non-adjusting ecotypes only presented strong relationships between $\pi_{o,w}$ and LMA. Light green points and lines represent ecotypes which had not osmotically adjusted, and darker green points represent those which had adjusted. Statistical significance; *p<0.05; **p<0.01; ***p<0.001.

Supplementary materials

Supplementary Data Captions (see attached Excel Workbook)

Table S4.1. Data for all 29 ecotypes of Arabidopsis thaliana from both control and drought treatments. Osmotic variables (i.e., $\pi_{o,w}$, $\pi_{o,d}$, and $\Delta\pi$) are tabled along with the contribution of $\Delta\pi$ and $\pi_{o,w}$, to the $\pi_{o,d}$, climate variables (see Table S4.2 for definitions, sources and units), and growth traits (i.e., relative growth rate, leaf, root and reproductive mass fraction, unit leaf rate, and leaf area ratio).

Table S4.2. Units, definitions, and sources for 47 climatic variables used to test for associations among osmotic adjustment, growth and climate throughout my study.

Table S4.3. All kinship informed correlations were performed across all genotypes, those which had adjusted (i.e., $\Delta\pi < 0$; adjusters), and those genotypes which did not adjust (i.e., $\Delta\pi < 0$). Tabled are the best fit correlations (i.e., untransformed or "raw" and log transformed) for osmotic, climate and growth variables for control and drought treated ecotypes of Arabidopsis thaliana.

Supplementary Figures

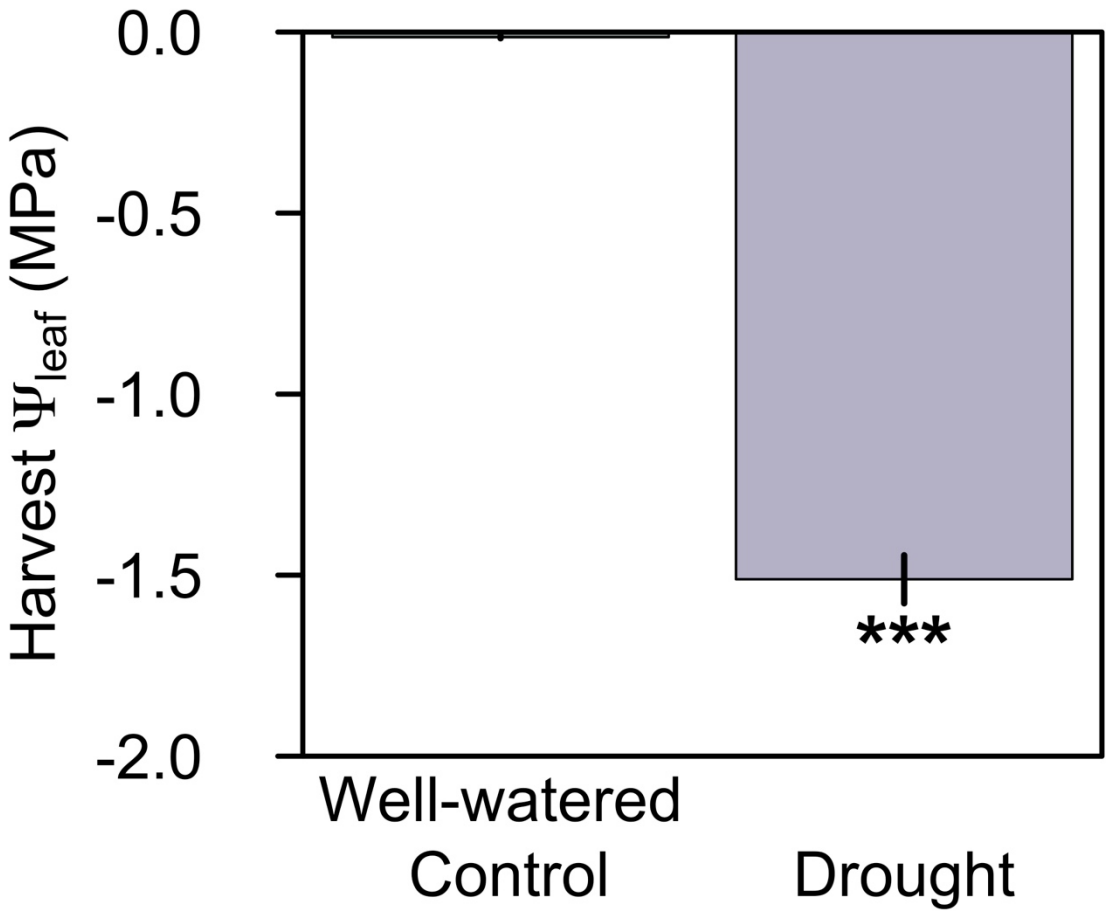

Figure S1. Harvest leaf water potential (Ψ_{leaf}) among well-watered control and droughted treatments. Stars indicate significant ($p<0.001$) Welch's Two-sample T-test.

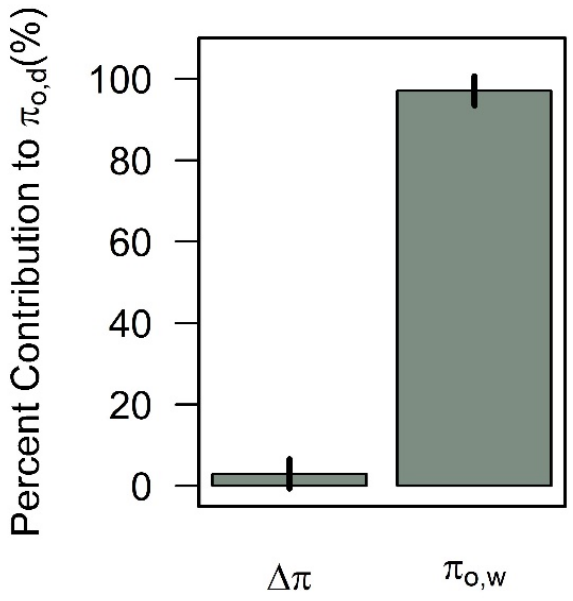

Figure S2. For each ecotype, I estimated the percent contribution of the change in osmotic potential ($\Delta\pi$) and the well-watered osmotic potential ($\pi_{o,w}$) to the final droughted osmotic potential at full turgor ($\pi_{o,d}$) (Equation 2-3). If the contribution of $\Delta\pi$ or $\pi_{o,w}$ for a given ecotype exceed 50%, then that variable was determined to be the more important determinant of the magnitude of $\pi_{o,d}$. Overall, $\pi_{o,w}$ contributed greatly to $\pi_{o,d}$ while $\Delta\pi$ contributed minimally.

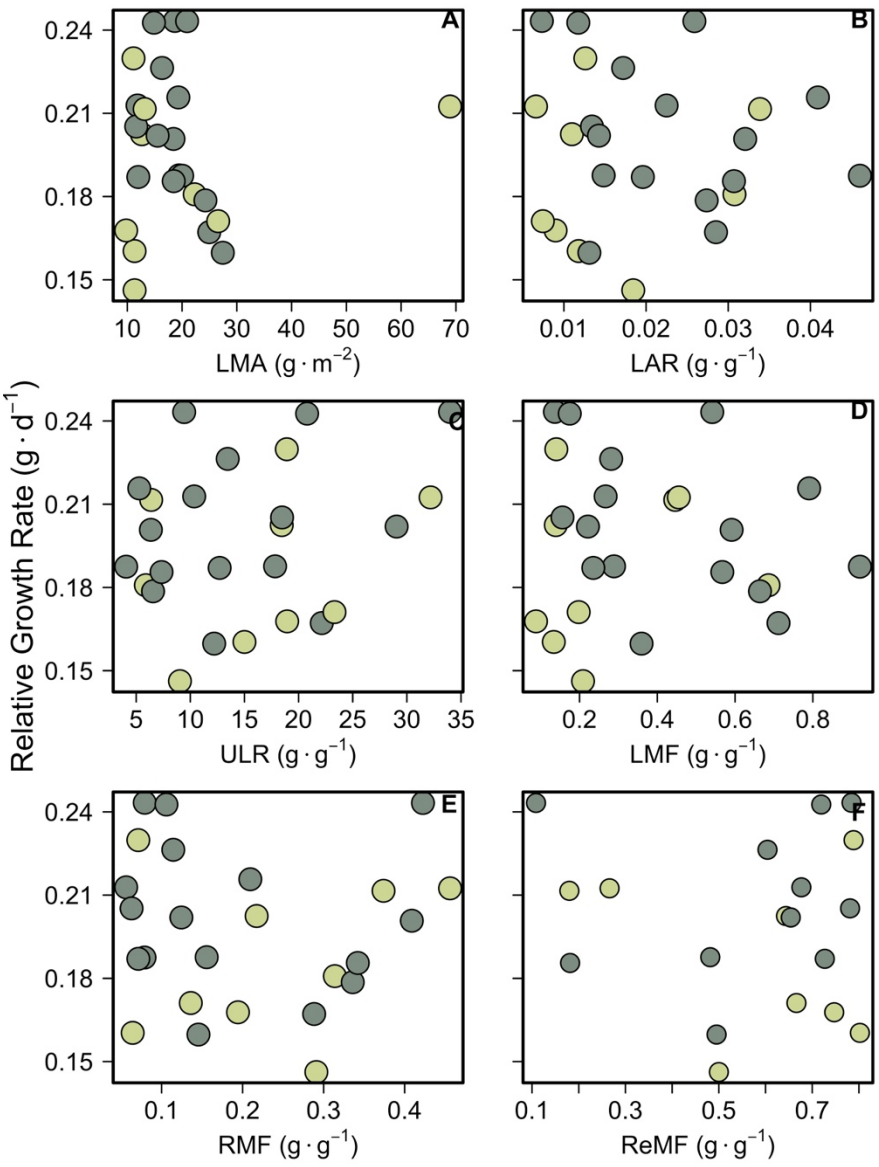

Figure S3. I grew 29 ecotypes of *Arabidopsis thaliana* estimating both their capacity to osmotically adjust and their subsequent growth response. Presented are the relationships between the relative growth rate (RGR), other growth parameters (i.e., leaf area ratio (LAR) and unit leaf rate (ULR)) and allocation (i.e., leaf mass per area (LMA), leaf mass fraction (LMF), root mass fraction (RMF) and reproductive mass fraction (ReMF)).

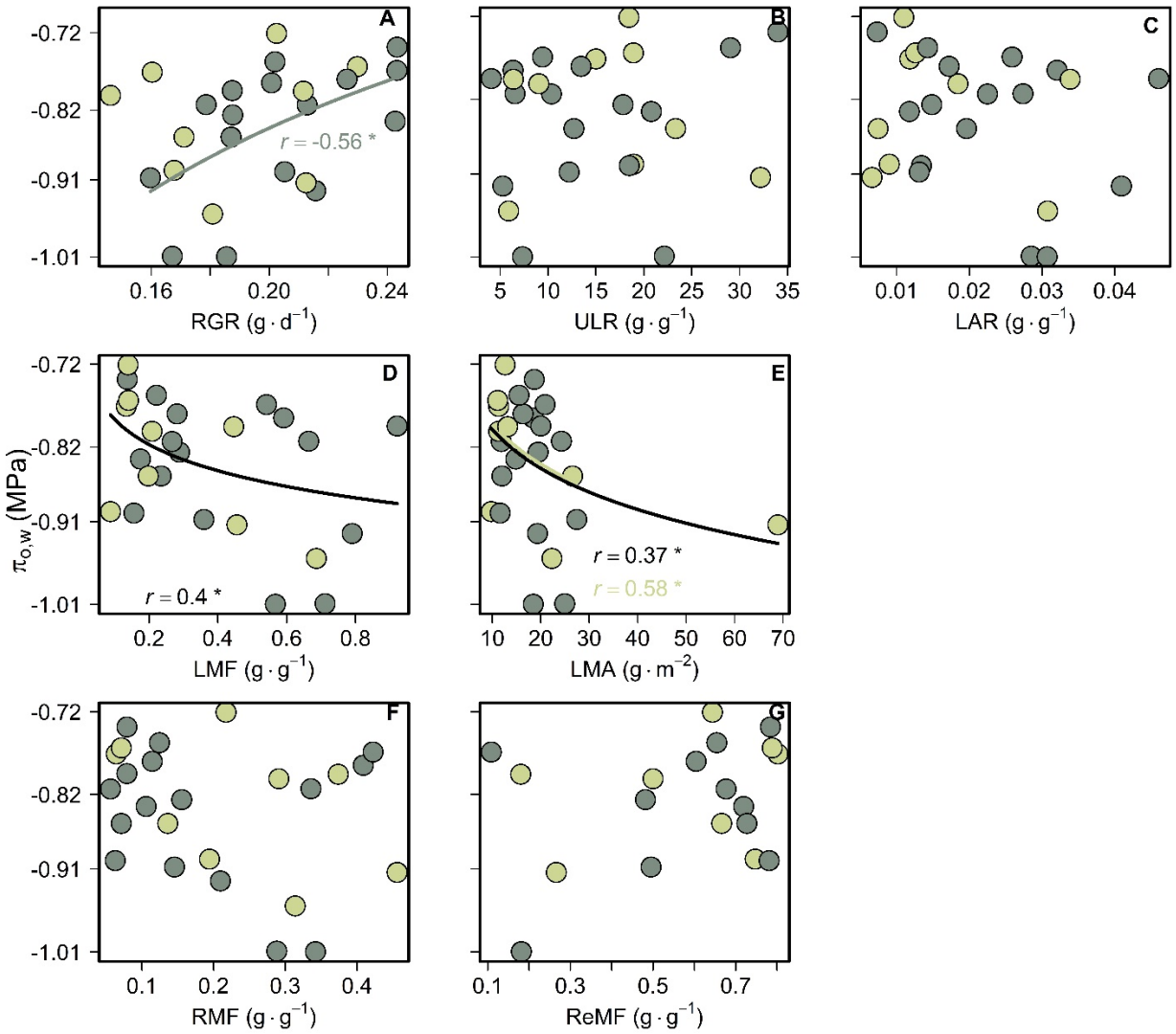

Figure S4. I tested for relationships among my ecotypes of *Arabidopsis thaliana* between their growth traits and their osmotic parameter. Presented are the relationships between the relative growth rate (RGR), other growth parameters (i.e., leaf area ratio (LAR) and unit leaf rate (ULR)) and allocation (i.e., leaf mass per area (LMA), leaf mass fraction (LMF), root mass fraction (RMF) and reproductive mass fraction (ReMF)) and well-watered osmotic potential at full turgor. Light green points and lines represent ecotypes which had not osmotically adjusted, and darker green points represent those which had adjusted. Statistical significance; *p<0.05; **p<0.01; ***p<0.001.

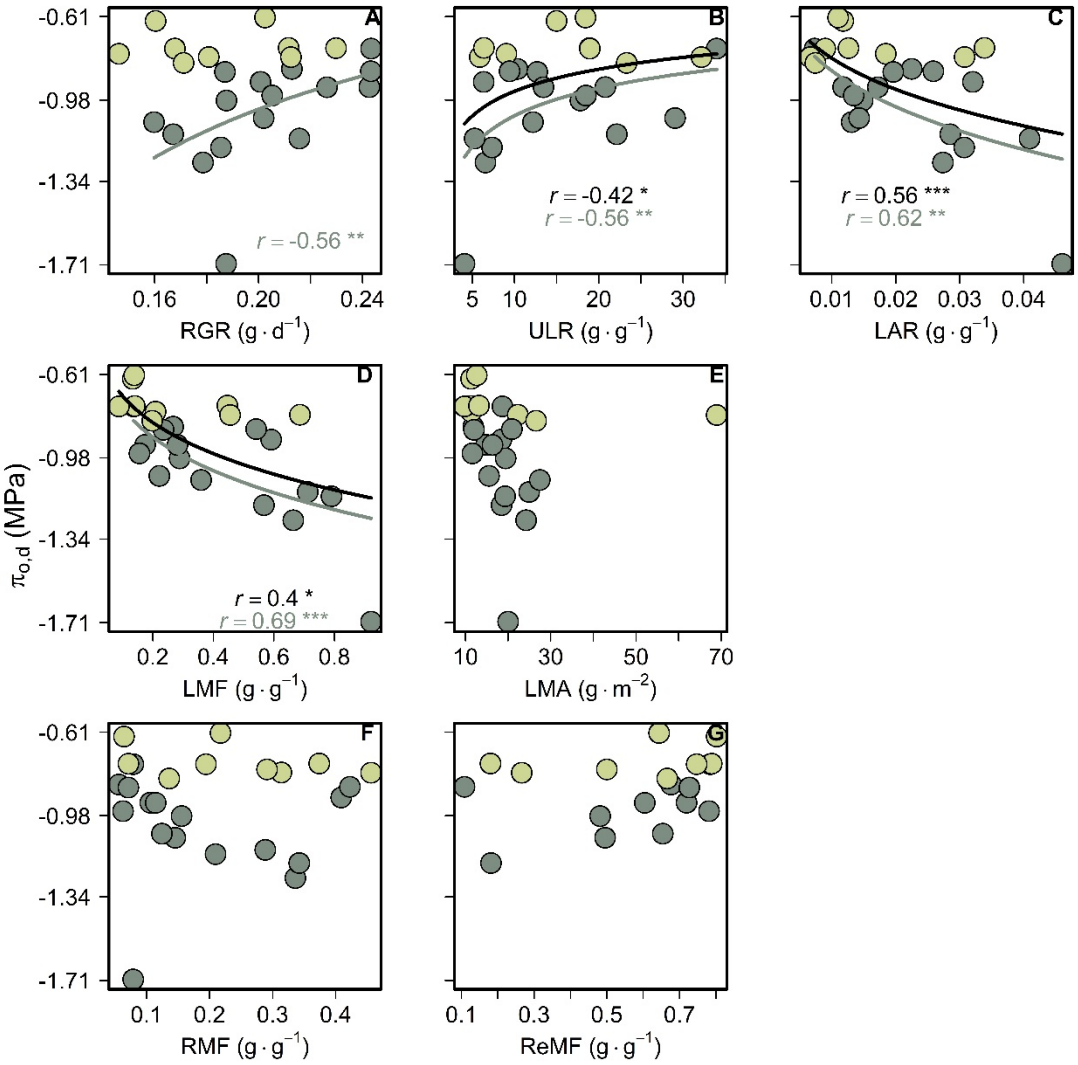

Figure S5. I tested for relationships among my ecotypes of *Arabidopsis thaliana* between their growth traits and their osmotic parameter. Presented are the relationships between the relative growth rate (RGR), other growth parameters (i.e., leaf area ratio (LAR) and unit leaf rate (ULR)) and allocation (i.e., leaf mass per area (LMA), leaf mass fraction (LMF), root mass fraction (RMF) and reproductive mass fraction (ReMF)) and well-watered osmotic potential at full turgor ($\pi_{o,d}$). Light green points and lines represent ecotypes which had not osmotically adjusted, and darker green points represent those which had adjusted. Statistical significance; *p<0.05; **p<0.01; ***p<0.001.

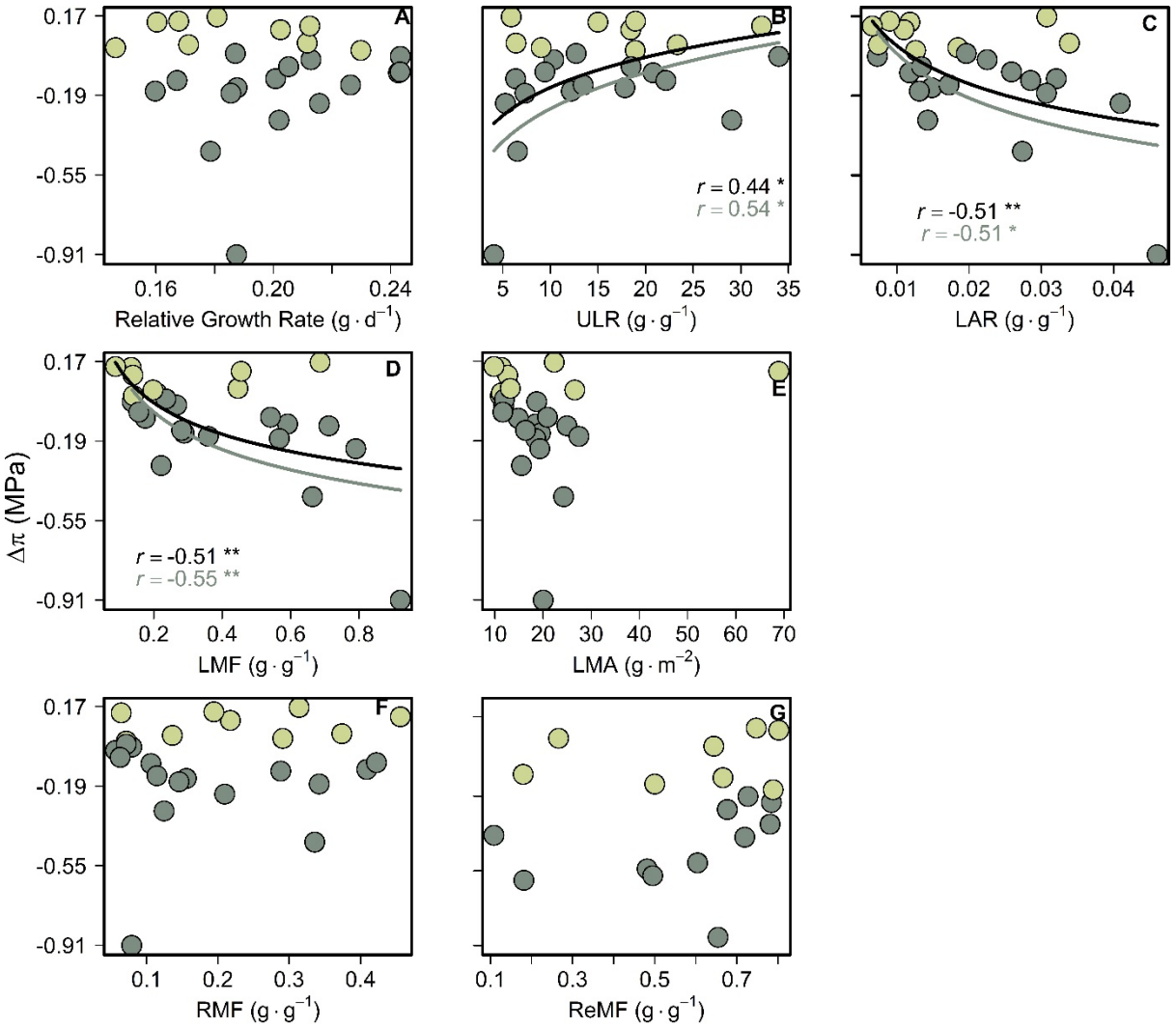

Figure S6. I tested for relationships among my ecotypes of *Arabidopsis thaliana* between their growth traits and their osmotic parameter. Presented are the relationships between the relative growth rate (RGR), other growth parameters (i.e., leaf area ratio (LAR) and unit leaf rate (ULR)) and allocation (i.e., leaf mass per area (LMA), leaf mass fraction (LMF), root mass fraction (RMF) and reproductive mass fraction (ReMF)) and well-watered osmotic potential at full turgor (Δπ). Light green points and lines represent ecotypes which had not osmotically adjusted, and darker green points represent those which had adjusted. Statistical significance; *p<0.05; **p<0.01; ***p<0.001.

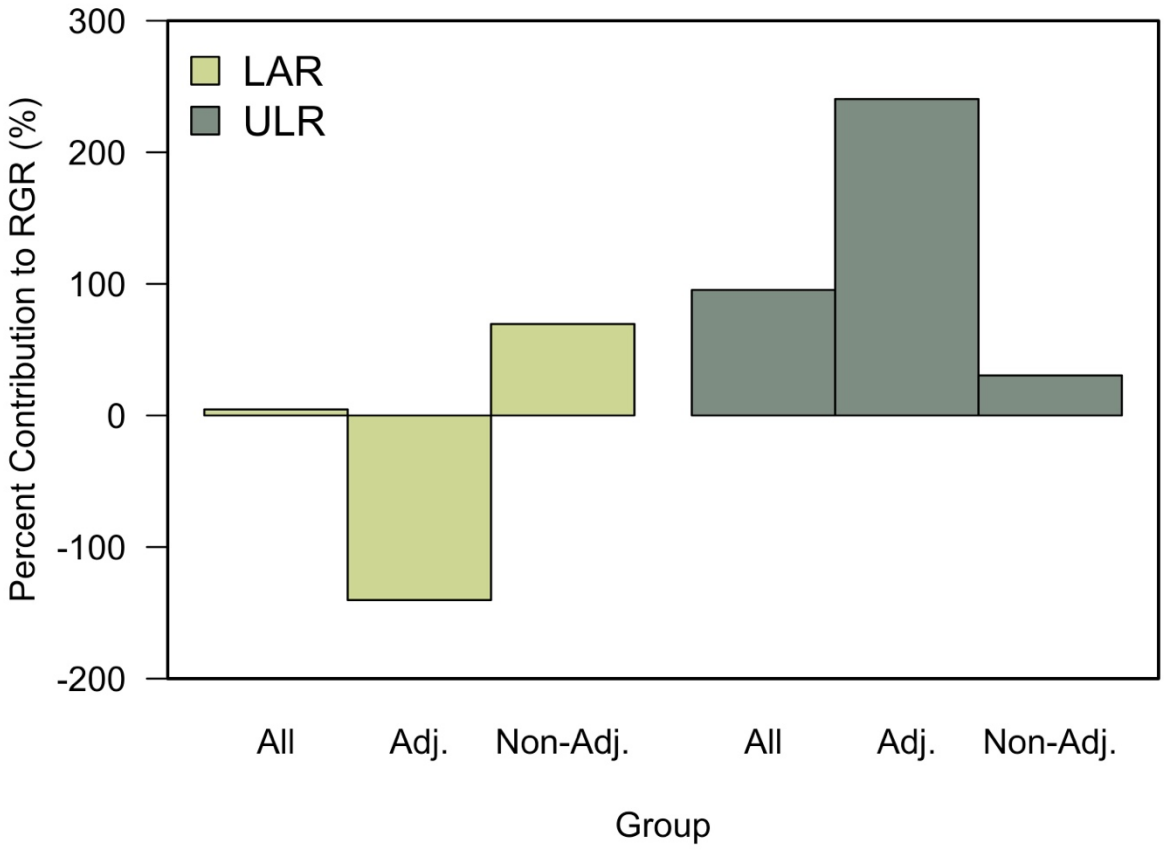

Figure S7. To determine the causal contribution of the components of relative growth rate (RGR) (i.e., leaf area ratio (LAR) and unit leaf rate (ULR)), I applied a causal partitioning analysis, which considers the function of RGR and estimates to infinitesimal change in RGR caused by each of its underlying components, integrated across all my genotypes, to provide the total contribution of each variable to the difference among genotypes. This approach avoids the influence of covariation among RGR components in correlations among those variables. I performed this analysis across all ecotypes, the adjusters, and non-adjusting ecotypes.

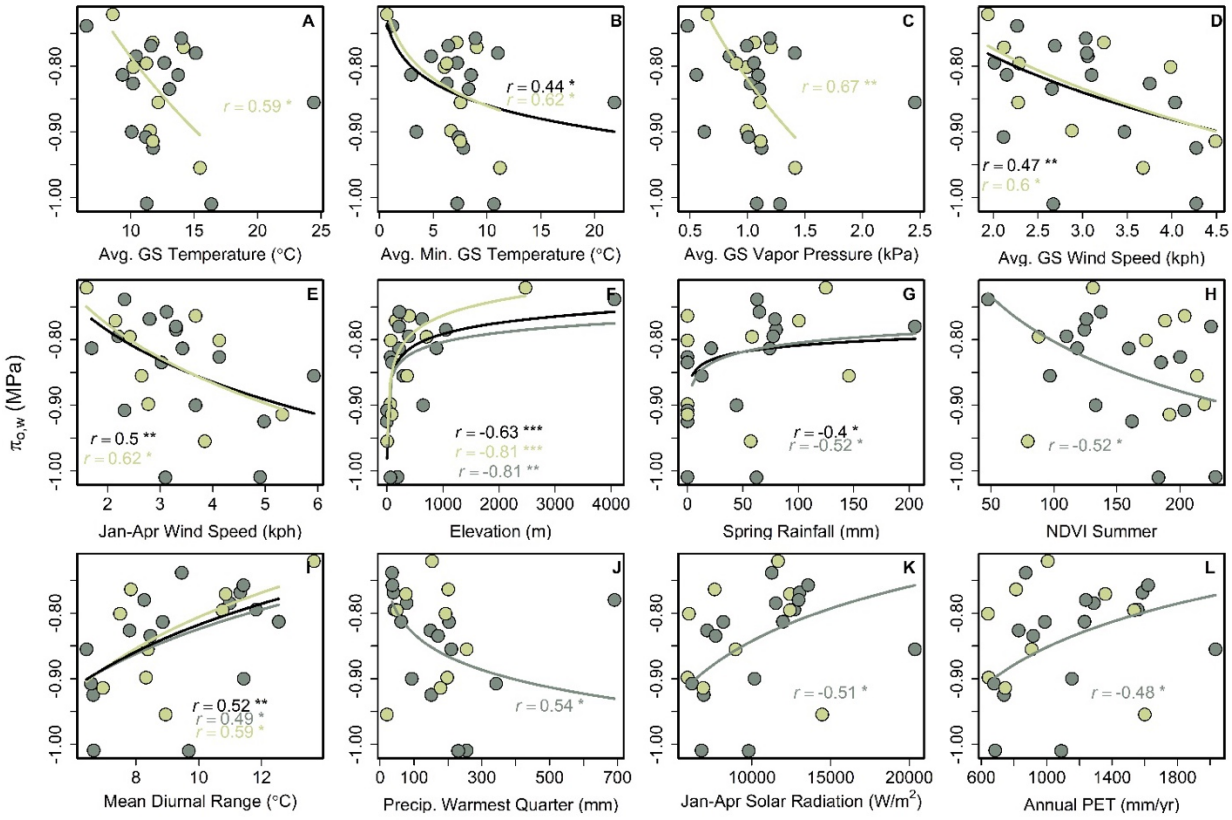

Figure S8. I assessed whether $\pi_{o,w}$, $\pi_{o,d}$ and $\Delta\pi$ were associated with the native climates of *A. thaliana* ecotypes. Presented are significant correlations among $\pi_{o,w}$ and climate variables. Light green points and lines represent ecotypes which had not osmotically adjusted, and darker green points represent those which had adjusted. Statistical significance; *p<0.05; **p<0.01; ***p<0.001.

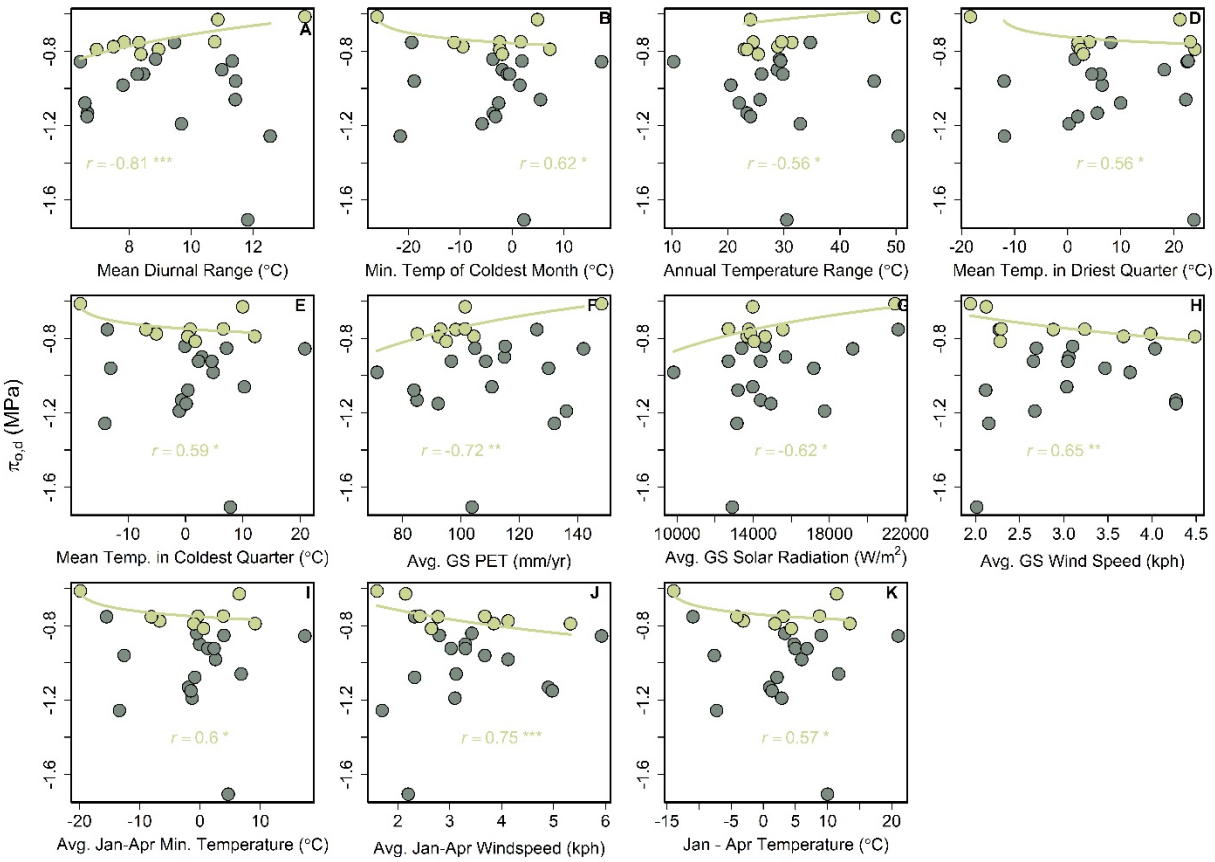

Figure S9. I assessed whether $\pi_{o,w}$, $\pi_{o,d}$ and $\Delta\pi$ were associated with the native climates of *A. thaliana* ecotypes. Presented are significant correlations among $\pi_{o,d}$ and climate variables. Light green points and lines represent ecotypes which had not osmotically adjusted, and darker green points represent those which had adjusted. Statistical significance; *p<0.05; **p<0.01; ***p<0.001.

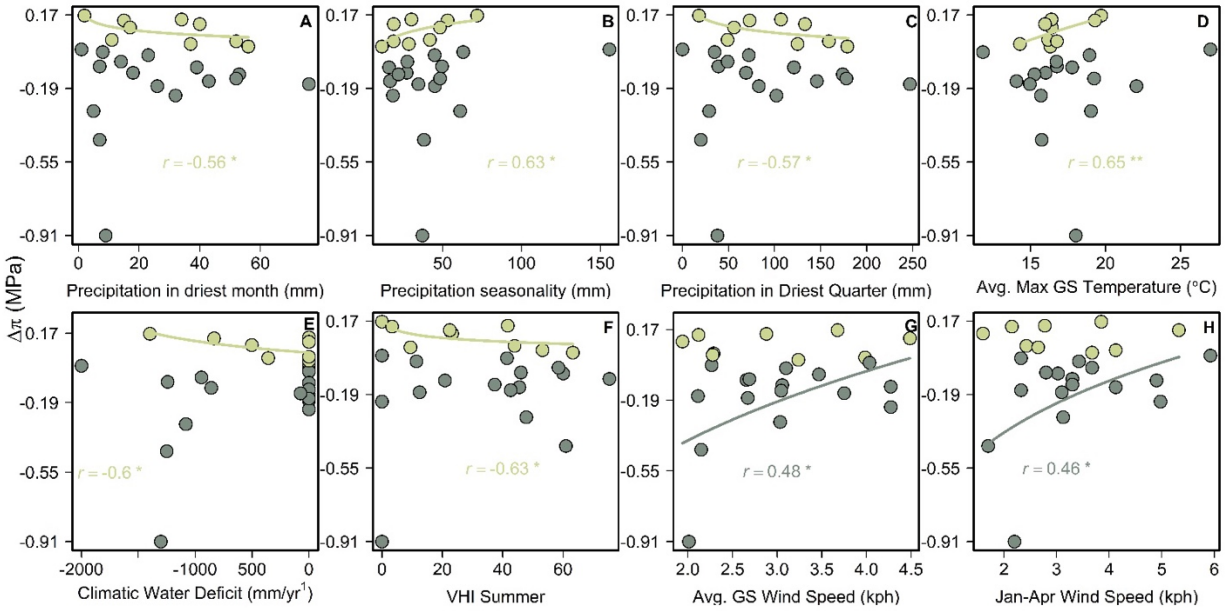

Figure S10. I assessed whether $\pi_{o,w}$, $\pi_{o,d}$ and $\Delta\pi$ were associated with the native climates of *A. thaliana* ecotypes. Presented are significant correlations among $\Delta\pi$ and climate variables. Light green points and lines represent ecotypes which had not osmotically adjusted, and darker green points represent those which had adjusted. Statistical significance; *p<0.05; **p<0.01; ***p<0.001.

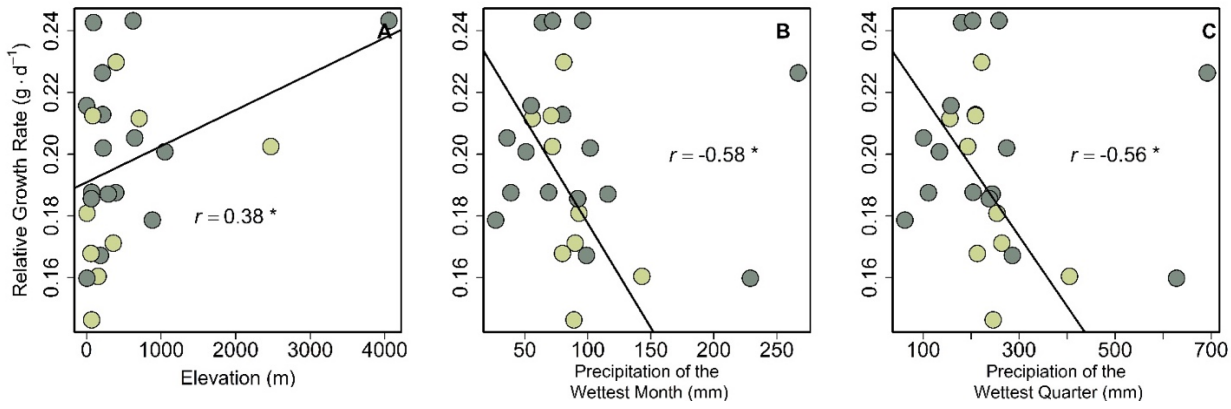

Figure S11. To determine associations between climate and growth (relative growth rate), I performed kinship-informed correlations among RGR and climate of ecotypes of *A.thaliana*. Presented are significant relationships between RGR, elevation, precipitation of the wettest month and quarter. Light green points and lines represent ecotypes which had not osmotically adjusted, and darker green points represent those which had adjusted. Solid black lines represent relationships drawn across all ecotypes. Statistical significance; *p<0.05; **p<0.01; ***p<0.001.

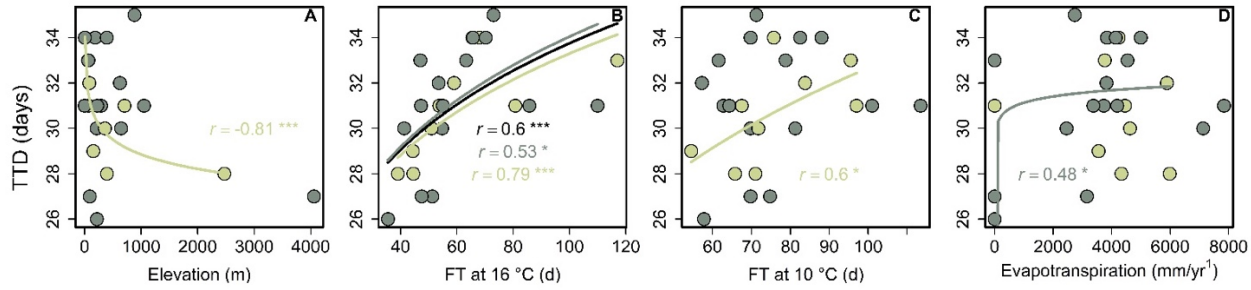

Figure S12. To determine associations between climate and survival time (TTD), I performed kinship-informed correlations among TTD and climate of ecotypes of *A.thaliana*. Presented are significant relationships between TTD, elevation (A), flowering time at 10°C (C) and 16°C (B), and evapotranspiration (D). Light green points and lines represent ecotypes which had not osmotically adjusted, and darker green points represent those which had adjusted. Statistical significance; *p<0.05; **p<0.01; ***p<0.001.

References

Allen, C.D., Macalady, A.K., Chenchouni, H., Bachelet, D., McDowell, N., Vennetier, M., Kitzberger, T., Rigling, A., Breshears, D.D., Hogg, E.H. (Ted), Gonzalez, P., Fensham, R., Zhang, Z., Castro, J., Demidova, N., Lim, J.-H., Allard, G., Running, S.W., Semerci, A., Cobb, N., 2010. A global overview of drought and heat-induced tree mortality reveals emerging climate change risks for forests. Forest Ecology and Management, Adaptation of Forests and Forest Management to Changing Climate 259, 660–684. https://doi.org/10.1016/j.foreco.2009.09.001

Alonso-Blanco, C., Andrade, J., Becker, C., Bemm, F., Bergelson, J., Borgwardt, K.M., Cao, J., Chae, E., Dezwaan, T.M., Ding, W., Ecker, J.R., Exposito-Alonso, M., Farlow, A., Fitz, J., Gan, X., Grimm, D.G., Hancock, A.M., Henz, S.R., Holm, S., Horton, M., Jarsulic, M., Kerstetter, R.A., Korte, A., Korte, P., Lanz, C., Lee, C.-R., Meng, D., Michael, T.P., Mott, R., Muliyati, N.W., Nägele, T., Nagler, M., Nizhynska, V., Nordborg, M., Novikova, P.Y., Picó, F.X., Platzer, A., Rabanal, F.A., Rodriguez, A., Rowan, B.A., Salomé, P.A., Schmid, K.J., Schmitz, R.J., Seren, Ü., Sperone, F.G., Sudkamp, M., Svardal, H., Tanzer, M.M., Todd, D., Volchenboum, S.L., Wang, C., Wang, G., Wang, X., Weckwerth, W., Weigel, D., Zhou, X., 2016a. 1,135 Genomes reveal the global pattern of polymorphism in Arabidopsis thaliana. Cell. https://doi.org/10.1016/j.cell.2016.05.063

Alonso-Blanco, C., Andrade, J., Becker, C., Bemm, F., Bergelson, J., Borgwardt, K.M., Cao, J., Chae, E., Dezwaan, T.M., Ding, W., Ecker, J.R., Exposito-Alonso, M., Farlow, A., Fitz, J., Gan, X., Grimm, D.G., Hancock, A.M., Henz, S.R., Holm, S., Horton, M., Jarsulic, M., Kerstetter, R.A., Korte, A., Korte, P., Lanz, C., Lee, C.-R., Meng, D., Michael, T.P.,

Mott, R., Muliyati, N.W., Nägele, T., Nagler, M., Nizhynska, V., Nordborg, M., Novikova, P.Y., Picó, F.X., Platzer, A., Rabanal, F.A., Rodriguez, A., Rowan, B.A., Salomé, P.A., Schmid, K.J., Schmitz, R.J., Seren, Ü., Sperone, F.G., Sudkamp, M., Svardal, H., Tanzer, M.M., Todd, D., Volchenboum, S.L., Wang, C., Wang, G., Wang, X., Weckwerth, W., Weigel, D., Zhou, X., 2016b. 1,135 Genomes reveal the global pattern of polymorphism in Arabidopsis thaliana. Cell. https://doi.org/10.1016/j.cell.2016.05.063

Bartlett, M.K., Detto, M., Pacala, S.W., 2019. Predicting shifts in the functional composition of tropical forests under increased drought and CO2 from trade-offs among plant hydraulic traits. Ecology Letters. https://doi.org/10.1111/ele.13168

Bartlett, M.K., Klein, T., Jansen, S., Choat, B., Sack, L., 2016. The correlations and sequence of plant stomatal, hydraulic, and wilting responses to drought. Proceedings of the National Academy of Sciences 113, 13098–13103. https://doi.org/10.1073/pnas.1604088113

Bartlett, M.K., Scoffoni, C., Ardy, R., Zhang, Y., Sun, S., Cao, K., Sack, L., 2012a. Rapid determination of comparative drought tolerance traits: using an osmometer to predict turgor loss point. Methods in Ecology and Evolution 3, 880–888. https://doi.org/10.1111/j.2041-210X.2012.00230.x

Bartlett, M.K., Scoffoni, C., Sack, L., 2012b. The determinants of leaf turgor loss point and prediction of drought tolerance of species and biomes: a global meta-analysis: Drivers of plant drought tolerance. Ecology Letters 15, 393–405. https://doi.org/10.1111/j.1461-0248.2012.01751.x

Bartlett, M.K., Zhang, Y., Kreidler, N., Sun, S., Ardy, R., Cao, K., Sack, L., 2014. Global analysis of plasticity in turgor loss point, a key drought tolerance trait. Ecol Lett 17, 1580–1590. https://doi.org/10.1111/ele.12374

Beers, Y., 1957. Introduction to the theory of error. Addison Wesley Publishing Co., Reading, Mass.

Binks, O., Meir, P., Rowland, L., da Costa, A.C.L., Vasconcelos, S.S., de Oliveira, A.A.R., Ferreira, L., Christoffersen, B., Nardini, A., Mencuccini, M., 2016. Plasticity in leaf-level water relations of tropical rainforest trees in response to experimental drought. New Phytologist 211, 477–488. https://doi.org/10.1111/nph.13927

Blum, A., 2017. Osmotic adjustment is a prime drought stress adaptive engine in support of plant production. Plant, Cell & Environment. https://doi.org/10.1111/pce.12800

Bolnick, D.I., Amarasekare, P., Araújo, M.S., Bürger, R., Levine, J.M., Novak, M., Rudolf, V.H.W., Schreiber, S.J., Urban, M.C., Vasseur, D.A., 2011. Why intraspecific trait variation matters in community ecology. Trends in Ecology & Evolution 26, 183–192. https://doi.org/10.1016/j.tree.2011.01.009

Brodribb, T.J., Powers, J., Cochard, H., Choat, B., 2020. Hanging by a thread? Forests and drought. Science. https://doi.org/10.1126/science.aat7631

Browne, M., Bartlett, M.K., Henry, C., Jarrahi, M., John, G., Scoffoni, C., Yardimci, N.T., Sack, L., 2023. Low baseline intraspecific variation in leaf pressure-volume traits: Biophysical basis and implications for spectroscopic sensing. *Physiologia Plantarum* 175, e13974. https://doi.org/10.1111/ppl.13974

Buckley, T.N., Diaz-Espejo, A., 2015. Partitioning changes in photosynthetic rate into contributions from different variables. Plant, Cell & Environment. https://doi.org/10.1111/pce.12459

de Bello, F., Lavorel, S., Albert, C.H., Thuiller, W., Grigulis, K., Dolezal, J., Janeček, Š., Lepš, J., 2011. Quantifying the relevance of intraspecific trait variability for functional diversity. Methods in Ecology and Evolution. https://doi.org/10.1111/j.2041-210X.2010.00071.x

Ding, Y., Zhang, Y., Zheng, Q.-S., Tyree, M.T., 2014. Pressure–volume curves: revisiting the impact of negative turgor during cell collapse by literature review and simulations of cell micromechanics. New Phytologist. https://doi.org/10.1111/nph.12829

Ferrero-Serrano, Á., Assmann, S.M., 2019. Phenotypic and genome-wide association with the local environment of Arabidopsis. Nature ecology & evolution 3, 274–285.

Fick, S.E., Hijmans, R.J., 2017. WorldClim 2: new 1-km spatial resolution climate surfaces for global land areas. International journal of climatology 37, 4302–4315.

Fletcher, L.R., Cui, H., Callahan, H., Scoffoni, C., John, G.P., Bartlett, M.K., Burge, D.O., Sack, L., 2018. Evolution of leaf structure and drought tolerance in species of Californian Ceanothus. American Journal of Botany 105, 1672–1687. https://doi.org/10.1002/ajb2.1164

Fletcher, L.R., Scoffoni, C., Farrell, C., Buckley, T.N., Pellegrini, M., Sack, L., 2022. Testing the association of relative growth rate and adaptation to climate across natural ecotypes of Arabidopsis. New Phytologist 236, 413–432. https://doi.org/10.1111/nph.18369

Girma, F.S., Krieg, D.R., 1992. Osmotic Adjustment in Sorghum 99, 6.

González, A., Martín, I., Ayerbe, L., 1999. Barley yield in water-stress conditions.: The influence of precocity, osmotic adjustment and stomatal conductance. Field Crops Research. https://doi.org/10.1016/S0378-4290(99)00002-7

Griffin-Nolan, R.J., Ocheltree, T.W., Mueller, K.E., Blumenthal, D.M., Kray, J.A., Knapp, A.K., 2019. Extending the osmometer method for assessing drought tolerance in herbaceous species. Oecologia 189, 353–363. https://doi.org/10.1007/s00442-019-04336-w

Harris, I., Jones, P.D., Osborn, T.J., Lister, D.H., 2014. Updated high-resolution grids of monthly climatic observations–the CRU TS3. 10 Dataset. International journal of climatology 34, 623–642.

Henry, C., John, G.P., Pan, R., Bartlett, M.K., Fletcher, L.R., Scoffoni, C., Sack, L., 2019. A stomatal safety-efficiency trade-off constrains responses to leaf dehydration. Nature Communications. https://doi.org/10.1038/s41467-019-11006-1

Hsiao, T.C., Acevedo, E., Fereres, E., Henderson, D.W., Monteith, J.L., Weatherley, P.E., 1976. Water stress, growth and osmotic adjustment. Philosophical Transactions of the Royal Society of London. B, Biological Sciences 273, 479–500. https://doi.org/10.1098/rstb.1976.0026

Huala, E., Dickerman, A.W., Garcia-Hernandez, M., Weems, D., Reiser, L., LaFond, F., Hanley, D., Kiphart, D., Zhuang, M., Huang, W., Mueller, L.A., Bhattacharyya, D., Bhaya, D., Sobral, B.W., Beavis, W., Meinke, D.W., Town, C.D., Somerville, C., Rhee, S.Y., 2001. The Arabidopsis Information Resource (TAIR): a comprehensive database and web-based information retrieval, analysis, and visualization system for a model plant. Nucleic Acids Research 29, 102–105. https://doi.org/10.1093/nar/29.1.102

IPCC, 2014. Climate change 2014: synthesis report.Contribution of working groups I, II and III to the fifth assessment report of the intergovernmental panel on climate change, 5th ed. IPCC, Geneva, Switzerland.

John, G.P., Scoffoni, C., Buckley, T.N., Villar, R., Poorter, H., Sack, L., 2017. The anatomical and compositional basis of leaf mass per area. Ecology Letters 20, 412–425. https://doi.org/10.1111/ele.12739

Kraft, N., 2016. Functional trait differences and the outcome of community assembly: an experimental test with vernal pool annual plants. Oikos. https://doi.org/10.1111/oik.03544

Lasky, J.R., Des Marais, D.L., McKAY, J.K., Richards, J.H., Juenger, T.E., Keitt, T.H., 2012. Characterizing genomic variation of Arabidopsis thaliana: the roles of geography and climate. Molecular Ecology 21, 5512–5529.

Maréchaux, I., Bartlett, M.K., Iribar, A., Sack, L., Chave, J., 2017. Stronger seasonal adjustment in leaf turgor loss point in lianas than trees in an Amazonian forest. Biology Letters. https://doi.org/doi:10.1098/rsbl.2016.0819

Marks, C. O. 2007. The causes of variation in tree seedling traits: The roles of environmental selection versus chance. *Evolution,* 61**,** 455-469.

Monroe, J.G., Powell, T., Price, N., Mullen, J.L., Howard, A., Evans, K., Lovell, J.T., McKay, J.K., 2018. Drought adaptation in Arabidopsis thaliana by extensive genetic loss-of-function. Elife 7, e41038.

Morgan, J., 1977. Differences in osmoregulation between wheat genotypes. Nature.

R Core Team, 2023. R: A language and environment for statistical computing (manual). R Foundation for Statistical Computing, Vienna, Austria.

Reich, P.B., 2014. The world-wide 'fast–slow' plant economics spectrum: a traits manifesto. Journal of Ecology. https://doi.org/10.1111/1365-2745.12211

Rosas, T., Mencuccini, M., Barba, J., Cochard, H., Saura-Mas, S., Martínez-Vilalta, J., 2019. Adjustments and coordination of hydraulic, leaf and stem traits along a water availability gradient. New Phytologist. https://doi.org/10.1111/nph.15684

Schindelin, J., Arganda-Carreras, I., Frise, E., Kaynig, V., Longair, M., Pietzsch, T., Preibisch, S., Rueden, C., Saalfeld, S., Schmid, B., Tinevez, J.-Y., White, D.J., Hartenstein, V., Eliceiri, K., Tomancak, P., Cardona, A., 2012. Fiji: an open-source platform for biological-image analysis. Nature Methods 9, 676.

Scoffoni, C., Pou, A., Aasamaaa, K., Sack, L., 2008. The rapid light response of leaf hydraulic conductance: new evidence from two experimental methods. Plant, Cell & Environment. https://doi.org/10.1111/j.1365-3040.2008.01884.x

Therneau, T.M., 2020. coxme: Mixed effects cox models (manual).

Trueba, S., Pan, R., Scoffoni, C., John, G.P., Davis, S.D., Sack, L., 2019. Thresholds for leaf damage due to dehydration: declines of hydraulic function, stomatal conductance and cellular integrity precede those for photochemistry. New Phytologist 0. https://doi.org/10.1111/nph.15779

Wright, I.J., Reich, P.B., Westoby, M., Ackerly, D.D., Baruch, Z., Bongers, F., Cavender-Bares, J., Chapin, T., Cornelissen, J.H., Diemer, M., 2004. The worldwide leaf economics spectrum. Nature.

Chapter 5: Conclusions and Future Directions

In this dissertation work, I resolved the limitations of estimating physiological traits, and extended the ability to discern the consequences of trait-trait relationships across scales for physiological function. I established a novel physically based remote sensing method, which would improve agricultural irrigation systems and enable noninvasive measurements of hydraulic decline (Browne et al., 2020). My work supports previous work showing that pressure-volume curves are tremendously useful for explaining how species confront drought, where species with a higher leaf water potential at their wilting point tend to be from more arid ecosystems (Bartlett et al., 2012). These traits are becoming more prominent in earth system models, where models including leaf water potential provide dynamic diurnal estimates of water stress and mechanistic understanding of ecosystem hydrology (Kennedy et al., 2019). Yet, few studies had considered variation across these traits within species (Bartlett et al., 2014), which can contribute considerably to across-species trends (Siefert et al., 2015), and to processes at ecosystem scale.

Approaches to the sensing of Ψ_{leaf} based on estimates of WMA have great urgency and importance across scales. My findings at leaf scale indicate that Ψ_{leaf} measurements could in principle be made in vivo, in situ, within a gas exchange system and that species-mean PV parameters could be used for such an application. At larger scales, measurements from a mounted in situ or remote system will improve estimates of drought-induced physiological responses at ecosystem scale (Konings et al., 2021; Momen et al., 2017; Rao et al., 2019), and enable the development of irrigation systems of crops and refinement of canopy flux measurements (Jepsen et al., 2011; Kennedy et al., 2019). While analysis of the ITV_{ref} leads to

important insights and applications at leaf scale, the range of applications at larger scales shows the increasingly need to quantify the ITV of pressure-volume parameters across many scales of ITV.

I also resolved mechanisms underlying the impacts of drought on shift on an annual species, responses that would scale up to influencing community structure (Brodribb et al., 2020; Kraft, 2016). Responses to drought can fall into three strategies. A species may be resistant to drought, and thus able to maintain cellular turgor, photosynthesis albeit at a lower rate, and sustain a relatively slow relative growth rate. Second, a species may avoid the drought, whereby they show sensitivity to hydraulic decline and stomatal closure and have rapid growth when water is available to mitigate the effects of the drought. Lastly, a species may be ambivalent, showing strong sensitivity to drought without necessarily compensating with rapid growth. My work showed that these three strategies could be discerned even among ecotypes of one widespread species, *A. thaliana*, which showed strong variation in native climate, ability to osmotically adjust and to survive an experimental drought. My work extends previous studies that found no association across ecotypes of *A.thaliana* of relative growth rate with native climate but ecotypes with a less negative $\pi_{o,w}$ were from less arid climates (Fletcher et al., 2022). My work shows a yet greater diversity of drought response strategies among ecotypes than shown in that previous work. Conservation of the multiple populations of a species should thus consider the potentially strong variation in drought response strategy and overall tolerance.

My future work will continue to explore the intricacies of physical relationships among plant functional traits and enhance the use of remotely sensing plant water with individual scale traits. New approaches are needed to clarify how pressure volume curve parameters may depend on pools of water in the leaf, and how they may be influenced by leaf dehydration due to loss of

rehydration capacity in dehydrated leaves, which when extreme can be lethal (Oppenheimer and Leshem, 1966). Pressure volume curves are constructed by repeatedly measuring leaf water status, as leaf water potential (Ψ_{leaf}), and leaf mass, which is represented as relative water content (RWC) given estimation of a saturated water content (SWC) (Sack and Pasquet-kok, 2011). Given the importance of hysteresis in cell volume due to dehydration, there is a need to establish a dynamic SWC to account for the percent loss in rehydration capacity and improve PV curve estimation and the quantification of leaf apoplastic fraction (a_f)). My work shows that increasingly detailed approaches to the analysis of plant water status provides new clarity and applications relevant to the biology of diverse species at a wide range of contexts and scales.

References

Bartlett, M.K., Scoffoni, C., Sack, L., 2012. The determinants of leaf turgor loss point and prediction of drought tolerance of species and biomes: a global meta-analysis: Drivers of plant drought tolerance. Ecology Letters 15, 393–405. https://doi.org/10.1111/j.1461-0248.2012.01751.x

Bartlett, M.K., Zhang, Y., Kreidler, N., Sun, S., Ardy, R., Cao, K., Sack, L., 2014. Global analysis of plasticity in turgor loss point, a key drought tolerance trait. Ecology Letters. https://doi.org/10.1111/ele.12374

Brodribb, T.J., Powers, J., Cochard, H., Choat, B., 2020. Hanging by a thread? Forests and drought. Science. https://doi.org/10.1126/science.aat7631

Browne, M., Yardimci, N.T., Scoffoni, C., Jarrahi, M., Sack, L., 2020. Prediction of leaf water potential and relative water content using terahertz radiation spectroscopy. Plant Direct. https://doi.org/10.1002/pld3.197

Fletcher, L.R., Scoffoni, C., Farrell, C., Buckley, T.N., Pellegrini, M., Sack, L., 2022. Testing the association of relative growth rate and adaptation to climate across natural ecotypes of Arabidopsis. New Phytologist 236, 413–432. https://doi.org/10.1111/nph.18369

Jepsen, P.U., Cooke, D.G., Koch, M., 2011. Terahertz spectroscopy and imaging : modern techniques and applications. Laser & Photonics Reviews 5, 124–166. https://doi.org/10.1002/lpor.201000011

John, G.P., Henry, C., Sack, L., 2018. Leaf rehydration capacity: associations with other indices of drought tolerance and environment. Plant, Cell & Environment 41, 2638–2653. https://doi.org/10.1111/pce.13390

Kennedy, D., Swenson, S., Oleson, K.W., Lawrence, D.M., Fisher, R., Lola da Costa, A.C., Gentine, P., 2019. Implementing Plant Hydraulics in the Community Land Model, Version 5. Journal of Advances in Modeling Earth Systems 11, 485–513. https://doi.org/10.1029/2018MS001500

Konings, A.G., Saatchi, S.S., Frankenberg, C., Keller, M., Leshyk, V., Anderegg, W.R.L., Humphrey, V., Matheny, A.M., Trugman, A., Sack, L., Agee, E., Barnes, M.L., Binks, O., Cawse-Nicholson, K., Christoffersen, B.O., Entekhabi, D., Gentine, P., Holtzman, N.M., Katul, G.G., Liu, Y., Longo, M., Martinez-Vilalta, J., McDowell, N., Meir, P., Mencuccini, M., Mrad, A., Novick, K.A., Oliveira, R.S., Siqueira, P., Steele-Dunne, S.C., Thompson, D.R., Wang, Y., Wehr, R., Wood, J.D., Xu, X., Zuidema, P.A., 2021. Detecting forest response to droughts with global observations of vegetation water content. Global Change Biology 27, 6005–6024. https://doi.org/10.1111/gcb.15872

Kraft, N., 2016. Functional trait differences and the outcome of community assembly: an experimental test with vernal pool annual plants. Oikos. https://doi.org/10.1111/oik.03544

Momen, M., Wood, J.D., Novick, K.A., Pangle, R., Pockman, W.T., McDowell, N.G., Konings, A.G., 2017. Interacting effects of leaf water potential and biomass on vegetation optical depth: effects of LWP and biomass on VOD. Journal of Geophysical Research: Biogeosciences 122, 3031–3046. https://doi.org/10.1002/2017JG004145

Oppenheimer, H.R., Leshem, B., 1966. Critical thresholds of dehydration in leaves of Nerium oleander L. Protoplasma 61, 302–321. https://doi.org/10.1007/BF01248987

Rao, K., Anderegg, W.R.L., Sala, A., Martínez-Vilalta, J., Konings, A.G., 2019. Satellite-based vegetation optical depth as an indicator of drought-driven tree mortality. Remote Sensing of Environment 227, 125–136. https://doi.org/10.1016/j.rse.2019.03.026

Sack, L., Pasquet-kok, J., 2011. Leaf pressure-volume curve parameters.

Siefert, A., Violle, C., Chalmandrier, L., Albert, C.H., Taudiere, A., Fajardo, A., Aarssen, L.W., Baraloto, C., Carlucci, M.B., Cianciaruso, M.V., de L. Dantas, V., de Bello, F., Duarte, L.D.S., Fonseca, C.R., Freschet, G.T., Gaucherand, S., Gross, N., Hikosaka, K., Jackson, B., Jung, V., Kamiyama, C., Katabuchi, M., Kembel, S.W., Kichenin, E., Kraft, N.J.B., Lagerström, A., Bagousse-Pinguet, Y.L., Li, Y., Mason, N., Messier, J., Nakashizuka, T., Overton, J.M., Peltzer, D.A., Pérez-Ramos, I.M., Pillar, V.D., Prentice, H.C., Richardson, S., Sasaki, T., Schamp, B.S., Schöb, C., Shipley, B., Sundqvist, M., Sykes, M.T., Vandewalle, M., Wardle, D.A., 2015. A global meta-analysis of the relative extent of intraspecific trait variation in plant communities. Ecology Letters. https://doi.org/10.1111/ele.12508

Trueba, S., Pan, R., Scoffoni, C., John, G.P., Davis, S.D., Sack, L., 2019. Thresholds for leaf damage due to dehydration: declines of hydraulic function, stomatal conductance and cellular integrity precede those for photochemistry. New Phytologist 0. https://doi.org/10.1111/nph.15779